LUMINESCENT MATERIALS AS DIAGNOSTIC REPORTERS IN LATERAL FLOW ASSAYS

by
Adheesha Nuwangi Danthanarayana

A dissertation submitted to the Department of Chemistry,
College of Natural Sciences and Mathematics
in partial fulfillment of the requirements for the degree of

DOCTOR OF PHILOSOPHY

in Chemistry

Chair of Committee: Dr. Jakoah Brgoch

Committee Member: Dr. Richard C. Willson

Committee Member: Dr. P. Shiv Halasyamani

Committee Member: Dr. Ding-Shyue (Jerry) Yang

Committee Member: Dr. Melissa Zastrow

University of Houston
May 2022

ACKNOWLEDGEMENTS

I would like to express my most sincere gratitude to my advisor, Dr. Jakoah Brgoch, and my co-advisor, Dr. Richard Willson for guiding, encouraging, and motivating me throughout my research. I highly appreciate their immense support during my difficult times as a Ph.D. student and for making me strive to achieve my maximum potential. I'm blessed to have both of you as my mentors. I would also like to thank my Ph.D. committee members, Drs. Shiv Halasyamani, Melissa Zastrow, and Jerry Yang for their time and effort in evaluating my research work and providing invaluable feedback.

I'm truly grateful to my dear parents, Sunil Danthanarayana and Priyangani Lelwala, for all the sacrifices they have silently made in helping me achieve my dreams. I cannot thank you enough for everything you have done for me. Thank you so much for all the love and support you have given me and for believing in me. I also want to thank my husband, Hiran Gunawardhana, for always being there for me. I would never have made it here without your love and support. I want to express my profound gratitude to my uncle, late Dr. Ranjith Lelwala, for inspiring me to pursue a Ph.D. Thank you for showing me the right path to achieve my ambition of becoming a scientist. You would have been proud of me if you were alive today.

I want to thank my undergraduate supervisors at the University of Colombo, Sri Lanka, Prof. Nalin de Silva and Prof. Rohini de Silva, for guiding, motivating, and supporting me to start my doctoral studies. I also want to thank all my teachers at Sanghamitta Balika Vidyalaya, Galle, Sri Lanka, for guiding me in my junior years to become the person I am today. I'm also thankful to all my relatives and friends who helped me in numerous ways throughout my life. I feel so lucky and blessed to have such supportive people around me.

I'm especially thankful to all my Sri Lankan friends in Houston who helped me when I first came to the United States. I also want to thank Celine and Aby for their generous support and kindness and for welcoming me warmly into their home anytime. Because of you all, I didn't feel that I'm far away from my home. I also thank Louise Marie, Ya Zhuo, Xiehong Xie, and Xiaojing Ma for the wonderful friendship and support and for making my years at the University of Houston more fun and memorable.

Finally, I would like to thank all the present and former members of the Brgoch group and the Willson group for providing help and advice on my research. I enjoyed working with you all. I especially thank Drs. Erin Finley and Heather Goux for training me when I started my research, Drs. Andrew Paterson and Balakrishnan Raja for providing help with smartphone-based imaging, and Drs. Katerina Kourentzi and Binh Vu for having many productive discussions with me on my research. I also want to acknowledge Drs. Bruno Travi and Jere McBride at the University of Texas Medical Branch at Galveston for their support and excellent collaboration.

ABSTRACT

The need for rapid and reliable point-of-care (POC) diagnostic testing has led to extensive research in developing new assays and associated reporter technologies. One of the most commonly used POC diagnostics is the lateral flow assay (LFA), most well-known for the home pregnancy test because of its simplicity, speed, low-cost, and portability. The reporter particles in the LFA play a crucial role in performing the diagnostic readout and dictating the test's sensitivity. Gold nanoparticles are often employed as the LFA reporters in commercial tests; however, their sensitivity is limited. Alternatively, work on luminescence-based reporter technologies has yielded improved LFA performance. These efforts have focused primarily on photoluminescent reporters, including organic fluorophores, quantum dots, lanthanide chelates, persistent luminescent phosphors, and upconversion phosphors. Chemiluminescent reporter techniques have also been investigated.

Herein, the mechanisms, advantages, and disadvantages of these different luminescent reporters and their potential benefits in LFAs are examined. Persistent luminescent phosphors were successfully applied in developing spatial and spectral multiplex assays for the simultaneous detection of model analytes: human chorionic gonadotropin (hCG) and prostate-specific antigen (PSA) with comparable limits of detection (LODs) to the commercially available single-target tests. Moreover, phosphors were applied in a nucleic acid-based LFA, combined with isothermal DNA amplification to detect cutaneous leishmaniasis. The LOD was compared with gold nanoparticles, and the phosphors were 50 - 100 times more sensitive in detecting *Leishmania* parasite DNA amplicons. Furthermore, chemiluminescence-based reporters were applied in LFAs to detect a tick-borne disease, human monocytic ehrlichiosis. An antigen detection LFA for specific tandem repeat proteins showed LODs in the range of 1 - 5 ng/mL in serum and blood. An antibody detection LFA was also developed using a tick-expressed protein with 89.5% sensitivity in initial clinical sample testing.

These LFAs were combined with smartphone-based detection to develop them as rapid, low-cost, and user-friendly POC devices. As a result, they are well-suited for POC medical diagnostics and they can also be applied in other fields such as the food and agricultural industry and environmental testing to obtain accurate and reliable results quickly rather than waiting hours or days for results from laboratory tests.

TABLE OF CONTENTS

LIST OF TABLES

LIST OF FIGURES

LIST OF ABBREVIATIONS

AFP - alpha fetoprotein

AMPPD - (3-(2′-spiroadamantane)-4-methoxy-4-(3′′-phosphoryloxy)phenyl-1,2-dioxetane disodium salt

AP - alkaline phosphatase

AUC - area under the curve

BSA- bovine serum albumin

CEA - carcinoembryonic antigen

CL - control line

CLFA - chemiluminescent lateral flow assay

CRP - C-reactive protein

cTnI - cardiac troponin I

dsDNA - double-stranded DNA

EDC - N-(3-Dimethylaminopropyl)-N′-ethylcarbodiimide hydrochloride

ELISA - enzyme-linked immunosorbent assay

ETU - energy-transfer upconversion

FA - folic acid

FITC/FAM - fluorescein

FRET - Förster resonance energy transfer

hCG - human chorionic gonadotropin

HME - human monocytic ehrlichiosis

HRP - horseradish peroxidase

HSV-2 - herpes simplex virus type 2

IL-6 - interleukin 6

kDNA - kinetoplast DNA

LFA - lateral flow assay

LOD - limit of detection

NHS - N-Hydroxysuccinimide

NT-proBNP - N-terminal fragment of B-type natriuretic peptide precursor

PBS - phosphate-buffered saline

PCR - polymerase chain reaction

PCT - procalcitonin

PEDV - porcine epidemic diarrhea virus

PLNPs - persistent luminescent nanophosphors

POC - point-of-care

PSA - prostate-specific antigen

PVP-40 - polyvinylpyrrolidone 40,000 avg. mol. wt.

QDs - quantum dots

RE - rare-earth ion

ROC - receiver operating characteristic

RPA - recombinase polymerase amplification

R-PE - R-phycoerythrin

SAO - $SrAl_2O_4:Eu^{2+},Dy^{3+}$

SBMSO - $(Sr_{0.625}Ba_{0.375})_2MgSi_2O_7:Eu^{2+},Dy^{3+}$ or $[(Sr_{0.625}Ba_{0.375})_{1.96}Eu_{0.01}Dy_{0.03}]MgSi_2O_7$

TCPO - (bis(2,4,6-trichlorophenyl) oxalate

TEM - transmission electron microscope

TEOS - tetraethyl orthosilicate

TESBA - triethoxysilylbutyraldehyde

TL - test line

TMB - 3,3′,5,5′-tetramethylbenzidine

TRP - tandem repeat protein

UCNPs - upconversion nanophosphors

UCPs - upconversion phosphors

XPS - X-ray photoelectron spectroscopy

CHAPTER 1

INTRODUCTION

Reproduced with permission from *the Journal of Applied Bio Materials*

(*Appl. Bio Mater.* 2022, 5, 1, 82–96)

DOI: 10.1021/acsabm.1c01051

Adheesha N. Danthanarayana,[1] Jakoah Brgoch,[1,*] and Richard C. Willson[2,3,*]

[1]Department of Chemistry, University of Houston, Houston, Texas 77204, USA

[2]Department of Chemical and Biomolecular Engineering, University of Houston, Houston, Texas 77204, USA

[3]Department of Biology and Biochemistry, University of Houston, Houston, Texas 77204, USA

1.1 Point-of-Care Diagnostics

Diagnostic testing plays a crucial role in all modern healthcare systems to identify the root cause of symptoms in a patient, monitor treatment efficacy, and screen for potential diseases in asymptomatic but high-risk populations. There have been significant advances in the availability of diagnostic testing methods such as polymerase chain reaction (PCR)[1] and enzyme-linked immunosorbent assay (ELISA).[2] However, these tests require sophisticated, expensive equipment, and highly trained personnel, necessitating advanced laboratory settings. Resource-limited locations tend to have inadequate facilities or support to host these systems, resulting in improper diagnosis and treatment that has been estimated to cause ~95% of the deaths due to infectious diseases in developing countries.[3, 4] For example, the shortage of medical infrastructure, including testing, results in *ca.* one million infant deaths per year in Africa due to malaria, even though it is a curable disease.[3]

Point-of-care (POC) diagnostic testing is one approach that can address many of the challenges stemming from limited diagnostic test availability. These tests have become an ever-growing research area because they are simple, rapid, and inexpensive, and administering the test requires minimal or no training.[3] They also enable healthcare providers to rapidly detect analytes near the patient, for instance, at a patient's home or bedside. This allows earlier diagnosis and faster medical decisions, leading to improved clinical and economic outcomes by implementing appropriate treatments at an earlier stage of the disease.[5, 6] Furthermore, POC testing is vital for epidemic response. The COVID-19 outbreak could readily have been tracked if immediate access to rapid detection platforms capable of identifying infections was available. POC testing will undoubtedly play a prominent role in maintaining global health in the future.

Among various POC diagnostic methods, lateral flow assays (LFAs) are among the most widely used due to their simple, rapid, affordable, and user-friendly nature. These tests are paper-based devices that can conduct an immunoassay for a target analyte in a liquid sample based on the binding between the target and antibody or other molecular recognition agent.[3, 7, 8] The sensitivity of LFAs depends significantly on the detectability of the reporter particle that reports the presence of the target analyte. Gold nanoparticles are the most commonly used reporters in LFAs because they show excellent chemical stability and size-tunable optical properties. They also are easy to functionalize. The test's output (line formation) can be easily read by the naked eye without using any external device.[7, 9] However, the sensitivity of gold-based tests tends to be limited because they are designed for colorimetric detection, which is of limited sensitivity. As a result, researchers have suggested using luminescence-based reporters to enhance the sensitivity of LFAs. Indeed, early proof-of-concept tests have shown that luminescent reporters can improve LFA sensitivity compared to conventional gold nanoparticles and other colorimetric methods.[9-13] In this chapter, the use of luminescence-based reporters in LFAs, including some of the most recent applications are discussed. Examining the variety of new approaches taken to modify this classic diagnostic test provides insight into innovative prospects to push the value of POC LFAs further.

1.2 Lateral Flow Assay

An LFA strip consists of four main components, illustrated in Figure 1.1. The sample is applied to a sample pad, usually made of cellulose and/or glass fiber, which functions to transport the sample to the conjugate-release pad in a smooth, continuous, and homogeneous manner. Conjugate-release pads store bioconjugated reporters and are made of materials such as glass fiber, cellulose, or polyester. The material used should be capable of immediately releasing the reporters upon contact with a moving liquid sample. The preparation of the reporters, the process of dispensing them onto the conjugate-release pad, and the efficiency of their release dramatically impact the assay's sensitivity. From the conjugate-release pad, the sample and reporters wick along a porous membrane (usually composed of nitrocellulose) to test and control lines of capture agents, usually antibodies. An ideal membrane should have a high affinity for proteins and other biomolecules and low non-specific adsorption in the regions of test and control lines. The wicking rate of the membrane is also significant for the sensitivity of the assay. Finally, the absorbent pad absorbs the excess liquid and helps maintain the flow rate over the membrane and prevent back-flow of the sample.[7, 8, 11]

There are two main formats of immunochromatographic lateral flow assays: the sandwich assay and the competitive assay. Each method has advantages and disadvantages depending on the analyte, the antibody, the sample matrix, and the concentration range of interest. Generally, the sandwich format has higher sensitivity than the competitive format. However, the sandwich format can give false negative results at high analyte concentrations due to the high-dose hook effect. The false negatives stem from excess analytes directly binding to the antibodies on the membrane without making a sandwich with the antibody-conjugated reporters. The competitive format is more suitable in these situations since it cannot have a high-dose hook effect.[14]

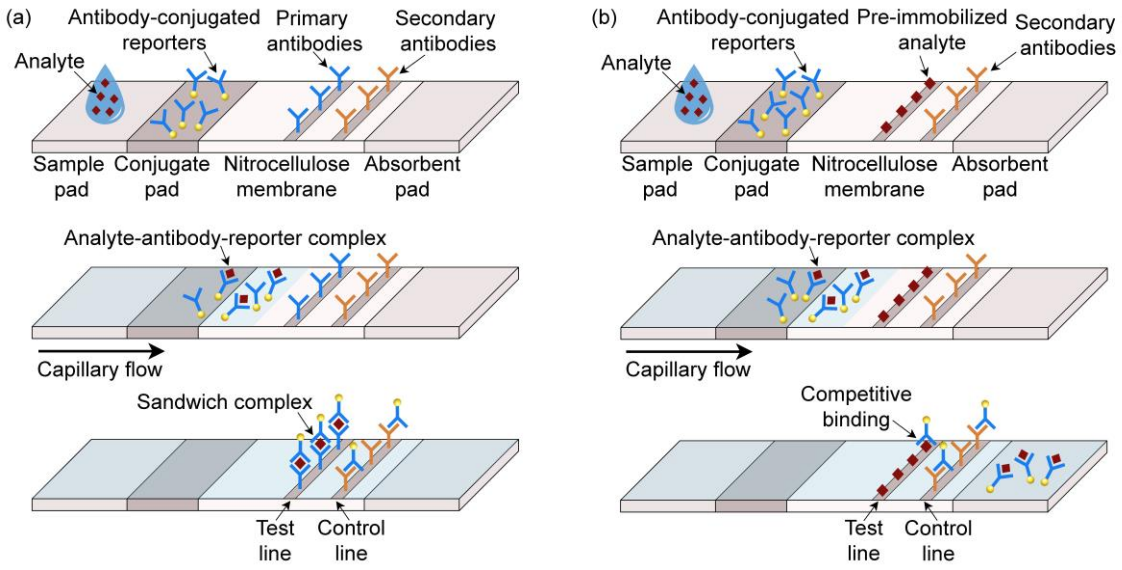

Figure 1.1. Different types of lateral flow assays. (a) In the sandwich assay, the analyte binds with the antibody-conjugated reporters on the conjugate pad. When this complex reaches the membrane, it binds with the primary antibodies on the test line forming the sandwich complex of primary antibody-antigen-antibody conjugated reporter. The excess antibody-conjugated reporters are captured at the control line. A positive test is when two lines appear, a test line and a control line. (b) In the competitive assay, the analyte in the sample first binds with antibody-conjugated reporters on the conjugate pad. When this complex reaches the membrane, it cannot bind with the pre-immobilized analyte on the test line since the antibodies conjugated to reporters are occupied with the analyte in the sample. If the test is positive, only one band appears due to the binding of excess antibody-conjugated reporters at the control line.

1.2.1 Sandwich Assay

The sandwich format (also called non-competitive or direct assay), illustrated in Figure 1.1a, is used for larger molecular weight analytes with multiple binding sites. A positive test is indicated by the appearance of the reporters at the test and control lines. In contrast, a negative test is indicated by the reporters appearing only at the control line. In the sandwich assay format, the analyte is applied to the sample pad and moves to the conjugate-release pad and binds to reporters conjugated with analyte-specific antibodies. The resulting analyte-antibody-reporter complex flows along the membrane, where another antibody specific to the analyte captures this complex at the test line. The sandwich binding of the antibodies conjugated to reporters and the capture antibodies mediated by the analyte's presence accumulates a signal from the

reporter at the test line that indicates the presence of the analyte in the sample. Secondary antibodies finally capture any excess antibody-conjugated reporters at the control line, confirming efficient flow.[7-9, 11]

1.2.2 Competitive Assay

The competitive format, illustrated in Figure 1.1b, is typically used for small molecular weight analytes with a single binding site. A positive test is represented by the absence of the reporters at the test line, and the signal intensity varies inversely with the amount of analyte present in the sample. A negative result is represented by reporters appearing at both the test and control lines. There are two styles of competitive assays. In the first, the analyte blocks the binding sites of the antibodies conjugated to reporters. Applying the sample containing the analyte to the sample pad causes it to first migrate to the conjugate-release pad and bind to analyte-specific antibodies conjugated to reporters, forming an analyte-antibody-reporter complex. On the nitrocellulose membrane, the test line contains pre-immobilized antigens (the analyte to be detected), which bind specifically to the antibodies conjugated to reporters. The control line contains pre-immobilized secondary antibodies that can bind with antibody-conjugated reporters. When the analyte-antibody-reporter complex reaches the test line, the pre-immobilized antigens cannot capture antibodies conjugated to reporters because the analyte in the sample already occupies these sites. Therefore, immobilized antigens on the test line can bind to the antibody-conjugated reporters, generating a signal at the test line only when the target analyte is absent from the sample solution. The excess antibody-conjugated reporters are captured at the control line by the secondary antibodies, confirming proper liquid flow through the strip. In the second competitive assay format, the analyte competes with an immobilized analyte analog conjugated with reporters to bind with the antibodies on the test line. The analyte-conjugated reporters are dispensed at the conjugate-release pad, while a primary antibody to the analyte is dispensed at the test line. When the sample with the analyte is applied to the sample pad, competition occurs between the analyte in the sample and the analyte conjugated with reporters to bind with the primary antibodies at the test line.[7, 8, 11]

Both assay formats have been widely used for POC diagnostic testing, but they often have limited sensitivity compared to laboratory diagnostic methods. However, the transition to luminescence-based reporter molecules and particles in place of conventional colorimetric reporters such as gold nanoparticles and colored latex beads has allowed LFAs to achieve dramatically improved limits of detection.[15-17] To establish the origin of these enhancements, it is essential first to understand the fundamental mechanisms governing the generation of light by these reporter molecules and materials.

1.3 Luminescence

Luminescence is the generic term for the spontaneous emission of light that is induced by an incident electron or photon, but it is not an effect of high temperature. Therefore, luminescence can be considered a form of cold-body radiation, which distinguishes the process of luminescence from incandescence. Luminescence can either be part of a chemical reaction, electrical energy, or a cause of subatomic motions, or stress on a crystal, among other sources. It is classified according to the mode of excitation and there are many different forms of luminescence including chemiluminescence, electroluminescence, photoluminescence, and mechanoluminescence.[18, 19] The work in this thesis focuses specifically on photoluminescence and chemiluminescence, their mechanisms, and applications in LFAs.

1.3.1 Photoluminescence: Fluorescence versus Phosphorescence

Photoluminescence is an optical phenomenon in which a material spontaneously re-emits absorbed light, generally, but not always, at a lower energy (longer wavelength). This process involves a molecule or material first absorbing a photon, causing an electron to transition to an excited state. Upon returning to the ground state, the excited electron's energy is released as a photon emission. There are two primary forms of photoluminescence: fluorescence and phosphorescence. The type of photoluminescence is assigned classically by the emission's duration or luminescence lifetime and, more recently, based on our improved understanding of the different photophysics controlling these optical processes.[18, 20]

Fluorescence is the immediate emission of light by a molecule or material following the absorption of a photon. The luminescence seemingly disappears simultaneously with the end of excitation because of the short (10^{-9} - 10^{-7} s) decay lifetime associated with fluorescence. In contrast, phosphorescence has a photon emission that persists on a significantly longer time scale. The lifetime of phosphorescence varies dramatically, ranging between 10^{-6} and 10^{0} s.[21] However, numerous examples do not comply with these definitions; for instance, there are long-lived fluorescent compounds like divalent europium salts and short-lived phosphorescence like the violet photoluminescence from zinc sulfide.[18] Quantum mechanics has provided a more thorough definition based on the different electronic transitions occurring in each process. Fluorescence arises from electronic transitions with a singlet state mechanism that involves "spin allowed" electronic transitions. Phosphorescence involves electronic transitions that change spin multiplicity, either from a singlet state to a triplet state or vice versa, resulting in "spin forbidden" electronic transitions.[18] These different processes are illustrated in Figure 1.2, using a modified Jablonski diagram.

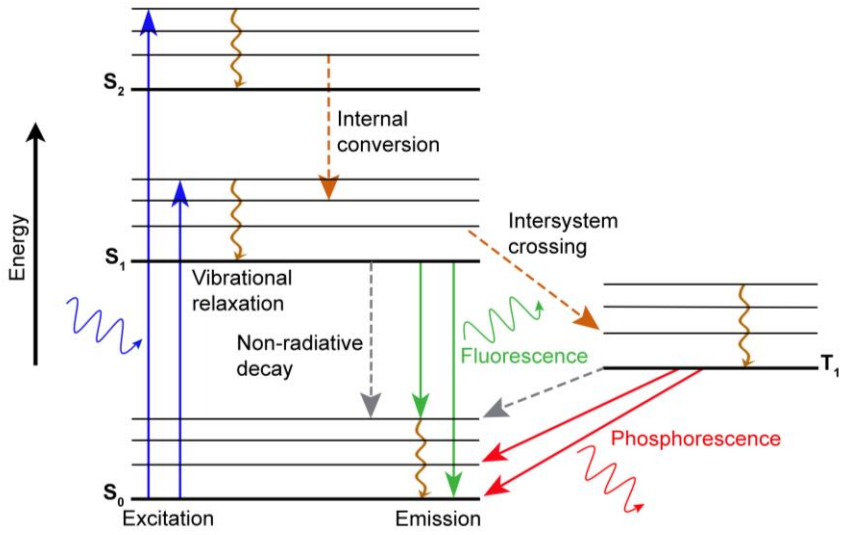

Figure 1.2. A modified Jablonski diagram illustrating fluorescence and phosphorescence. Absorption of incident photons causes an electron in the ground state (S_0) to enter an excited state (S_1, S_2, S_n,…). A portion of the initial energy is lost via non-radiative relaxation (internal conversion and vibrational relaxation) to the lowest vibrational level of the first excited state. The electron then relaxes back to the ground state (S_0) by emitting a photon resulting in "fluorescence" or further non-radiative decay. If the electron's spin in the singlet excited states (S_n) undergoes intersystem crossing generating a triplet excited state (T_n), the electron will then slowly decay back to the ground state (S_0) from the first triplet excited state (T_1). This process is called "phosphorescence".

The fluorescence process consists of three main steps. First, a photon of excitation light is absorbed by an electron of a fluorescent molecule or material in its ground electronic state (S_0). The molecule or material is then excited to a higher energy level (the excited state, S_n), which only takes femtoseconds (10^{-15} s). The excited-state electron then undergoes vibrational relaxation and internal conversion to the lowest energy level of the excited state (S_1). This process is slightly slower than the excitation process and can be measured in picoseconds (10^{-12} s). Finally, the electron can return to the ground state either by non-radiative relaxation, producing heat, or through photon emission, which is fluorescence. This emission takes a much longer time, on the order of nanoseconds (10^{-9} s). During this entire process, the spin multiplicity of the electron does not change. Further, the emitted photon has less energy and, therefore, a longer wavelength than the excitation light because of internal conversion; this phenomenon is called the "Stokes shift".[21-23]

Phosphorescent compounds, on the other hand, emit light for longer times than fluorescent materials. The detectable luminescence can typically last milliseconds to seconds after the excitation source is switched off.[20, 21] The phosphorescence excitation process is identical to that of fluorescence, but the emission pathway is different. The excited electron releases the energy through vibrational relaxation and internal conversion to the lowest energy level of the singlet excited state while maintaining the same spin. However, at this point, the electron undergoes a spin-flip and converts to a triplet excited state (T_1). This process is called "intersystem crossing". The spin selection rules forbid it as the transition occurs between two states of different spin multiplicity. Nevertheless, the interactions between magnetic dipoles generated by the spin of the electron and orbital motion of the electron couple the spin and orbital components so that the singlet and triplet characters mix. Since these states are no longer pure spin states, the electrons move from S_1 to T_1. This phenomenon is spurred by "spin-orbit coupling".[24, 25] Subsequently, electrons in the T_1 state cannot easily relax back to the ground state since the transition is again spin-forbidden. As a result, relaxation back to the ground state is a much slower process resulting in a weaker, longer lifetime emission.[21, 23, 26]

The different types of fluorescent compounds, such as fluorophores and quantum dots, have excited lifetimes on the order of nanoseconds.[20] Lanthanide chelates, some transition metal chelates like bisimidazolyl carbazolide ligand-based platinum(II) alkynyls,[27] and purely organic non-metal chelates like β-hydroxyvinylimine boron compounds[28] are examples of phosphorescent molecules; their lifetimes generally are in the range of microseconds to milliseconds.[29, 30]

1.3.2 Chemiluminescence

Chemiluminescence is the emission of light as a result of a chemical reaction. The energy produced by the chemical reaction induces an electron of a product molecule to transfer to its excited state, and subsequently when the electron decays back to its ground state, the energy is lost as a photon resulting in chemiluminescence. Chemiluminescence can reach greater sensitivities of detection compared to absorbance and fluorescence assays, since chemiluminescent assays have a lower background signal as they do not involve the initial absorption of light. Not only are their lower limits of detection, but chemiluminescent assays have other advantages such as no radioactive waste, relatively simple instrumentation requirements, and a wide dynamic range leading to their application in clinical analysis.[31, 32]

Unfortunately, chemiluminescence reactions generally produce weak luminescence due to their low quantum efficiency. The chemical interferences and non-linear behavior can also complicate the chemiluminescence systems. These factors are the main challenges for the more widespread application of chemiluminescence in analytical assays. The introduction of nanomaterials with unique optical, electronic, and catalytic properties which can be used as catalyzers and fluorescence acceptors has improved the performance of chemiluminescent assays.[32, 33]

In general, two major mechanisms are used for chemiluminescent immunoassays:[31]

(1) Label Chemical Directly Involved in the Light Emission Reaction

This technique directly detects the emission of light from the chemiluminescent reagent (label) to determine the presence of an analyte. The chemical label can transfer to its excited state through chemical reaction and upon relaxation back to the ground state, the label emits light. An example is acridinium ester and its derivatives, which after exposure to alkaline hydrogen peroxide (H_2O_2), a photon emission is generated. The mechanism of acridinium ester-mediated chemiluminescence is shown in Figure 1.3. [31, 34, 35]

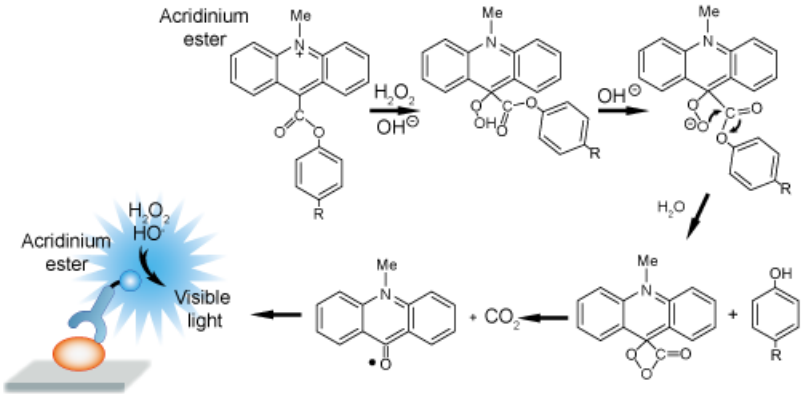

Figure 1.3. Mechanism of acridinium ester-mediated chemiluminescence (Reproduced from reference 34).

(2) Enzyme-Catalyzed Light Emission Reaction

In this technique, an enzyme is used as the label and the chemiluminescent substrate undergoes enzyme-catalyzed oxidation in the presence of a suitable oxidant, producing light.[31] The most commonly used enzymes are horseradish peroxidase (HRP) and alkaline phosphatase (AP). The mechanism of HRP enzyme-catalyzed chemiluminescence is shown in Figure 1.4a. In the presence of H_2O_2, HRP catalyzes the decomposition of luminol, which acts as the chemiluminescent substrate and produces an excited state intermediate. Upon the decay of the excited state intermediate back to the ground state, light is emitted in the form of chemiluminescence. The mechanism of AP enzyme-catalyzed chemiluminescence is shown in Figure 1.4b. A derivative of 1,2-dioxetane, (3-(2′-spiroadamantane)-4-methoxy-4-(3″-phosphoryloxy)phenyl-1,2-dioxetane disodium salt (AMPPD) acts as the substrate for AP. The phosphate

group of AMPPD undergoes enzymatic cleavage in the presence of AP, becoming destabilized. It then decomposes via an intermediate anion, AMPD, which is moderately stable, and its energy is released as light.[34, 35]

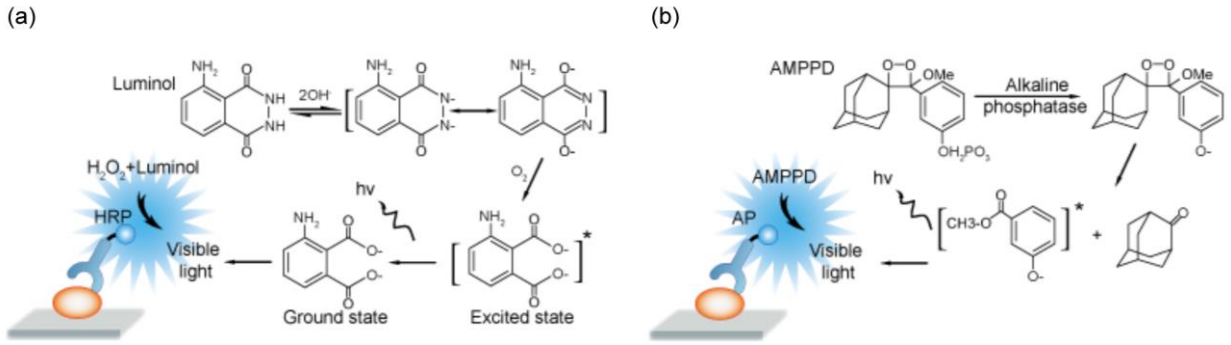

Figure 1.4. Mechanism of (a) Luminol-HRP and (b) AMPPD-AP chemiluminescence system (Reproduced from reference 34).

In addition to the mechanisms described above, there are other indirect chemiluminescence mechanisms where the energy from the chemical reagent excites another luminescent material that acts as the label. A typical example of this type of chemiluminescence is the reaction between oxalic acid diester (bis(2,4,6-trichlorophenyl) oxalate or TCPO) and H_2O_2. These compounds react to produce a highly energetic intermediate (1,2-dioxetanedione) which is unstable and decomposes, releasing CO_2 while the luminescent material absorbs the released energy activating the molecule to the excited state. As it relaxes back to the ground state, photons are released, emitting light as shown in Figure 1.5.[33, 35, 36]

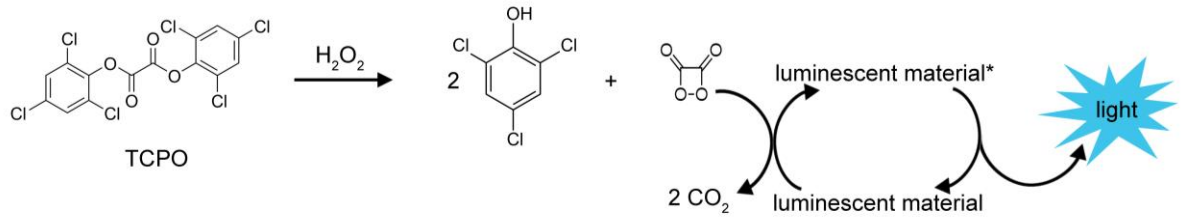

Figure 1.5. Mechanism of chemiluminescence reaction between an oxalic acid diester (TCPO) and H_2O_2.

1.4 Photoluminescent Reporters and Their Application in LFAs

1.4.1 Organic Fluorophores

Organic fluorophores are typically polyaromatic compounds that consist of a conjugated π electron system. Fluorophores used in biological applications can be divided into two main categories: intrinsic and extrinsic. Intrinsic fluorophores occur naturally, whereas extrinsic fluorophores are added to a compound that otherwise does not display any spectral properties, or to change the compound's spectral properties. The most common intrinsic fluorophores include aromatic amino acids, reduced nicotinamide adenine dinucleotide (NADH), the oxidized forms of flavins, and derivatives of pyridoxal and chlorophyll. Intrinsic fluorescence is highly sensitive to the local environment of these residues and is therefore widely used to study conformational changes and intermolecular interactions of biomolecules.[20, 21] However, most of the intrinsic fluorophores require high-energy excitation by ultraviolet light, which can be detrimental to live cells. The brightness and quantum yield of many intrinsic fluorophores are also relatively low, and they have photostability issues that limit practical applications. Therefore, biomolecules are typically modified to include ("labeled with") extrinsic fluorescent molecules with favorable optical properties such as absorption at longer wavelengths, higher quantum yields, and improved photostability.[21]

Fluorescence was first observed in nature, and then the fluorescent compounds were extracted and eventually synthesized due to their unique properties. For example, in 1845, Sir John Herschel observed the glow exhibited by a solution of quinine in sunlight. It was not until 1852 that Sir George Gabriel Stokes named the phenomenon now known as "fluorescence".[18] The first synthetic organic fluorescent molecule, Mauveine, was created by William Henry Perkin in 1856 while attempting to synthesize quinine.[37] Since then, thousands of organic fluorescent dyes have been discovered. Some of the most common include dansyl, fluorescein, and rhodamine.[20] These fluorophores often are modified to react with specific functional groups of biomolecules such as amino groups resulting in improved fluorescence at a particular

wavelength.[20, 21] This allows these compounds to be used in many biomedical fields such as spectroscopy, bioimaging, and diagnostic applications.[20, 38]

Organic Fluorophores as Reporters in LFAs:

Incorporating fluorophores in an LFA allows much higher sensitivity than conventional gold nanoparticles. A fluorescent dye, R-phycoerythrin (R-PE) was used by Lee *et al.* to develop a low-cost, high-performance POC diagnostic system for the quantitative and sensitive detection of target analytes. Fluorescence detection with R-PE and absorbance detection with colloidal gold has been directly compared using a home-built reader system with an LED light source, readily available plastic and colored glass filters and plastic lenses. The images were captured using an iPhone 4 camera. The signals were compared in sandwich LFA format using two different model analytes: biotinylated bovine serum albumin (BSA) and human chorionic gonadotropin (hCG). For the biotinylated BSA system, fluorescence provided linear data from 0.4 - 4000 ng/mL with a 1000-fold signal change, whereas colloidal gold provided a non-linear response over a range of 16 - 4000 ng/mL with a 10-fold signal change. The hCG system has shown a similar improvement in sensitivity and dynamic range in the fluorescent system compared to colloidal gold.[10]

Although organic fluorophores show higher sensitivity than colorimetric reporters, their poor photostability can result in lower sensitivity than other photoluminescent reporters. They also can suffer from chemical and metabolic degradation.[7] Researchers have made efforts to improve their photostability and chemical stability to enhance their diagnostic performance. One method is doping fluorescent dyes into nanomaterials such as silica[39] and polystyrene nanoparticles.[40, 41] For instance, Cai *et al.* synthesized Nile red dye-doped polystyrene nanoparticles for the detection of C-reactive protein (CRP), a biomarker of acute inflammatory and cardiovascular diseases. They developed a sandwich LFA, and the fluorescence intensity at the test line and control line was measured using a laboratory-prepared strip reader. The limit of detection (LOD) was 0.091 μg/mL, which is lower than many other available CRP detection methods. Moreover, the

concentration of CRP could be measured over a wide dynamic range in plasma (0.1 - 160 µg/mL) with a rapid detection time (3 min). This method also displayed improved reproducibility and stability since the coating protects the dye from the surrounding environment.[40]

Förster resonance energy transfer (FRET) based fluorescent probes also significantly enhance the sensitivity of LFAs.[41] Recently, Yang *et al.* developed a FRET-based "traffic light" lateral flow assay for the qualitative and quantitative analysis of prostate-specific antigen (PSA) in 10 min from a drop of whole blood. In this assay, in the presence of PSA, anti-PSA (detection) conjugated semiconducting polymer dots (PF-TC6FQ) and anti-PSA (capture) conjugated coumarin derivative polymer (PCA) nanoparticles form a sandwich-type complex on the test line. FRET occurs between the PCA nanoparticles and the PF-TC6FQ polymer dots, generating an emission color transition from sky blue to orange-red. Energy transfer occurs depending on the target concentration and produces signals that the naked eye can qualitatively detect under a portable 410 nm flashlight. For quantitative analysis, the fluorescence intensity of the emission was measured using the images captured by a Nikon D7500 digital camera under irradiation with 410 nm UV light, with appropriate filters. This assay showed an outstanding detection sensitivity of 0.32 ng/mL of PSA in 10% human serum, which is about 1 order of magnitude lower than conventional fluorometric immunoassay systems. This assay was also tested in real human whole blood, and the results suggest the potential of this FRET-based immunoassay for use in clinical analysis. Moreover, they have developed a multiplex assay to detect two cancer biomarkers, carcinoembryonic antigen (CEA) and PSA, simultaneously on a single strip taking advantage of the traffic light signals.[42] The limits of detection for several analytes with organic fluorophores are given in Table 1.1.

Table 1.1. Organic Fluorophore-based Lateral Flow Assays.

analyte	LFA format	limit of detection	applied range	analysis time	reference
PSA	sandwich	0.32 ng/mL	2 - 10 ng/mL	10 min	42
CRP	sandwich	0.091 mg/L	0.1 - 160 mg/L	3 min	40
CRP	sandwich	0.133 mg/L	0 - 10 mg/L	10 min	43
influenza A	sandwich	0.25 µg/mL	0 - 1.5 µg/mL	30 min	39
avian influenza H7N1	sandwich	5.34×10^2 PFU/mL	2.67×10^2 - 6.83×10^4 PFU/mL	15 min	44
procalcitonin (PCT)	sandwich	0.1 µg/L	0 - 101.36 µg/L	15 min	45
interleukin 6 (IL-6)	sandwich	7.15 pg/mL	0.2 - 5 ng/mL	N/A	46
tumor necrosis factor alpha	sandwich	10.7 pg/mL	1 - 15 ng/mL	N/A	46

1.4.2 Quantum Dots

Quantum dots (QDs) are semiconductor nanocrystals with diameters ≈ 1 - 10 nm.[47, 48] They have a core-shell structure in which the core is usually composed of elements from groups II-VI such as CdSe, CdS, or CdTe, groups III-V such as InP or InAs, or groups IV-VI such as PbSe, and the shell is usually composed of ZnS.[48] Even though typically QDs are made of binary compounds, there are other compositions such as multinary (ternary, quaternary) nanocrystals[49, 50] and perovskite quantum dots.[51] Due to their composition and dimensionality, QDs have properties falling between bulk semiconductors and discrete atoms or molecules. The resulting "quantum confinement effect" generates unique optical properties such as size-tunable absorption and emission profiles, high emission quantum yield, and narrow emission spectral band.

Unlike organic fluorophores, QDs also exhibit high photostability. All these properties make QDs ideally suitable for biosensing and bioimaging applications. The only current limitations are that QDs suffer from photoblinking and cytotoxicity.[47, 48, 52] Moreover, they are generally incompatible with polar solvents, limiting their use in biological applications without further derivatization.[53] Nevertheless, QDs are used in many biological applications such as *in-vitro* diagnostics, drug delivery, and bioimaging.[48, 52, 53]

Quantum Dots as Reporters in LFAs:

Yang *et al.* compared quantum dots and colloidal gold as reporters in an LFA test for syphilis. According to their results, the naked-eye LOD of colloidal gold-based lateral flow test strips could only reach 20 ng/mL of polyclonal anti-TP47 syphilis antibody solution. In contrast, the naked-eye detection (under a portable UV lamp) of the fluorescent signal of CdTe QD-based test strips can reliably achieve a LOD of 2 ng/mL of polyclonal anti-TP47 syphilis antibody solution. This 10-fold improvement is impressive, considering the only change is using a different reporter. Moreover, the clinical sensitivity of colloidal gold was 82%, whereas that of the QD-based test was 100%.[54] In 2019, Wang *et al.* reported a Cu:Zn−In−S/ZnS QD-based sandwich LFA for detecting the tetanus antibody. This assay can be completed in 30 min, and the fluorescence intensity was recorded using a commercial fluorescent reader (ESEQuant LFR). The results showed a LOD of 0.001 IU/mL in buffer, ten times lower than gold nanoparticle-based tetanus LFA tests. This system was also successfully applied for the detection of the tetanus antibody in human serum.[55]

Different core-shell structures have been introduced to further improve the sensitivity of QDs by suppressing exciton leakage and thereby obtaining a high quantum yield. For example, Shen *et al.* successfully deposited a CdS/$Cd_xZn_{1-x}S$/ZnS multishell on a ZnSe/CdSe core, increasing fluorescence quantum yields from 28% to 75% along with improving stability in various physiological conditions. These QDs were applied to detect human hepatitis B surface antigen. The fluorescence signal was observed by a fluorescence detector with a 370 nm LED lamp as the light source. The results showed a sensitivity as high

as 0.05 ng/mL.[56] Furthermore, polymer encapsulation has been proposed to prepare poly QDs with stronger photoluminescence intensity and better optical properties than single QDs.[41, 57, 58] Hu *et al.* developed fluorescent nanosphere reporters to detect CRP in LFA, where each poly(styrene/acrylamide) copolymer nanosphere contains 332 ± 8 CdSe/ZnS QDs. This assay can be completed in 20 min, and the fluorescence intensity was measured using the images acquired with an EMCCD single-photon detector mounted on an inverted fluorescence microscope. The resulting luminescence signal was 380-fold stronger than a single QD. This allowed QD fluorescent nanospheres to achieve a LOD of 27.8 pM of CRP in buffer, which is 257-fold more sensitive than gold nanoparticle-based CRP detection LFAs. This assay showed a LOD of 34.8 pM in serum and it was also applied to quantitatively detect CRP in peripheral blood plasma samples from cancer patients.[57] The limits of detection for several analytes with quantum dots are given in Table 1.2.

Table 1.2. Quantum Dot-based Lateral Flow Assays.

analyte	LFA format	limit of detection	applied range	analysis time	reference
hCG	sandwich	0.016 IU/L	0 - 1000 IU/L	20 min	58
hCG	sandwich	0.5 IU/L	0 - 50 IU/L	10 min	59
PSA	sandwich	0.33 ng/mL	0 - 128 ng/mL	15 min	60
PSA	sandwich	1.0754 ng/mL	0 - 100 ng/mL	10 min	61
hepatitis B virus surface antigen	sandwich	75 pg/mL	75 pg/mL - 75 ng/mL	15 min	62
hepatitis B virus surface antigen	sandwich	0.05 ng/mL	0 - 5 ng/mL	20 min	56
syphilis	sandwich	2 ng/mL	0.2 ng/mL - 2 µg/mL	10 min	54

Table 1.2 (continued).

tetanus	sandwich	0.001 IU/mL	0.005 - 0.1 IU/mL	30 min	55
CRP	sandwich	27.8 pM	0.178 - 11.4 nM	20 min	57
CRP	sandwich	0.3 ng/mL	0.5 ng/mL - 1 µg/mL	3 min	63
alpha fetoprotein (AFP)	sandwich	1 ng/mL	0 - 100 ng/mL	10 min	64
AFP	sandwich	3 ng/mL	0 - 150 ng/mL	15 min	65
CEA	sandwich	2 ng/mL	0 - 150 ng/mL	15 min	65
IL-6	sandwich	1.995 pg/mL	10 - 4000 pg/mL	18 min	66
human foreskin fibroblast exosomes	sandwich	117.94 exosome/µL	100 - 1000 exosomes/µL	10 min	67
nitrated ceruloplasmin	sandwich	1 ng/mL	1 ng/mL - 10 µg/mL	10 min	68
influenza A virus subtypes H5 and H9	sandwich	subtype H5: 0.016 HAU subtype H9: 0.25 HAU	1/128 - 128 HAU	15 min	69
zika virus non-structural protein 1	sandwich	0.045 ng/mL	0.01- 1000 ng/mL	20 min	70

1.4.3 Lanthanide Chelates

A lanthanide chelate consists of a rare-earth lanthanide ion complexed with one or more organic chelating ligands. The lanthanide ion binds with the ligands *via* electron transfer through *f*-orbitals, with highly electronegative donor atoms such as N and O. Some of the most commonly used lanthanide ions are Sm(III), Eu(III), Tb(III), and Dy(III) which show significantly different emission wavelengths.[30, 71] The lanthanide ions themselves show very weak absorption and emission profiles as the transitions of interest are generally forbidden (by the Spin and Laporte rule).[30] However, chelating with appropriate ligands enhances the luminescence *via* the "antenna effect" where energy is efficiently absorbed by the chelating ligands and transferred to the coordinated lanthanide ion.[47, 71] In lanthanide chelates, luminescence generally originates from 4f-4f transitions, and it offers unique optical properties. Due to 5s and 5p shielding effects, the 4f orbitals do not directly participate in chemical bonding with the surrounding environment. Therefore, the emission is minimally perturbed by the surrounding matrix and ligand field. The emission is strongly affected only by the first coordination sphere and is mainly specific to the metal ion. This results in a narrow emission spectrum, which can be tuned by varying the lanthanide ion. The forbidden nature of these transitions causes lanthanide chelates to exhibit long decay times (spanning microseconds to milliseconds) and large Stokes shifts. These properties make them exciting alternatives to typical fluorescent reporters. The extended emission lifetime of lanthanide chelates allows time-resolved luminescent measurements to minimize background interference from excitation light and autofluorescence from biological media. It enhances the signal-to-noise ratio and reduces the cost of the reader by eliminating advanced optical components.[25, 47, 71] The main drawback of most lanthanide chelates is their luminescence emission typically is susceptible to quenching by coordinated water molecules in aqueous systems. The lanthanide complexes also tend to undergo dissociation in some assay conditions.[71] Moreover, although lanthanide chelates are more photostable than fluorophores, they tend to have photostability issues when excited with continuous exposure under an intense excitation source. Therefore, the time delay needs to be carefully defined; otherwise, the sensitivity can be significantly reduced when involved in time-resolved measurements.[72]

The long luminescence lifetime of lanthanide chelates is generated through a distinct mechanism of luminescence (shown in Figure 1.6a) compared to typical fluorescence or phosphorescence mechanisms described in section 1.3.1. When a strongly absorbing chelating ligand (antenna) is bound to the lanthanide ion, it harvests energy to the ligand's singlet excited state, followed by intersystem crossing to the longer-lived triplet excited state of the ligand. The antenna then transfers energy to the excited state ^5D_J of the lanthanide ion. The transition of electrons from the excited ^5D_J to ^7F_J state results in luminescence emission. These electronic transitions typically result in a series of bands in the visible and near-IR region. Figure 1.6b shows the luminescence emission spectrum for an Eu(III) complex and its $^5D_0$ to ^7F_J transitions (where J = 0 to 5), which give six distinct bands. The change in spin multiplicity during the transition (from 5 to 7) in Eu(III) results in a forbidden transition with a long luminescence lifetime.[29, 30, 71]

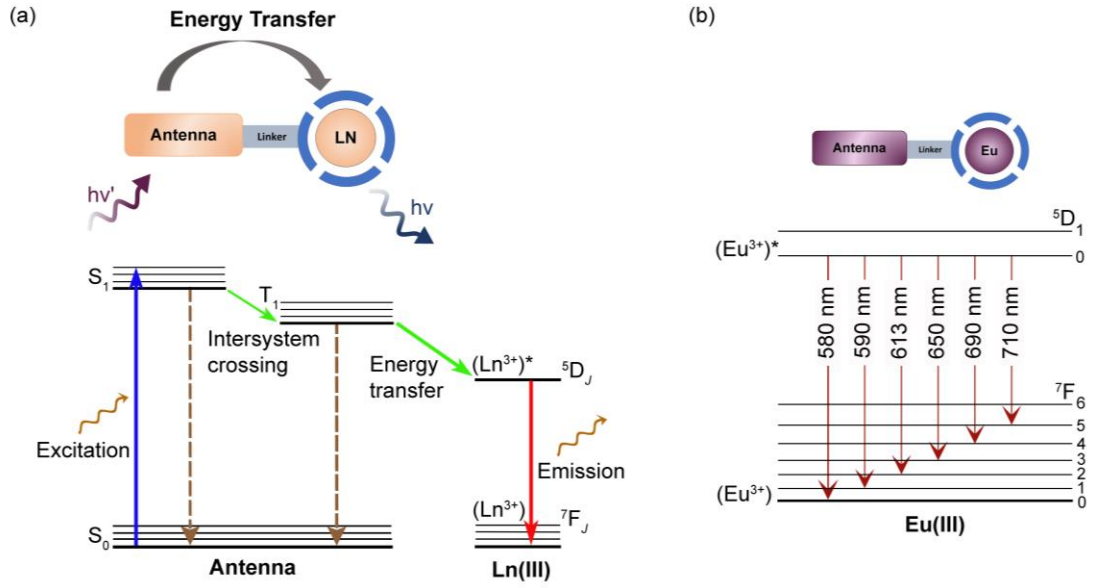

Figure 1.6. The luminescence mechanism of lanthanide chelates. First, the strongly absorbing ligand (antenna) harvests the energy to the singlet excited state (S_1), and the excited electron then travels to the triplet excited state (T_1) *via* intersystem crossing. The antenna then transfers energy to the excited state of the lanthanide ion, and finally, the electron decays back to the ground state, resulting in phosphorescence. (b) The Eu(III) complex's luminescence emission spectrum gives six distinct bands from its $^5D_0$ to ^7F_J transitions (where J = 0 - 5) (Adapted from reference 30 Copyright 2013 American Chemical Society).

Lanthanide Chelates as Reporters in LFAs:

Eu(III) is one of the most used lanthanide labels, and Eu(III) chelates have been doped into microparticles/ nanoparticles *via* covalent interactions to enhance the signal intensity.[41] Liang *et al.* used Eu(III) chelate microparticles to develop a direct competitive LFA to quantitatively detect antibodies to hepatitis B core antigen (anti-HBc). The fluorescence intensities of the lines were measured using an aQcare TRF reader, and the results showed a LOD of 0.31 IU/mL in buffer and a wide linear range from 0.63 to 640 IU/mL. This assay was also tested in human serum and compared to results from commercially available anti-HBc kits. The results showed a good agreement and comparable sensitivity and specificity, suggesting that this assay can be effectively applied for the quantitative determination of anti-HBc in human serum. Moreover, compared to the commercially available anti-HBc kits, this method shows advantages in the maximum measurable concentration of anti-HBc whereby only a 1/100 to 1/10,000 (100-fold increase) dilution is required when the anti-HBc level is >640 IU/mL. This means that in detecting high anti-HBc concentration samples, dilution and detection times using this method were less than other methods. This method has a fast turnaround time (15 min for a complete analysis) compared to other quantitative anti-HBc methods.[73] Recently, Liu *et al.* reported an Eu(III) chelate microparticle-based sandwich LFA to detect porcine epidemic diarrhea virus (PEDV), the predominant cause of severe enteropathogenic diarrhea in swine. The fluorescence intensities of the lines were measured using a quantitative fluorescence immunoassay reader, and the LOD of the assay was 10 $TCID_{50}$/mL of PEDV, making it better than reverse transcription-PCR and a commercial immunochromatographic assay kit (100 $TCID_{50}$/mL). Furthermore, the analysis using field samples containing various PEDV strains and other viruses showed 97.8% sensitivity and 100% specificity.[74]

Juntunen *et al.* carried out a comparative study of the performance of Eu(III) chelate-doped polystyrene nanoparticles and colloidal gold particles in lateral flow assays. They compared colloidal gold and Eu(III) nanoparticles using both PSA and biotinylated-BSA as antigens. The reflectance measurement of colloidal

gold was done with a USB flatbed scanner. A Victor X4 multilabel reader was used to measure the time-resolved fluorescence of Eu(III) nanoparticles. A Canon Powershot SX130 IS digital camera was used with an optical bandpass filter and hand-held UV lamp (as the excitation source) for the conventional fluorescence detection without a time delay between excitation and measurement. The analytical sensitivities with each detection method were compared. The time-resolved fluorescence measurement and the conventional fluorescence photography measurement did not significantly differ in this assay. However, when compared to reflectometric measurements of colloidal gold, the fluorescence measurements of the PSA assay showed 7-fold higher sensitivity, and the biotinylated-BSA assay showed 300-fold higher sensitivity.[75] The limits of detection for several analytes with lanthanide chelates are given in Table 1.3.

Table 1.3. Lanthanide Chelate-based Lateral Flow Assays.

analyte	LFA format	limit of detection	applied range	analysis time	reference
PSA	sandwich	0.07 ng/mL	5 pg/mL - 0.1 µg/mL	1 - 1.5 hrs	75
PSA	sandwich	0.01 ng/mL	0.01 - 5 ng/mL	21 min	76
PSA	sandwich	193 ng/L	1 - 100,000 ng/L	N/A	77
cardiac troponin I (cTnI)	sandwich	2039 ng/L	1 - 100,000 ng/L	N/A	77
cTnI	competitive	97 pg/mL	0 - 1.16 ng/mL	N/A	78
CRP	sandwich	0.2 ng/mL	0.2 - 100 ng/mL	30 min	79
hepatitis B virus core antigen	competitive	0.31 IU/mL	0.63 - 640 IU/mL	15 min	73
hepatitis B virus surface antigen	sandwich	0.03 µg/L	0.05 - 3.13 µg/L	30 min	80

Table 1.3 (continued).

AFP	sandwich	0.1 IU/mL	1 - 1000 IU/mL	15 min	81
PCT	sandwich	0.08 ng/mL	0 - 40 ng/mL	15 min	82
SARS-CoV-2	sandwich	1000 TU/mL	10^3 - 10^7 TU/mL	< 1 hr	83
eosinophil protein X	sandwich	0.082 µg/L	0.13 - 200 µg/L	N/A	84
human neutrophil lipocalin	sandwich	0.05 µg/L	0.13 - 200 µg/L	N/A	84

1.4.4 Persistent Luminescent Phosphors

The term "phosphor" generally refers to any solid luminescent material that emits light after exposure to high-energy radiation (typically UV or visible light). It was derived from the Greek word "fosforos", meaning light bearer. It was first identified in the early 17th century with the discovery of the Bologna stone, which emitted red light in the dark after exposure to sunlight. Since then, this term has remained virtually unchanged and is used to describe both fluorescent and phosphorescent materials.[85-87]

Persistent luminescent phosphors are a unique subclass of materials with properties very closely resembling phosphorescent materials but photophysics related to fluorescent materials. As a result, in the literature, these two terms are sometimes used interchangeably. Like phosphorescent materials, persistent luminescent phosphors have very long lifetimes, emitting light for several minutes to hours after the excitation light ceases. However, while the long lifetime of phosphorescence arises from forbidden electronic transitions within the luminescent center, transitions in persistent luminescence are not necessarily forbidden, and the excitation energy is stored in trap centers that differ from the luminescent center.[88] The crystalline host material is typically an insulator with a wide band gap that incorporates with two types of active centers;

emission centers and trap centers. The emission center is generally a rare-earth (lanthanide) ion (e.g., Eu^{2+}, Ce^{3+} with 5d to 4f or 4f to 4f transitions) or a transition metal ion (e.g., Cr^{3+}, Mn^{2+} with 3d to 3d transitions). Trap centers can be lattice defects (e.g., oxygen vacancies, antisite defects), impurities, or intentionally introduced codopants (e.g., Dy^{3+} in $SrAl_2O_4:Eu^{2+}$).[86] Since emission after excitation involves trapping and detrapping of charge carriers (electrons/holes), the lifetimes of persistent luminescent phosphors are several orders of magnitude longer than the spin-forbidden transitions of phosphorescent materials.[89, 90] Therefore, they are widely used in "glow-in-the-dark" applications such as safety signs, emergency displays, and luminescent paints. More recently, they have been used as optical reporters in biological applications as their long emission lifetime makes them ideal for use in time-resolved measurements to avoid background interferences.[90, 91]

Persistent luminescence is a special case of thermally stimulated luminescence at room temperature.[88, 92] Different mechanisms have been proposed to explain the persistent luminescence, and the actual mechanism is still under debate; however, there is a general agreement on the involvement of charge carrier trapping and detrapping.[88, 93]

The first model of persistent luminescence (Figure 1.7a) was introduced by Matsuzawa *et al.*[89] in 1996 upon discovering $SrAl_2O_4:Eu^{2+},Dy^{3+}$. In this model, holes are assumed to be the primary charge carriers. When a Eu^{2+} ion is excited by a photon, a hole escapes to the valence band, generating a Eu^{+} ion. The hole is then trapped by a trivalent rare-earth ion such as Dy^{3+}, creating a Dy^{4+} ion. Thermal energy (kT) is then required to stimulate the slow release of the trapped hole back to the valence band. The hole then recombines with the Eu^{+} ion and recreates the ground state Eu^{2+}, causing the emission of a photon. The suggested oxidation of Dy^{3+} to Dy^{4+} was accepted because tetravalent Dy^{4+} and Nd^{4+} are known to exist in some phosphors like $Cs_3DyF_7:Dy^{4+}$ or $Cs_3NdF_7:Nd^{4+}$.[89] However, this model does not explain the persistent luminescence of non-codoped $SrAl_2O_4:Eu^{2+}$. It is also not plausible to generate monovalent Eu^{+} and tetravalent Dy^{4+} ions in

the material with low-energy photons. Therefore, other models have been proposed to describe persistent luminescence, with the Dorenbos model becoming the most popular.[94, 95]

In the Dorenbos model (Figure 1.7b), the photoexcitation of Eu^{2+} ion causes an electron to move into 5d-orbitals. Since 5d-orbitals are close to the conduction band, with the continuous excitation, the electron can jump into the conduction band, where it is subsequently captured by a trivalent rare-earth codopant ion. Thus, Eu^{2+} would become oxidized, and the rare-earth codopant would become reduced. The trapped electron is then released by the thermal energy (kT) and recombines with the luminescent center. This model does not require the existence of Eu^{+} and RE^{4+} (RE = rare-earth ion). However, similar to the Matsuzawa model, it cannot explain persistent luminescence in the absence of a RE codopant.[94, 95]

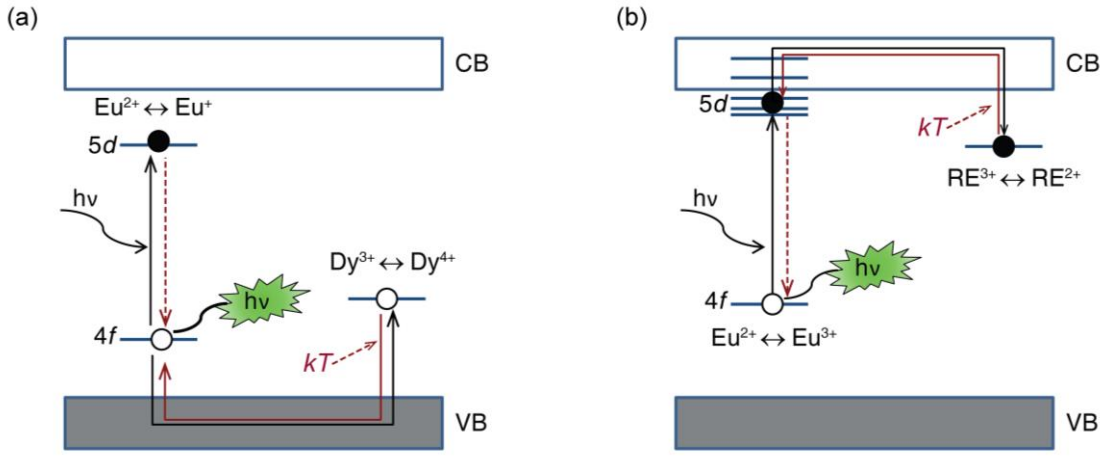

Figure 1.7. Proposed persistent luminescence mechanism of $SrAl_2O_4:Eu^{2+},Dy^{3+}$: (a) the Matsuzawa model and (b) the Dorenbos model. The excitation and trapping are black lines, and thermal release and relaxation are red lines. An electron is a filled black circle, whereas a hole is an open circle (Reproduced with permission from reference 95).

Persistent luminescent phosphors with transition metal ions as the activation center have a different mechanism since the excitation and emission occur entirely within 3d-orbitals. One of the mechanisms for these materials has been suggested based on the $ZnGa_2O_4:Cr^{3+}$ system (Figure 1.8). It is generally agreed that persistent luminescence arises from lattice defects, and although $ZnGa_2O_4:Cr^{3+}$ is a simple AB_2O_4

compound with a spinel structure, it exhibits antisite defects where Zn and Ga exchange. When the compound absorbs UV/visible light, an electron-hole pair in the ground state ($^4A_2$) is excited to a $^4T_1(^4F)$ excited state. The pair is then trapped by a neighboring antisite defect that acts as the trap state. Thermal energy (*kT*) causes the electron-hole pair to be released to the lower-energy excited state, ^2E, and then it decays back to the ground state resulting in the emission of a photon in the form of near-IR light. However, the effects of adding codopants into these materials still need to be investigated. Moreover, studies of the local structure of some spinel-type structures reveal that an increase in lattice defects quenches persistent luminescence in Cr^{3+} substituted phosphors, which contradicts the findings in Eu^{2+} substituted materials. Therefore, further investigations are required to understand persistent luminescent phosphors with transition metal ions.[95, 96]

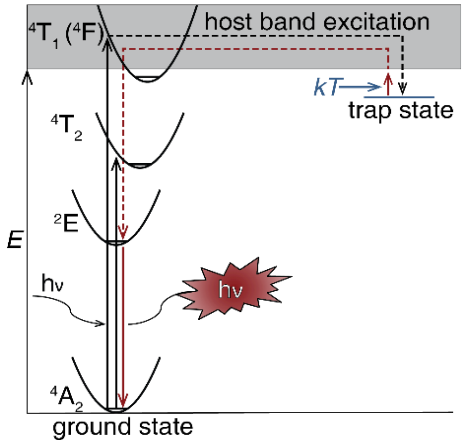

Figure 1.8. Proposed general model of the persistent luminescence mechanism of $ZnGa_2O_4:Cr^{3+}$. The excitation and trapping are black arrows, and relaxation and detrapping are red arrows (Reproduced with permission from reference 95).

Persistent Luminescent Phosphors as Reporters in LFAs:

Persistent luminescent phosphors were first used as LFA reporters by Paterson *et al.*, who applied commercially-purchased $SrAl_2O_4:Eu^{2+},Dy^{3+}$ as the reporter. Most phosphors are produced as bulk powder with large particle size (>8 μm). Paterson *et al.* ball-milled and size-fractionated by differential centrifugal sedimentation to produce smaller (~250 nm) nanoparticles suitable for reasonable flow through the strip

membrane. Moreover, $SrAl_2O_4:Eu^{2+},Dy^{3+}$ readily hydrolyzes in water and loses its luminescent properties. Therefore, after size fractionation, the nanoparticles were silica-encapsulated using a modified Stöber process to make them water stable. The silica-encapsulated nanoparticles were then conjugated to NeutrAvidin and used to detect the model analyte biotinylated lysozyme in buffer using monoclonal anti-lysozyme antibodies at the test line. The LOD was below 100 pg/mL, approximately an order of magnitude more sensitive than colloidal gold.[91] Later, this system was coupled with a time-gated smartphone-based imaging system as an efficient and sensitive POC device. A 3D-printed attachment costing ≈USD 5 was used as the imaging compartment to position the LFA strip in front of the smartphone camera and block out the background light for sensitive luminescence imaging. The attachment used minimal optical hardware, containing a lens, a bundle of inexpensive plastic optical fibers, and no electronic components. An in-house-built smartphone application was used to operate the smartphone flash as the excitation source and camera to capture the images of the luminescence signal. This imaging format was used to detect hCG with a LOD of 45 pg/mL in buffer, comparable with the commercially available lateral flow hCG tests.[97] Moreover, persistent luminescent $SrAl_2O_4:Eu^{2+},Dy^{3+}$ nanoparticles were applied to develop a smartphone-based serological LFA to detect herpes simplex virus type 2 (HSV-2) in human plasma/serum with initial 96.7% sensitivity and 100% specificity. Compared to the other available rapid HSV-2 assays, this assay showed the highest sensitivity reported at the time. This technology is particularly beneficial for private self-testing of sexually transmitted diseases as individuals often spread the condition due to unawareness of their infection, in part because of the social stigma associated with in-clinic testing for sexually transmitted infections.[98] The limits of detection for several analytes with persistent luminescent phosphors are given in Table 1.4.

The main drawback of persistent luminescent phosphors is their need to undergo a series of size-reduction steps to obtain nanoparticles since they are synthesized as bulk powder, which is time and labor-intensive. Moreover, only a few highly efficient persistent luminescent nanophosphors are suitable as optical reporters

in lateral flow assays, and therefore, their use in multiplex assays is limited. Persistent luminescent nanophosphors with different optical properties can be synthesized by band gap engineering strategies, including adding codopant ions, altering their ratios, and preparing a solid solution series of phosphors. Kim *et al.* recently reported a novel method of improving the luminescence intensity and lifetime of phosphors based on the energy transfer effect by chemical mixing of different phosphors with distinct optical properties. The energy transfer efficiency depends on the extent of spectral overlap between the donor emission and acceptor absorption spectra. Therefore, a higher luminescence efficiency is expected from the spectrally close donor phosphors. For example, the luminescence efficiency of the green-emitting phosphor can be improved by transferring the energy from the blue-emitting calcium aluminate phosphor to the green-emitting alkaline-earth aluminate phosphor ($SrAl_2O_4:Eu^{2+},Dy^{3+}$). Similarly, the luminescence efficiency of the blue-emitting phosphor can be improved by the energy transfer from a violet-emitting to the blue-emitting phosphor.[99]

Table 1.4. Persistent Luminescent Phosphor-based Lateral Flow Assays.

analyte	LFA format	limit of detection	applied range	analysis time	reference
hCG	sandwich	45 pg/mL	0.02 - 4.55 ng/mL	N/A	97
PSA	sandwich	0.1 ng/mL	0.02 - 10 ng/mL	20 min	9

1.4.5 Upconversion Phosphors

The subgroup of phosphors called upconversion phosphors (UCPs) is unique in absorbing low-energy photons and emitting higher-energy photons. UCPs are particles composed of an inorganic host lattice doped with rare-earth ions (e.g., Yb^{3+}, Er^{3+}, and Tm^{3+}) or transition metal ions.[100, 101] They have the unique ability to absorb infrared radiation and emit at visible wavelengths by a sequential process of multiphoton absorption, accumulation *via* equally spaced long-lived excited states of lanthanide dopants, and subsequent

emission. The anti-Stokes emission of UCPs enables background-free detection since it can be efficiently spectrally resolved from the Stokes shifted autofluorescence, eliminating the need for time-resolved measurements. Moreover, UCPs show narrow emission spectra and no photobleaching at their excitation wavelengths, enabling long observation times and multiplexed detection.[101-103] These characteristics make UCPs an ideal luminescent label for *in-vivo* biomedical applications such as bioimaging and therapeutics.[100, 104] Three basic mechanisms have been proposed to explain the lanthanide upconversion processes: excited-state absorption, energy-transfer upconversion, and photon avalanche. Among them, excited-state absorption and energy-transfer upconversion are the most common mechanisms in nanoscale lanthanide materials.[100, 104]

Excited-state absorption (Figure 1.9a), mainly observed in singly-doped upconversion materials, involves a sequential multistep absorption process. Under suitable excitation, an electron absorbs a photon and travels from ground state E_0 to the excited metastable state E_1, then absorbs another photon while at the excited state E_1 and jumps to the higher excited state E_2. When the electron returns to the ground state E_0 from the higher excited state E_2, upconversion emission occurs.[100, 104] A low active ion concentration in the doped particles favors this process as it reduces transfer losses through cross-relaxation between the luminescent centers and increases the gain in the excited-state absorption process.[104]

Energy-transfer upconversion (ETU) is considered the most efficient upconversion process in lanthanide-doped upconversion materials. Different types of ETU mechanisms have been reported, and among them, resonant non-radiative transfer and phonon-assisted non-radiative transfer are essential to describe the ETU process in two ion-involved systems (Figure 1.9b). In the resonant non-radiative energy transfer mechanism, a sensitizer ion (S) at its excited state transfers energy to the activator ion (A), exciting A from its ground state before S emits a photon. This can occur only when the energy differences between the ground state and the excited state are nearly equal for both sensitizer and activator ions, and the distance

between the two ions is small enough. If the energy differences between the ground state and the excited state of the S and A ions are different, phonon assistance is necessary to compensate for the energy mismatch. Therefore, energy transfer occurs *via* a phonon-assisted non-radiative process. The concentration of lanthanide ions should be sufficiently high to induce the energy-transfer process *via* ion-ion interactions. An advantage of energy-transfer upconversion, compared to excited-state absorption, is that only one pump source is needed and is independent of the pump power. [100, 104, 105]

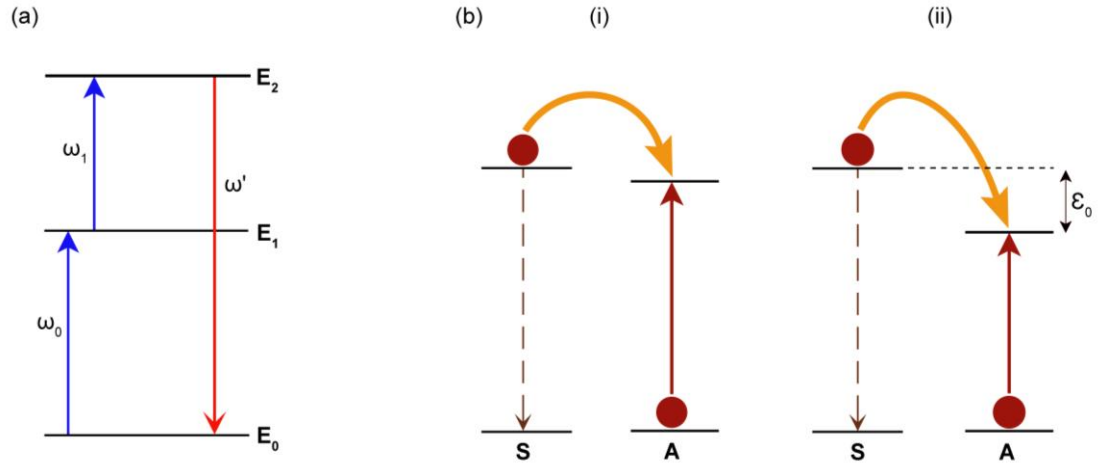

Figure 1.9. Schematic diagrams of upconversion mechanisms. (a) Excited-state absorption ($\omega' > \omega_1, \omega_0$): E_0, E_1, and E_2 represent the ground state, intermediate state, and excited state, respectively. (b) Energy transfer processes between two ions: (i) resonant non-radiative transfer, (ii) phonon-assisted non-radiative transfer (S = sensitizer ions, A = activator ions, ε_0 = energy mismatch).

Upconversion Phosphors as Reporters in LFAs:

Upconversion nanophosphors (UCNPs) have also been used to make LFAs with high sensitivity and specificity. The limits of detection for several analytes with upconversion phosphors are given in Table 1.5. Yang *et al.* used $NaYF_4$:Yb^{3+},Er^{3+} UCNPs to develop a sandwich LFA for the quantitative detection of N-terminal fragment of B-type natriuretic peptide precursor (NT-proBNP), a biomarker used to diagnose acute heart failure, in plasma samples. The UCNPs were excited using infrared light (980 nm), and their visible light emission (541.5 nm) was measured using a strip reader of upconverting phosphor technology-based

biosensor. The assay can be completed in less than 20 min. The limit of detection was 116 ng/L, which is lower than the clinical diagnosis cutoff (150 ng/L), and the linear range was 50 - 35,000 ng/L.[106]

Although UCNPs show many advantages over other luminescent reporters, their luminescence efficiency is limited by low absorption efficiency, non-negligible surface defects, and concentration quenching. Therefore, various strategies, including attaching organic dye molecules as antennas,[107] suppression of surface-related concentration quenching,[108, 109] and confining energy migration[110] have been proposed to enhance the upconversion luminescence.[111] These approaches could be used to further improve the sensitivity of UCNP-based LFAs. He *et al.* developed highly doped UCNPs to increase the concentration of emitters within small nanocrystals to improve sensitivity. They used highly Er^{3+} doped and Tm^{3+} doped $NaYF_4$:Yb^{3+},Er^{3+}/Tm^{3+} UCNPs for the ultrasensitive quantitative detection of low abundance biomarkers for early-stage cancer detection. The UCNPs were excited using a 980 nm laser diode, and the emission signal was detected using a smartphone camera as the readout element. The highly doped UCNPs were used as two independent reporters on two-color LFA for the quantitative multiplex detection of PSA and ephrin type-A receptor 2 with limits of detection of 89 and 400 pg/mL, respectively.[112]

Table 1.5. Upconversion Phosphor-based Lateral Flow Assays.

analyte	LFA format	limit of detection	applied range	analysis time	reference
hCG	sandwich	100 pg/mL	0 - 10 ng/mL	30 min	101
cTnI	sandwich	30 ng/L	30 - 10,000 ng/L	45 min	113
cTnI	sandwich	41 ng/L	1 - 100,000 ng/L	N/A	77
PSA	sandwich	556 ng/L	1 - 100,000 ng/L	N/A	77
PSA	sandwich	89 pg/mL	0.01 - 100 ng/mL	30 min	112

Table 1.5 (continued).

ephrin type-A receptor 2	sandwich	400 pg/mL	0.01 - 100 ng/mL	30 min	112
NT-proBNP	sandwich	116 ng/L	50 - 35,000 ng/L	20 min	106
hepatitis B virus surface antigen	sandwich	0.1 IU/mL	0.01 - 12.8 IU/mL	30 min	114
hepatitis B virus surface antibody	sandwich	20 mIU/mL	20 - 900 mIU/ mL	10 min	115
interleukin 10	sandwich	30 pg/mL	0 - 3000 pg/mL	40 min	116
Francisella tularensis	sandwich	10^4 CFU/mL	10^3 - 10^9 CFU/mL	15 min	117
Schistosoma circulating anodic antigen	sandwich	0.5 pg/mL	0.5 - 500 pg/mL	1.5 - 2 hrs	118
brain natriuretic peptide	sandwich	5 pg/mL	0 - 100 pg/mL	20 min	119
suppression of tumorigenicity 2	sandwich	1 ng/mL	0 - 25 ng/mL	20 min	119

1.5 Application of Chemiluminescent Reporters in LFAs

Chemiluminescence is useful in the POC diagnostic field because, compared to other optical methods, chemiluminescence has a high signal-to-noise ratio, resulting in increased sensitivity. Moreover, the readout instruments of the chemiluminescent signal are more straightforward than other optical readout systems. Therefore, researchers have paid attention to incorporating chemiluminescence into LFAs to develop

simple, rapid, and sensitive POC assays.[120] The limits of detection for several analytes with chemiluminescent reporters are given in Table 1.6.

Although there are different chemiluminescent methods, the luminol-HRP detection system is the widely used method in chemiluminescent lateral flow assays (CLFAs). Wang *et al.* developed a CLFA to detect synthetic nucleic acid sequences representative of *Trypanosoma* mRNA, the causative agent for African sleeping sickness, which is endemic in sub-Saharan African countries. They used HRP conjugated nucleic acid probes as the reporter system, which catalyzes luminol to produce a signal at the test line and control line in the presence of H_2O_2. The intensity of the chemiluminescent signal was evaluated using a CCD camera and as well as a microtiter plate reader. This on-membrane enzymatic signal amplification was able to reach sub-femtomolar level limit of detection, meaning 0.5 fmols of the nucleic acid target could be detected without the need for target amplification and costly equipment.[121] Moreover, CLFAs have been developed using luminol-HRP detection system for the detection of cardiac troponin I with a LOD of 5.6 pg/mL[12] and cortisol with a LOD of 0.342 µg/dL[122] in human serum.

This reported CLFA also has improved sensitivity over gold nanoparticles. Indeed, a CLFA developed by Han *et al.* showed 110-fold improvement of the analytical sensitivity compared to gold nanoparticle-based colorimetric LFA in detecting cardiac troponin I in human serum.[12] Kim *et al.* developed highly sensitive CLFA using HRP conjugated antibodies, and luminol as the substrate for the detection of myoglobin. The intensity of the chemiluminescent signal was measured using a CCD system, and the LOD was found to be less than 10 ng/mL. The sensitivity of this assay improved as much as 100-fold compared to the gold nanoparticle-based colorimetric LFA.[13] Moreover, Chen *et al.* developed a dual-readout multiplex CLFA for the simultaneous detection of cancer biomarkers, AFP and CEA. In this assay, HRP and the detection antibodies are simultaneously conjugated onto gold nanoparticles producing a dual readout as a visual colorimetric readout by the accumulation of captured gold nanoparticles. A chemiluminescence readout is

then produced as the HRP on the surface of gold nanoparticles catalyzes the chemiluminescence reaction of luminol to amplify the signal. A portable custom-made chemiluminescence analyzer was used to detect the chemiluminescent signal. The colorimetric limit of detection of AFP and CEA by the naked eye was 5 ng/mL and 5 ng/mL, respectively. Using the chemiluminescent signal as the readout, the LOD can reach 0.21 ng/mL for AFP and 0.2 ng/mL for CEA. It shows that CLFA is more sensitive than conventional colorimetric LFA, and also it can be successfully employed in quantitative multiplex detection.[123]

Even with these successful examples, the use of chemiluminescence in the POC diagnostic field remains limited. This is largely due to the need for complex reagents. Some reagents need to be freshly prepared right before the test, and some need to be stored at low temperatures. Deng *et al*. developed a self-contained CLFA to minimize many of these problems and make CLFA as a rapid and convenient platform for POC testing. There are three parts of this LFA: the LFA strip, the chemiluminescent substrate pad, and the polycarbonate holder. The LFA strip is similar to a conventional gold nanoparticle-based LFA, but the gold nanoparticles are conjugated with the detection antibody and HRP simultaneously. The substrate pad contains a lyophilized chemiluminescent substrate mixture of luminol and sodium perborate. (Sodium perborate was used as the oxidant since H_2O_2 decomposes during lyophilization.) This test first gives a colorimetric qualitative analysis by the naked eye. Then the substrate is dissolved with deionized water, and the substrate pad is kept on top of the LFA strip to transfer the substrate onto the nitrocellulose membrane. It reacts under the catalysis of HRP and generates a chemiluminescent signal and it was measured using a customized chemiluminescence analyzer. This CLFA format allows quantitative detection, and it has been applied to detect macromolecules and small molecules using model analytes, AFP and folic acid (FA), respectively. The AFP limit of detection of chemiluminescence-based readout was 0.27 ng/mL and it is 20 times lower than the gold nanoparticle-only readout. This CLFA shows excellent analytical performance compared to most of the other AFP detection LFA platforms. Moreover, the chemiluminescence-based LOD of FA was 0.22 ng/mL and the signal for FA showed a broader detection

range from 0.5 - 50 ng/mL compared to gold nanoparticle-based colorimetric LFA (0.1 - 2 ng/mL).[124] Lyophilization of the chemiluminescent substrate allows long-term storage, minimizes the user intervention, and makes it easy to use in resource-limited settings. Furthermore, Liu *et al.* developed a nanozyme-based chemiluminescent lateral flow assay for rapid and sensitive detection of SARS-CoV-2 antigen, which can be completed within 16 min. They used Co–Fe@hemin-peroxidase nanozyme that catalyzes chemiluminescence comparable with natural HRP and thus amplifies chemiluminescent signal. The signal was detected using a camera of a smartphone, and the LOD for recombinant spike antigen of SARS-CoV-2 was 0.1 ng/mL. Here, Co–Fe@hemin-peroxidase nanozyme was used in place of HRP because natural enzymes are unstable, complex to produce, and expensive. According to the results of this study, Co–Fe@hemin-peroxidase nanozyme is more stable at high temperatures and alkaline conditions compared with HRP and as efficient as HRP. Therefore, the nanozyme CLFA can be stored stably at ambient temperature, benefiting transportation and field application.[125]

Table 1.6. Chemiluminescent Reporter-based Lateral Flow Assays.

analyte	LFA format	limit of detection	applied range	analysis time	reference
Trypanosoma mRNA	sandwich	0.5 fmols	0 - 10 fmols	70 min	121
cTnI	sandwich	5.6 pg/mL	0 - 10^4 pg/mL	25 min	12
cortisol	sandwich	0.342 µg/dL	0.78 - 12.5 µg/dL	13 min	122
CEA	sandwich	0.17 ng/mL	5 - 200 ng/mL	15 min	123
PCT	sandwich	0.02 pg/mL	1 - 1000 pg/mL	15 - 30 min	123
myoglobin	sandwich	< 10 ng/mL	10 ng/mL - 10 mg/mL	N/A	13
AFP	sandwich	0.27 ng/mL	1 - 200 ng/mL	18 min	124

Table 1.6 (continued).

FA	competitive	0.22 ng/mL	0.5 - 50 ng/mL	18 min	124
SARS-CoV-2 antigen	sandwich	0.1 ng/mL	0.2 - 100 ng/mL	16 min	125
high sensitivity-CRP	sandwich	1.05 ng/mL	1 - 10,000 ng/mL	10 - 12 min	126

1.6 Research Goals and Organization of the Thesis

The main goal of the research presented in this thesis is to develop highly sensitive lateral flow assays using luminescence-based reporters for more reliable point-of-care diagnosis. In this research work, a series of photoluminescent reporters and chemiluminescent reporters have been used to achieve better limits of detection compared to conventional gold nanoparticles. Moreover, the resulting luminescence-based LFAs can be coupled with smartphone-based detection to create fast, cheap, and user-friendly POC tests that enable individuals to monitor their health anytime and anywhere.

The second chapter describes the development of a multicolor multiplex LFA for high sensitivity analyte detection using a pair of persistent luminescent nanophosphors. Green-emitting and blue-emitting persistent luminescent nanophosphors were incorporated in a duplex LFA using hCG and PSA as model analytes to show that they can be successfully used for spatial or spectral detection of two different analytes simultaneously. Further development of this smartphone-based multiplex assay with realistic targets can help to reduce the time and cost and improve the precision of POC diagnostics.

The third chapter describes about increasing the sensitivity of a nucleic acid-based LFA for detecting cutaneous leishmaniasis using blue-emitting persistent luminescent nanophosphors as reporters. This work

shows how a highly sensitive nucleic acid-based POC test can be developed using an isothermal DNA amplification technique, recombinase polymerase amplification (RPA), combined with a traditional LFA as the readout. The amplified product was detected using gold nanoparticles and blue-emitting persistent luminescent nanophosphors to compare the sensitivities. This work shows that the higher sensitivity of persistent luminescent nanophosphors combined with isothermal nucleic acid amplification and smartphone-based detection helps to develop rapid, low-cost, more accurate nucleic acid-based POC tests to control infectious diseases, especially in resource-limited parts of the world.

The fourth chapter describes the construction of chemiluminescence-based lateral flow assays to detect human monocytic ehrlichiosis (HME), which is an infectious disease caused by the bacterium, *Ehrlichia chaffeensis*, and transmitted to humans by tick bites. We first developed a direct antigen detection LFA using fluorescent reporters as the label and TCPO and H_2O_2 as chemiluminescent reagents to detect *Ehrlichia* tandem repeat proteins (TRPs) that can serve as the target for POC diagnostics. Coupling the direct antigen LFA with smartphone-based imaging makes it suitable for highly sensitive POC diagnosis of HME, including in resource-limited areas, supporting early diagnosis and effective treatment. We also developed a serological assay to detect a tick-expressed protein (A9) in human serum, which could also serve as the basis for developing HME POC diagnostics for earlier diagnosis of the disease. Here, we used HRP as the label and compared the colorimetric response of the 3,3′,5,5′-tetramethylbenzidine (TMB) substrate and chemiluminescent response of luminol-H_2O_2, showing better sensitivity. We also tested some clinical samples using chromogenic detection by adding TMB to demonstrate the feasibility of this LFA in the application of clinical diagnosis.

1.7 Acknowledgements

This work was funded in part by NIAID/NIH (Grant No. 1R43AI118180-01A1 and 1R01AR072742-01) and CDC (Grant No. 1U01CK000512-01 and Contract No. 200-2017-M-94591). The authors also

acknowledge the NIH Rapid Acceleration of Diagnostics (RADx) Project #7720 DOD CDMRP W81XWH-21-1-0975 (CA200041).

Bibliography

(1) Valones, M. A. A.; Guimarães, R. L.; Brandão, L. A. C.; De Souza, P. R. E.; de Albuquerque Tavares Carvalho, A.; Crovela, S. Principles and Applications of Polymerase Chain Reaction in Medical Diagnostic Fields: A Review. *Brazilian J. Microbiol.* **2009**, *40* (1), 1–11.

(2) Alhajj, M.; Farhana, A. Enzyme Linked Immunosorbent Assay. In *StatPearls*; StatPearls Publishing, 2021.

(3) Hu, J.; Wang, S. Q.; Wang, L.; Li, F.; Pingguan-Murphy, B.; Lu, T. J.; Xu, F. Advances in Paper-Based Point-of-Care Diagnostics. *Biosens. Bioelectron.* **2014**, *54*, 585–597.

(4) Lee, W. G.; Kim, Y. G.; Chung, B. G.; Demirci, U.; Khademhosseini, A. Nano/Microfluidics for Diagnosis of Infectious Diseases in Developing Countries. *Adv. Drug Delivery Rev.* **2010**, *62* (4-5), 449–457.

(5) Price, C. P. Point of Care Testing. *BMJ.* **2001**, *322* (7297), 1285–1288.

(6) Vashist, S. K. Point-of-Care Diagnostics: Recent Advances and Trends. *Biosensors* **2017**, *7* (4), 62.

(7) Sajid, M.; Kawde, A. N.; Daud, M. Designs, Formats and Applications of Lateral Flow Assay: A Literature Review. *J. Saudi Chem. Soc.* **2015**, *19* (6), 689–705.

(8) Koczula, K. M.; Gallotta, A. Lateral Flow Assays. *Essays Biochem.* **2016**, *60* (1), 111–120.

(9) Danthanarayana, A. N.; Finley, E.; Vu, B.; Kourentzi, K.; Willson, R. C.; Brgoch, J. A Multicolor Multiplex Lateral Flow Assay for High-Sensitivity Analyte Detection Using Persistent Luminescent Nanophosphors. *Anal. Methods* **2020**, *12* (3), 272–280.

(10) Lee, L. G.; Nordman, E. S.; Johnson, M. D.; Oldham, M. F. A Low-Cost, High-Performance System for Fluorescence Lateral Flow Assays. *Biosensors* **2013**, *3* (4), 360–373.

(11) Juntunen, E. Lateral Flow Immunoassays with Fluorescent Reporter Technologies. Ph.D. Dissertation, University of Turku, Turku, Finland, 2018 (accessed May 08, 2021).

(12) Han, G. R.; Kim, M. G. Highly Sensitive Chemiluminescence-Based Lateral Flow Immunoassay for Cardiac Troponin I Detection in Human Serum. *Sensors* **2020**, *20* (9), 2593.

(13) Kim, H. S.; Ko, H.; Kang, M. J.; Pyun, J. C. Highly Sensitive Rapid Test with Chemiluminescent Signal Bands. *Biochip J.* **2010**, *4* (2), 155–160.

(14) https://www.abingdonhealth.com/competitive-inhibition-sandwich-immunoassay-formats-lateral-flow/ (accessed May 14, 2021).

(15) Bahadır, E. B.; Sezgintürk, M. K. Lateral Flow Assays: Principles, Designs and Labels. *TrAC, Trends Anal. Chem.* **2016**, *82*, 286–306.

(16) Huang, Y.; Xu, T.; Wang, W.; Wen, Y.; Li, K.; Qian, L.; Zhang, X.; Liu, G. Lateral Flow

Biosensors Based on the Use of Micro- and Nanomaterials: A Review on Recent Developments. *Microchim. Acta* **2020**, *187* (1), 70.

(17) Quesada-González, D.; Merkoçi, A. Nanoparticle-Based Lateral Flow Biosensors. *Biosens. Bioelectron.* **2015**, *73*, 47–63.

(18) Valeur, B.; Berberan-Santos, M. N. A Brief History of Fluorescence and Phosphorescence before the Emergence of Quantum Theory. *J. Chem. Educ.* **2011**, *88* (6), 731–738.

(19) https://www.leica-microsystems.com/science-lab/basic-principles-of-luminescence/ (accessed September 4, 2021).

(20) Lakowicz, J. R. *Principles of Fluorescence Spectroscopy*, 3rd ed.; Lakowicz, J. R., Ed.; Springer, 2006.

(21) Jain, A.; Blum, C.; Subramaniam, V. Fluorescence Lifetime Spectroscopy and Imaging of Visible Fluorescent Proteins. In *Advances in Biomedical Engineering*, 1st ed.; Verdonck, P., Ed.; Elsevier, 2009; pp 147–176.

(22) https://micro.magnet.fsu.edu/primer/techniques/fluorescence/fluorescenceintro.html (accessed May 18, 2021).

(23) https://www.chemistryviews.org/details/education/10468955/What_are_Fluorescence_and_Phosphorescence.html (accessed May 18, 2021).

(24) Baryshnikov, G.; Minaev, B.; Ågren, H. Theory and Calculation of the Phosphorescence Phenomenon. *Chem. Rev.* **2017**, *117* (9), 6500–6537.

(25) Penfold, T. J.; Gindensperger, E.; Daniel, C.; Marian, C. M. Spin-Vibronic Mechanism for Intersystem Crossing. *Chem. Rev.* **2018**, *118* (15), 6975–7025.

(26) https://www.leica-microsystems.com/science-lab/an-introduction-to-fluorescence/ (accessed May 18, 2021).

(27) Liska, T.; Swetz, A.; Lai, P. N.; Zeller, M.; Teets, T. S.; Gray, T. G. Room-Temperature Phosphorescent Platinum(II) Alkynyls with Microsecond Lifetimes Bearing a Strong-Field Pincer Ligand. *Chem. - Eur. J.* **2020**, *26* (38), 8417–8425.

(28) Mukherjee, S.; Thilagar, P. Recent Advances in Purely Organic Phosphorescent Materials. *Chem. Commun.* **2015**, *51* (55), 10988–11003.

(29) Hagan, A. K.; Zuchner, T. Lanthanide-Based Time-Resolved Luminescence Immunoassays. *Anal. Bioanal. Chem.* **2011**, *400* (9), 2847–2864.

(30) Heffern, M. C.; Matosziuk, L. M.; Meade, T. J. Lanthanide Probes for Bioresponsive Imaging. *Chem. Rev.* **2014**, *114* (8), 4496–4539.

(31) Wu, J.; Ju, H. X. Clinical Immunoassays and Immunosensing. In *Comprehensive Sampling and Sample Preparation*; Pawliszyn, J., Ed.; Academic Press, 2012; pp 143–167.

(32) Zhu, X.; Gao, T. Spectrometry. In *Nano-Inspired Biosensors for Protein Assay with Clinical Applications*; Li, G., Ed.; Elsevier, 2019; pp 237–264.

(33) Delafresnaye, L.; Bloesser, F. R.; Kockler, K. B.; Schmitt, C. W.; Irshadeen, I. M.; Barner-Kowollik, C. All Eyes on Visible-Light Peroxyoxalate Chemiluminescence Read-Out Systems. *Chem. - Eur. J.* **2020**, *26* (1), 114–127.

(34) https://www.creative-diagnostics.com/Chemiluminescence-Immunoassay-guide.htm (accessed September 8, 2021).

(35) Dodeigne, C.; Thunus, L.; Lejeune, R. Chemiluminescence as Diagnostic Tool. A Review. *Talanta* **2000**, *51* (3), 415–439.

(36) Yuan, D. Q.; Kishikawa, N.; Yang, C.; Koga, K.; Kuroda, N.; Fujita, K. Fluorophore-Capped Cyclodextrins as Efficient Chemical-to-Light Energy Converters. *Chem. Commun.* **2003**, *3* (3), 416–417.

(37) Travis, A. S. Perkin's Mauve: Ancestor of the Organic Chemical Industry. *Technology and Culture* **1990**, *31* (1), 51–82.

(38) Svechkarev, D.; Mohs, A. M. Organic Fluorescent Dye-Based Nanomaterials: Advances in the Rational Design for Imaging and Sensing Applications. *Curr. Med. Chem.* **2019**, *26* (21), 4042–4064.

(39) Bamrungsap, S.; Apiwat, C.; Chantima, W.; Dharakul, T.; Wiriyachaiporn, N. Rapid and Sensitive Lateral Flow Immunoassay for Influenza Antigen Using Fluorescently-Doped Silica Nanoparticles. *Microchim. Acta* **2014**, *181* (1-2), 223–230.

(40) Cai, Y.; Kang, K.; Liu, Y.; Wang, Y.; He, X. Development of a Lateral Flow Immunoassay of C-Reactive Protein Detection Based on Red Fluorescent Nanoparticles. *Anal. Biochem.* **2018**, *556*, 129–135.

(41) Gong, X.; Cai, J.; Zhang, B.; Zhao, Q.; Piao, J.; Peng, W.; Gao, W.; Zhou, D.; Zhao, M.; Chang, J. A Review of Fluorescent Signal-Based Lateral Flow Immunochromatographic Strips. *J. Mater. Chem. B* **2017**, *5* (26), 5079–5091.

(42) Yang, Y. Q.; Yang, Y. C.; Liu, M. H.; Chan, Y. H. FRET-Created Traffic Light Immunoassay Based on Polymer Dots for PSA Detection. *Anal. Chem.* **2020**, *92* (1), 1493–1501.

(43) Ahn, J. S.; Choi, S.; Jang, S. H.; Chang, H. J.; Kim, J. H.; Nahm, K. B.; Oh, S. W.; Choi, E. Y. Development of a Point-of-Care Assay System for High-Sensitivity C-Reactive Protein in Whole Blood. *Clin. Chim. Acta* **2003**, *332* (1-2), 51–59.

(44) Yeo, S. J.; Choi, K.; Cuc, B. T.; Hong, N. N.; Bao, D. T.; Ngoc, N. M.; Le, M. Q.; Hang, N. L. K.; Thach, N. C.; Mallik, S. K.; Kim, H. S.; Chong, C. K.; Choi, H. S.; Sung, H. W.; Yu, K.; Park, H. Smartphone-Based Fluorescent Diagnostic System for Highly Pathogenic H5N1 Viruses. *Theranostics* **2016**, *6* (2), 231–242.

(45) Wang, H.; Wang, H.; Chen, S.; Dzakah, E. E.; Kang, K.; Wang, J.; Wang, J. Development of a Fluorescent Immnunochromatographic Assay for the Procalcitonin Detection of Clinical Patients in China. *Clin. Chim. Acta* **2015**, *444*, 37–42.

(46) Worsley, G. J.; Attree, S. L.; Noble, J. E.; Horgan, A. M. Rapid Duplex Immunoassay for Wound Biomarkers at the Point-of-Care. *Biosens. Bioelectron.* **2012**, *34* (1), 215–220.

(47) Hötzer, B.; Medintz, I. L.; Hildebrandt, N. Fluorescence in Nanobiotechnology: Sophisticated Fluorophores for Novel Applications. *Small* **2012**, *8* (15), 2297–2326.

(48) Samir, T. M.; Mansour, M. M. H.; Kazmierczak, S. C.; Azzazy, H. M. E. Quantum Dots: Heralding a Brighter Future for Clinical Diagnostics. *Nanomedicine* **2012**, *7* (11), 1755–1769.

(49) Aldakov, D.; Lefrançois, A.; Reiss, P. Ternary and Quaternary Metal Chalcogenide Nanocrystals:

Synthesis, Properties and Applications. *J. Mater. Chem. C* **2013**, *1* (24), 3756–3776.

(50) Fan, F. J.; Wu, L.; Yu, S. H. Energetic I-III-VI_2 and I_2-II-IV-VI_4 Nanocrystals: Synthesis, Photovoltaic and Thermoelectric Applications. *Energy Environ. Sci.* **2014**, *7* (1), 190–208.

(51) Protesescu, L.; Yakunin, S.; Bodnarchuk, M. I.; Krieg, F.; Caputo, R.; Hendon, C. H.; Yang, R. X.; Walsh, A.; Kovalenko, M. V. Nanocrystals of Cesium Lead Halide Perovskites ($CsPbX_3$, X = Cl, Br, and I): Novel Optoelectronic Materials Showing Bright Emission with Wide Color Gamut. *Nano Lett.* **2015**, *15* (6), 3692–3696.

(52) Chandan, H. R.; Schiffman, J. D.; Balakrishna, R. G. Quantum Dots as Fluorescent Probes: Synthesis, Surface Chemistry, Energy Transfer Mechanisms, and Applications. *Sen. Actuators B Chem.* **2018**, *258*, 1191–1214.

(53) Walling, M. A.; Novak, J. A.; Shepard, J. R. E. Quantum Dots for Live Cell and *In Vivo* Imaging. *Int. J. Mol. Sci.* **2009**, *10* (2), 441–491.

(54) Yang, H.; Li, D.; He, R.; Guo, Q.; Wang, K.; Zhang, X.; Huang, P.; Cui, D. A Novel Quantum Dots-Based Point of Care Test for Syphilis. *Nanoscale Res. Lett.* **2010**, *5* (5), 875–881.

(55) Wang, J.; Meng, H. M.; Chen, J.; Liu, J.; Zhang, L.; Qu, L.; Li, Z.; Lin, Y. Quantum Dot-Based Lateral Flow Test Strips for Highly Sensitive Detection of the Tetanus Antibody. *ACS Omega* **2019**, *4* (4), 6789–6795.

(56) Shen, H.; Yuan, H.; Niu, J. Z.; Xu, S.; Zhou, C.; Ma, L.; Li, L. S. Phosphine-Free Synthesis of High-Quality Reverse Type-I ZnSe/CdSe Core with CdS/Cd_xZn_{1-x}S/ZnS Multishell Nanocrystals and Their Application for Detection of Human Hepatitis B Surface Antigen. *Nanotechnology* **2011**, *22* (37) 375602.

(57) Hu, J.; Zhang, Z. L.; Wen, C. Y.; Tang, M.; Wu, L. L.; Liu, C.; Zhu, L.; Pang, D. W. Sensitive and Quantitative Detection of C-Reaction Protein Based on Immunofluorescent Nanospheres Coupled with Lateral Flow Test Strip. *Anal. Chem.* **2016**, *88* (12), 6577–6584.

(58) Li, X.; Gong, X.; Zhang, B.; Liu, Y.; Chang, J.; Zhang, X. Ultrasensitive Lateral-Flow Assays Based on Quantum Dot Encapsulations with Signal Amplification. *J. Nanopart. Res.* **2018**, *20* (5), 139.

(59) Zhou, C.; Yuan, H.; Shen, H.; Guo, Y.; Li, X.; Liu, D.; Xu, L.; Ma, L.; Li, L. S. Synthesis of Size-Tunable Photoluminescent Aqueous CdSe/ZnS Microspheres *via* a Phase Transfer Method with Amphiphilic Oligomer and Their Application for Detection of HCG Antigen. *J. Mater. Chem.* **2011**, *21* (20), 7393–7400.

(60) Li, X.; Li, W.; Yang, Q.; Gong, X.; Guo, W.; Dong, C.; Liu, J.; Xuan, L.; Chang, J. Rapid and Quantitative Detection of Prostate Specific Antigen with a Quantum Dot Nanobeads-Based Immunochromatography Test Strip. *ACS Appl. Mater. Interfaces* **2014**, *6* (9), 6406–6414.

(61) Bock, S.; An, J.; Kim, H. M.; Kim, J.; Jung, H. S.; Pham, X. H.; Rho, W. Y.; Jun, B. H. A Lateral Flow Immunoassay for Prostate-Specific Antigen Detection Using Silica-Coated CdSe@ZnS Quantum Dots. *Bull. Korean Chem. Soc.* **2020**, *41* (10), 989–993.

(62) Shen, J.; Zhou, Y.; Fu, F.; Xu, H.; Lv, J.; Xiong, Y.; Wang, A. Immunochromatographic Assay for Quantitative and Sensitive Detection of Hepatitis B Virus Surface Antigen Using Highly Luminescent Quantum Dot-Beads. *Talanta* **2015**, *142*, 145–149.

(63) Wu, R.; Zhou, S.; Chen, T.; Li, J.; Shen, H.; Chai, Y.; Li, L. S. Quantitative and Rapid Detection

of C-Reactive Protein Using Quantum Dot-Based Lateral Flow Test Strip. *Anal. Chim. Acta* **2018**, *1008*, 1–7.

(64) Yang, Q.; Gong, X.; Song, T.; Yang, J.; Zhu, S.; Li, Y.; Cui, Y.; Li, Y.; Zhang, B.; Chang, J. Quantum Dot-Based Immunochromatography Test Strip for Rapid, Quantitative and Sensitive Detection of Alpha Fetoprotein. *Biosens. Bioelectron.* **2011**, *30* (1), 145–150.

(65) Wang, C.; Hou, F.; Ma, Y. Simultaneous Quantitative Detection of Multiple Tumor Markers with a Rapid and Sensitive Multicolor Quantum Dots Based Immunochromatographic Test Strip. *Biosens. Bioelectron.* **2015**, *68*, 156–162.

(66) Tang, J.; Wu, L.; Lin, J.; Zhang, E.; Luo, Y. Development of Quantum Dot-Based Fluorescence Lateral Flow Immunoassay Strip for Rapid and Quantitative Detection of Serum Interleukin-6. *J. Clin. Lab. Anal.* **2021**, *35* (5), e23752.

(67) Kim, H. M.; Oh, C.; An, J.; Baek, S.; Bock, S.; Kim, J.; Jung, H. S.; Song, H.; Kim, J. W.; Jo, A.; Kim, D. E.; Rho, W. Y.; Jang, J. Y.; Cheon, G. J.; Im, H. J.; Jun, B. H. Multi-Quantum Dots-Embedded Silica-Encapsulated Nanoparticle-Based Lateral Flow Assay for Highly Sensitive Exosome Detection. *Nanomaterials* **2021**, *11* (3), 768.

(68) Li, Z.; Wang, Y.; Wang, J.; Tang, Z.; Pounds, J. G.; Lin, Y. Rapid and Sensitive Detection of Protein Biomarker Using a Portable Fluorescence Biosensor Based on Quantum Dots and a Lateral Flow Test Strip. *Anal. Chem.* **2010**, *82* (16), 7008–7014.

(69) Wu, F.; Yuan, H.; Zhou, C.; Mao, M.; Liu, Q.; Shen, H.; Cen, Y.; Qin, Z.; Ma, L.; Li, L. S. Multiplexed Detection of Influenza A Virus Subtype H5 and H9 via Quantum Dot-Based Immunoassay. *Biosens. Bioelectron.* **2016**, *77*, 464–470.

(70) Rong, Z.; Wang, Q.; Sun, N.; Jia, X.; Wang, K.; Xiao, R.; Wang, S. Smartphone-Based Fluorescent Lateral Flow Immunoassay Platform for Highly Sensitive Point-of-Care Detection of Zika Virus Nonstructural Protein 1. *Anal. Chim. Acta* **2019**, *1055*, 140–147.

(71) Gudgin Dickson, E. F.; Pollak, A.; Diamandis, E. P. Time-Resolved Detection of Lanthanide Luminescence for Ultrasensitive Bioanalytical Assays. *J. Photochem. Photobiol. B Biol.* **1995**, *27* (1), 3–19.

(72) Ye, Z.; Tan, M.; Wang, G.; Yuan, J. Novel Fluorescent Europium Chelate-Doped Silica Nanoparticles: Preparation, Characterization and Time-Resolved Fluorometric Application. *J. Mater. Chem.* **2004**, *14*, 851–856.

(73) Liang, R. L.; Deng, Q. T.; Chen, Z. H.; Xu, X. P.; Zhou, J. W.; Liang, J. Y.; Dong, Z. N.; Liu, T. C.; Wu, Y. S. Europium (III) Chelate Microparticle-Based Lateral Flow Immunoassay Strips for Rapid and Quantitative Detection of Antibody to Hepatitis B Core Antigen. *Sci. Rep.* **2017**, *7* (1), 14093.

(74) Liu, J.; Shi, H.; Cong, G.; Chen, J.; Zhang, X.; Shi, D.; Cao, L.; Wang, X.; Zhang, J.; Ji, Z.; Jing, Z.; Feng, L. Development of a Rapid and Sensitive Europium (III) Chelate Microparticle-Based Lateral Flow Test Strip for the Detection and Epidemiological Surveillance of Porcine Epidemic Diarrhea Virus. *Arch. Virol.* **2020**, *165* (5), 1049–1056.

(75) Juntunen, E.; Myyryläinen, T.; Salminen, T.; Soukka, T.; Pettersson, K. Performance of Fluorescent Europium(III) Nanoparticles and Colloidal Gold Reporters in Lateral Flow Bioaffinity Assay. *Anal. Biochem.* **2012**, *428* (1), 31–38.

(76) Salminen, T.; Juntunen, E.; Talha, S. M.; Pettersson, K. High-Sensitivity Lateral Flow

Immunoassay with a Fluorescent Lanthanide Nanoparticle Label. *J. Immunol. Methods* **2019**, *465*, 39–44.

(77) Juntunen, E.; Arppe, R.; Kalliomäki, L.; Salminen, T.; Talha, S. M.; Myyryläinen, T.; Soukka, T.; Pettersson, K. Effects of Blood Sample Anticoagulants on Lateral Flow Assays Using Luminescent Photon-Upconverting and Eu(III) Nanoparticle Reporters. *Anal. Biochem.* **2016**, *492*, 13–20.

(78) Lee, K. W.; Kim, K. R.; Chun, H. J.; Jeong, K. Y.; Hong, D. K.; Lee, K. N.; Yoon, H. C. Time-Resolved Fluorescence Resonance Energy Transfer-Based Lateral Flow Immunoassay Using a Raspberry-Type Europium Particle and a Single Membrane for the Detection of Cardiac Troponin I. *Biosens. Bioelectron.* **2020**, *163*, 112284.

(79) Song, X.; Knotts, M. Time-Resolved Luminescent Lateral Flow Assay Technology. *Anal. Chim. Acta* **2008**, *626* (2), 186–192.

(80) Xia, X.; Xu, Y.; Zhao, X.; Li, Q. Lateral Flow Immunoassay Using Europium Chelate-Loaded Silica Nanoparticles as Labels. *Clin. Chem.* **2009**, *55* (1), 179–182.

(81) Liang, R. L.; Xu, X. P.; Liu, T. C.; Zhou, J. W.; Wang, X. G.; Ren, Z. Q.; Hao, F.; Wu, Y. S. Rapid and Sensitive Lateral Flow Immunoassay Method for Determining Alpha Fetoprotein in Serum Using Europium (III) Chelate Microparticles-Based Lateral Flow Test Strips. *Anal. Chim. Acta* **2015**, *891*, 277–283.

(82) Shao, X. Y.; Wang, C. R.; Xie, C. M.; Wang, X. G.; Liang, R. L.; Xu, W. W. Rapid and Sensitive Lateral Flow Immunoassay Method for Procalcitonin (PCT) Based on Time-Resolved Immunochromatography. *Sensors* **2017**, *17* (3), 480.

(83) Wang, D.; He, S.; Wang, X.; Yan, Y.; Liu, J.; Wu, S.; Liu, S.; Lei, Y.; Chen, M.; Li, L.; Zhang, J.; Zhang, L.; Hu, X.; Zheng, X.; Bai, J.; Zhang, Y.; Zhang, Y.; Song, M.; Tang, Y. Rapid Lateral Flow Immunoassay for the Fluorescence Detection of SARS-CoV-2 RNA. *Nat. Biomed. Eng.* **2020**, *4* (12), 1150–1158.

(84) Rundström, G.; Jonsson, A.; Mårtensson, O.; Mendel-Hartvig, I.; Venge, P. Lateral Flow Immunoassay Using Europium (III) Chelate Microparticles and Time-Resolved Fluorescence for Eusonophils and Neutrophils in Whole Blood. *Clin. Chem.* **2007**, *53* (2), 342–348.

(85) *Phosphor Handbook*, 2nd ed.; Yen, W. M., Shionoya, S., Yamamoto, H., Eds.; CRC Press: Boca Raton, FL, 2007.

(86) Xu, J.; Tanabe, S. Persistent Luminescence Instead of Phosphorescence: History, Mechanism, and Perspective. *J. Lumin.* **2019**, *205*, 581–620.

(87) Paterson, A. S. Persistent Luminescent Nanophosphors as Reporters for Sensitive Diagnostics. Ph.D. Dissertation, University of Houston, Houston, TX, 2016.

(88) Brito, H. F.; Hölsä, J.; Laamanen, T.; Lastusaari, M.; Malkamäki, M.; Rodrigues, L. C. V. Persistent Luminescence Mechanisms: Human Imagination at Work. *Opt. Mater. Express* **2012**, *2* (4), 371–381.

(89) Matsuzawa, T.; Aoki, Y.; Takeuchi, N.; Murayama, Y. A New Long Phosphorescent Phosphor with High Brightness, $SrAI_2O_4:Eu^{2+},Dy^{3+}$. *J. Electrochem. Soc.* **1996**, *143* (8), 2670–2673.

(90) Finley, E.; Cobb, A.; Duke, A.; Paterson, A.; Brgoch, J. Optimizing Blue Persistent Luminescence in $(Sr_{1-\delta}Ba_\delta)_2MgSi_2O_7:Eu^{2+},Dy^{3+}$ via Solid Solution for Use in Point-of-Care Diagnostics. *ACS*

Appl. Mater. Interfaces **2016**, *8* (40), 26956–26963.

(91) Paterson, A. S.; Raja, B.; Garvey, G.; Kolhatkar, A.; Hagström, A. E. V.; Kourentzi, K.; Lee, T. R.; Willson, R. C. Persistent Luminescence Strontium Aluminate Nanoparticles as Reporters in Lateral Flow Assays. *Anal. Chem.* **2014**, *86* (19), 9481–9488.

(92) Lastusaari, M.; Jungner, H.; Kotlov, A.; Laamanen, T.; Rodrigues, L. C. V.; Brito, H. F.; Hölsä, J. Understanding Persistent Luminescence: Rare-Earth- and Eu^{2+}-Doped $Sr_2MgSi_2O_7$. *Z. Naturforsch., B: J. Chem. Sci.* **2014**, *69* (2), 171–182.

(93) Lécuyer, T.; Teston, E.; Ramirez-Garcia, G.; Maldiney, T.; Viana, B.; Seguin, J.; Mignet, N.; Scherman, D.; Richard, C. Chemically Engineered Persistent Luminescence Nanoprobes for Bioimaging. *Theranostics* **2016**, *6* (13), 2488–2524.

(94) Van den Eeckhout, K.; Smet, P. F.; Poelman, D. Persistent Luminescence in Eu^{2+}-Doped Compounds: A Review. *Materials* **2010**, *3* (4), 2536–2566.

(95) Finley, E. Structure-Composition Relationships and Their Influence on Long Luminescent Lifetimes in Persistent Luminescent Phosphors. Ph.D. Dissertation, University of Houston, Houston, TX, 2019.

(96) Bessière, A.; Sharma, S. K.; Basavaraju, N.; Priolkar, K. R.; Binet, L.; Viana, B.; Bos, A. J. J.; Maldiney, T.; Richard, C.; Scherman, D.; Gourier, D. Storage of Visible Light for Long-Lasting Phosphorescence in Chromium-Doped Zinc Gallate. *Chem. Mater.* **2014**, *26* (3), 1365–1373.

(97) Paterson, A. S.; Raja, B.; Mandadi, V.; Townsend, B.; Lee, M.; Buell, A.; Vu, B.; Brgoch, J.; Willson, R. C. A Low-Cost Smartphone-Based Platform for Highly Sensitive Point-of-Care Testing with Persistent Luminescent Phosphors. *Lab Chip* **2017**, *17* (6), 1051–1059.

(98) Goux, H. J.; Raja, B.; Kourentzi, K.; Trabuco, J. R. C.; Vu, B. V.; Paterson, A. S.; Kirkpatrick, A.; Townsend, B.; Lee, M.; Truong, V. T. T.; Pedroza, C.; Willson, R. C. Evaluation of a Nanophosphor Lateral-Flow Assay for Self-Testing for Herpes Simplex Virus Type 2 Seropositivity. *PLoS One* **2019**, *14* (12), e0225365.

(99) Kim, D.; Kim, H. E.; Kim, C. H. Enhancement of Long-Persistent Phosphorescence by Solid-State Reaction and Mixing of Spectrally Different Phosphors. *ACS Omega* **2020**, *5* (19), 10909–10918.

(100) Chen, J.; Zhao, J. X. Upconversion Nanomaterials: Synthesis, Mechanism, and Applications in Sensing. *Sensors* **2012**, *12* (3), 2414–2435.

(101) Hampl, J.; Hall, M.; Mufti, N. A.; Yao, Y. M. M.; MacQueen, D. B.; Wright, W. H.; Cooper, D. E. Upconverting Phosphor Reporters in Immunochromatographic Assays. *Anal. Biochem.* **2001**, *288* (2), 176–187.

(102) Tanke, H. J.; Zuiderwijk, M.; Wiesmeijer, K. C.; Breedveld, R. N.; Abrams, W. R.; de Dood, C. J.; Tjon Kon Fat, E. M.; Corstjens, P. L. A. M. The Use of Upconverting Phosphors in Point-of-Care (POC) Testing. In *Imaging, Manipulation, and Analysis of Biomolecules, Cells, and Tissues XII*; Farkas, D.L., Nicolau, D.V., Leif, R.C., Eds.; Proceedings of SPIE, Vol. 8947; SPIE, Bellingham, WA, 2014.

(103) Sirkka, N.; Lyytikäinen, A.; Savukoski, T.; Soukka, T. Upconverting Nanophosphors as Reporters in a Highly Sensitive Heterogeneous Immunoassay for Cardiac Troponin I. *Anal. Chim. Acta* **2016**, *925*, 82–87.

(104) Zhou, J.; Liu, Q.; Feng, W.; Sun, Y.; Li, F. Upconversion Luminescent Materials: Advances and

Applications. *Chem. Rev.* **2015**, *115* (1), 395–465.

(105) Auzel, F. Upconversion and Anti-Stokes Processes with f and d Ions in Solids. *Chem. Rev.* **2004**, *104* (1), 139–173.

(106) Yang, X.; Liu, L.; Hao, Q.; Zou, D.; Zhang, X.; Zhang, L.; Li, H.; Qiao, Y.; Zhao, H.; Zhou, L. Development and Evaluation of Up-Converting Phosphor Technology-Based Lateral Flow Assay for Quantitative Detection of NT-ProBNP in Blood. *PLoS One* **2017**, *12* (2), e0171376.

(107) Zou, W.; Visser, C.; Maduro, J. A.; Pshenichnikov, M. S.; Hummelen, J. C. Broadband Dye-Sensitized Upconversion of Near-Infrared Light. *Nat. Photonics* **2012**, *6* (8), 560–564.

(108) Wang, F.; Wang, J.; Liu, X. Direct Evidence of a Surface Quenching Effect on Size-Dependent Luminescence of Upconversion Nanoparticles. *Angew. Chem., Int. Ed.* **2010**, *49* (41), 7456–7460.

(109) Bian, W.; Lin, Y.; Wang, T.; Yu, X.; Qiu, J.; Zhou, M.; Luo, H.; Yu, S. F.; Xu, X. Direct Identification of Surface Defects and Their Influence on the Optical Characteristics of Upconversion Nanoparticles. *ACS Nano* **2018**, *12* (4), 3623–3628.

(110) Chen, X.; Jin, L.; Kong, W.; Sun, T.; Zhang, W.; Liu, X.; Fan, J.; Yu, S. F.; Wang, F. Confining Energy Migration in Upconversion Nanoparticles towards Deep Ultraviolet Lasing. *Nat. Commun.* **2016**, *7*, 10304.

(111) Zhu, X.; Zhang, J.; Liu, J.; Zhang, Y. Recent Progress of Rare-Earth Doped Upconversion Nanoparticles: Synthesis, Optimization, and Applications. *Adv. Sci.* **2019**, *6* (22), 1901358.

(112) He, H.; Liu, B.; Wen, S.; Liao, J.; Lin, G.; Zhou, J.; Jin, D. Quantitative Lateral Flow Strip Sensor Using Highly Doped Upconversion Nanoparticles. *Anal. Chem.* **2018**, *90* (21), 12356–12360.

(113) Bayoumy, S.; Martiskainen, I.; Heikkilä, T.; Rautanen, C.; Hedberg, P.; Hyytiä, H.; Wittfooth, S.; Pettersson, K. Sensitive and Quantitative Detection of Cardiac Troponin I with Upconverting Nanoparticle Lateral Flow Test with Minimized Interference. *Sci. Rep.* **2021**, *11* (1), 18698.

(114) Martiskainen, I.; Talha, S. M.; Vuorenpää, K.; Salminen, T.; Juntunen, E.; Chattopadhyay, S.; Kumar, D.; Vuorinen, T.; Pettersson, K.; Khanna, N.; Batra, G. Upconverting Nanoparticle Reporter-Based Highly Sensitive Rapid Lateral Flow Immunoassay for Hepatitis B Virus Surface Antigen. *Anal. Bioanal. Chem.* **2021**, *413* (4), 967–978.

(115) Li, L.; Zhou, L.; Yu, Y.; Zhu, Z.; Lin, C.; Lu, C.; Yang, R. Development of Up-Converting Phosphor Technology-Based Lateral-Flow Assay for Rapidly Quantitative Detection of Hepatitis B Surface Antibody. *Diagn. Microbiol. Infect. Dis.* **2009**, *63* (2), 165–172.

(116) Corstjens, P. L. A. M.; de Dood, C. J.; van der Ploeg-van Schip, J. J.; Wiesmeijer, K. C.; Riuttamäki, T.; van Meijgaarden, K. E.; Spencer, J. S.; Tanke, H. J.; Ottenhoff, T. H. M.; Geluk, A. Lateral Flow Assay for Simultaneous Detection of Cellular- and Humoral Immune Responses. *Clin. Biochem.* **2011**, *44* (14-15), 1241–1246.

(117) Hua, F.; Zhang, P.; Zhang, F.; Zhao, Y.; Li, C.; Sun, C.; Wang, X.; Yang, R.; Wang, C.; Yu, A.; Zhou, L. Development and Evaluation of an Up-Converting Phosphor Technology-Based Lateral Flow Assay for Rapid Detection of *Francisella Tularensis*. *Sci. Rep.* **2015**, *5*, 17178.

(118) Corstjens, P. L. A. M.; van Lieshout, L.; Zuiderwijk, M.; Kornelis, D.; Tanke, H. J.; Deelder, A. M.; van Dam, G. J. Up-Converting Phosphor Technology-Based Lateral Flow Assay for Detection of *Schistosoma* Circulating Anodic Antigen in Serum. *J. Clin. Microbiol.* **2008**, *46* (1), 171–176.

(119) You, M.; Lin, M.; Gong, Y.; Wang, S.; Li, A.; Ji, L.; Zhao, H.; Ling, K.; Wen, T.; Huang, Y.; Gao, D.; Ma, Q.; Wang, T.; Ma, A.; Li, X.; Xu, F. Household Fluorescent Lateral Flow Strip Platform for Sensitive and Quantitative Prognosis of Heart Failure Using Dual-Color Upconversion Nanoparticles. *ACS Nano* **2017**, *11* (6), 6261–6270.

(120) Nguyen, V. T.; Song, S.; Park, S.; Joo, C. Recent Advances in High-Sensitivity Detection Methods for Paper-Based Lateral-Flow Assay. *Biosens. Bioelectron.* **2020**, *152*, 112015.

(121) Wang, Y.; Fill, C.; Nugen, S. R. Development of Chemiluminescent Lateral Flow Assay for the Detection of Nucleic Acids. *Biosensors* **2012**, *2* (1), 32–42.

(122) Kim, H. T.; Jin, E.; Lee, M. H. Portable Chemiluminescence-Based Lateral Flow Assay Platform for the Detection of Cortisol in Human Serum. *Biosensors* **2021**, *11* (6), 191.

(123) Chen, Y.; Sun, J.; Xianyu, Y.; Yin, B.; Niu, Y.; Wang, S.; Cao, F.; Zhang, X.; Wang, Y.; Jiang, X. A Dual-Readout Chemiluminescent-Gold Lateral Flow Test for Multiplex and Ultrasensitive Detection of Disease Biomarkers in Real Samples. *Nanoscale* **2016**, *8* (33), 15205–15212.

(124) Deng, J.; Yang, M.; Wu, J.; Zhang, W.; Jiang, X. A Self-Contained Chemiluminescent Lateral Flow Assay for Point-of-Care Testing. *Anal. Chem.* **2018**, *90* (15), 9132–9137.

(125) Liu, D.; Ju, C.; Han, C.; Shi, R.; Chen, X.; Duan, D.; Yan, J.; Yan, X. Nanozyme Chemiluminescence Paper Test for Rapid and Sensitive Detection of SARS-CoV-2 Antigen. *Biosens. Bioelectron.* **2020**, *173*, 112817.

(126) Joung, H. A.; Oh, Y. K.; Kim, M. G. An Automatic Enzyme Immunoassay Based on a Chemiluminescent Lateral Flow Immunosensor. *Biosens. Bioelectron.* **2014**, *53*, 330–335.

CHAPTER 2

A MULTICOLOR MULTIPLEX LATERAL FLOW ASSAY FOR HIGH-SENSITIVITY ANALYTE DETECTION USING PERSISTENT LUMINESCENT NANOPHOSPHORS

Reproduced with permission from *the Journal of Analytical Methods*

(*Anal. Methods* 2020, 12, 3, 272–280)

DOI: 10.1039/C9AY02247C

Adheesha N. Danthanarayana,[1] Erin Finley,[1] Binh Vu,[2] Katerina Kourentzi,[2] Richard C. Willson,[2,3,4,*] and Jakoah Brgoch[1,*]

[1]Department of Chemistry, University of Houston, Houston, Texas 77204, USA

[2]Department of Chemical and Biomolecular Engineering, University of Houston, Houston, Texas 77204, USA

[3]Department of Biology and Biochemistry, University of Houston, Houston, Texas 77204, USA

[4]Escuela de Medicina y Ciencias de Salud, Tecnológico de Monterrey, Monterrey, Nuevo León 64710, Mexico

2.1 Introduction

Point-of-care (POC) testing is a critical and ever-growing research area in the medical and biotechnological fields. It provides significant advantages to healthcare providers by allowing immediate and convenient testing in low-resource settings such as less-developed countries or a patient's home. Indeed, these tests allow quicker clinical decisions without the need for sophisticated and expensive instrumentation or highly trained personnel.[1-3] Among POC testing methods, lateral flow assays (LFAs) have gained significant attention because of their simplicity, low-cost, and user-friendly format.[4-6] LFAs are wicking-membrane-

based devices (the components are shown in Figure 2.1) that can conduct an immunoassay for a target analyte in a liquid sample based on the biorecognition between a target antigen and antibody or other molecular recognition agent. When the sample containing the analyte (antigen) is applied to the sample pad, it first migrates to the conjugate pad where it binds to analyte-specific antibodies that have been conjugated to reporter labels. The resulting analyte-antibody-reporter complex then continues to flow along the porous LFA membrane where another antibody that is primary to the analyte, captures this complex at a test line. The sandwich binding of the labeled and primary antibodies mediated by the presence of the analyte produces a response, typically as simple as the appearance of a color, at the test line that indicates the presence of the analyte in the sample. Any excess antibody-conjugated reporters are finally captured by secondary antibodies at the control line, indicating the proper liquid flow through the strip.[3, 5, 6]

For given antibodies, the test sensitivity primarily depends on the detectability of the reporter. Some commonly used reporters are gold nanoparticles, colored latex nanobeads, organic fluorophores, and quantum dots.[5-8] Gold nanoparticles are the most commonly used reporters due to their ease of functionalization, size-tunable optical properties, and excellent chemical stability.[5] Colored latex beads are also easy to functionalize, and they are available at a relatively low-cost.[8] Organic fluorophores show enhanced sensitivity while quantum dots show resistance to photobleaching and they have unique size-tunable optical properties.[5, 8] Unfortunately, there are drawbacks for each of these reporters. For example, gold nanoparticles and colored latex beads have limited sensitivity because they are colorimetric methods.[9, 10] Fluorophores and quantum dots exhibit better sensitivity than gold nanoparticles and colored latex beads;[11, 12] however, fluorophores are not photostable[5, 13] and quantum dots are costly and have intermittent on/off behavior.[14] Moreover, quantum dots are generally incompatible with aqueous environments.[5, 15] These fluorescent reporters also require nearly continuous excitation, which leads to an increase in the background from scattered excitation light as well as autofluorescence, and greatly complicates the optical components required to read them.[7] To reduce the background autofluorescence and the cost of the reader

by eliminating advanced optical components, time-gated measurements were introduced using long-lived luminescent reporters such as lanthanide-chelates.[16] They have a longer emission lifetime than typical fluorescent reporters and therefore, a short time delay can be introduced between the excitation and measurement for the decay of the background signal. Although functional, these molecules tend to have photostability issues and therefore, the time delay needs to be carefully defined, or the sensitivity can be greatly reduced when involved in time-gated measurements.[7]

To overcome many of these problems, we recently introduced persistent luminescent nanophosphors (PLNPs) as reporters for the LFA.[7, 17] In the last decade, PLNPs have gained great attention in biomedical applications such as bioimaging and photothermal therapies, owing to their unique optical characteristics.[18, 19] PLNPs generate a photon emission lasting for several minutes to hours after photoexcitation, vastly longer than the nanosecond lifetime of most fluorescent materials, allowing separation of emission signal from excitation light by time-gated measurements.[7, 20] PLNPs also show excellent photostability.[7] The combination of these properties allowed us to demonstrate a highly sensitive LFA for the detection of model protein human chorionic gonadotropin (hCG) with a limit of detection of ≈ 0.05 ng/mL using a green-emitting $SrAl_2O_4:Eu^{2+},Dy^{3+}$ (SAO) PLNP that could be detected and analyzed using smartphone-based time-gated imaging.[17, 21] SAO PLNPs were briefly excited with the phone's flash, followed by switching off the flash and collecting the emitted luminescence on the test and control lines with the smartphone's camera.[17]

Even with the resounding success of this initial demonstration, many practical limitations of this test would best be addressed by the creation of a multiplex LFA, which can save time and costs and improve diagnostic precision.[22, 23] Multiplex LFAs have been reported with different types of reporters, including gold nanoparticles[24], colored latex beads[25], fluorophores,[26] and quantum dots.[27, 28] Yet, these multiplex LFAs have the same limitations of sensitivity and reliability owing to the drawbacks of these reporters, as

described above. In this study, we developed a new approach for a highly sensitive multiplex LFA using multiple PLNPs emitting at different wavelengths and coupled it with smartphone-based time-gated imaging. Our recent research suggested the best options for two PLNPs are the blue-emitting $(Sr_{0.625}Ba_{0.375})_2MgSi_2O_7:Eu^{2+},Dy^{3+}$ (SBMSO) PLNPs, which can be detected using the smartphone-based imaging as well as our previously used SAO PLNPs.[20, 29] Therefore, as illustrated in Figure 2.1, SAO and SBMSO compounds were used in tandem as reporters to build a novel smartphone-based multiplex LFA that can simultaneously detect two model analytes; prostate-specific antigen (PSA) and hCG for which commercial high-affinity antibodies exist.

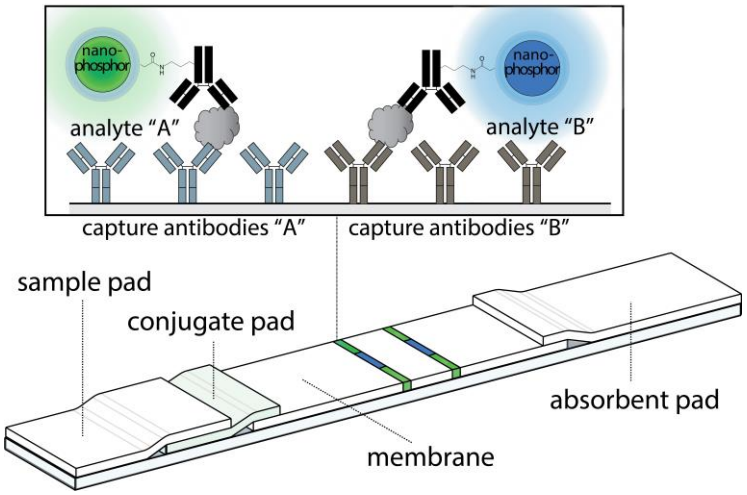

Figure 2.1. Schematic representation of a duplex lateral flow assay where the green-emitting $SrAl_2O_4:Eu^{2+},Dy^{3+}$ (SAO) and blue-emitting $(Sr_{0.625}Ba_{0.375})_2MgSi_2O_7:Eu^{2+},Dy^{3+}$ (SBMSO) PLNPs are employed as reporters.

Employing two different phosphors emitting at different wavelengths is especially important to analyze a sample with antibodies that are not specific to a particular pathogen. Most multiplex tests rely on spatial multiplexing, where the analytes are captured on two or more test lines using the same optical reporter. However, if there is significant non-specific binding, the test can produce erroneous results. Associating a different color with each pathogen and subsequently analyzing the composition of the test region color would be a more robust approach to examine samples containing several antibodies that are not pathogen-

specific. This has been investigated previously using colored latex beads[25] and silver nanoparticles[30] as reporters. Although these results are encouraging, the colorimetric optical reporters may limit the test's sensitivity. In this work, we have used multiple PLNPs as reporters to achieve a highly sensitive and reliable LFA as a versatile multiplex POC test for the quantitative detection of multiple analytes simultaneously.

2.2 Experimental Section

2.2.1 Nanophosphor Preparation, Milling, and Fractionation

$SrAl_2O_4:Eu^{2+},Dy^{3+}$ (SAO) was purchased from Glow Inc. and the starting particle size (d_{50} = 5 - 15 μm) was reduced by dispersing 10 g of powder in 100 mL of anhydrous ethanol (Decon) and ball milling for 10 days in a ceramic milling jar with zirconia grinding media.[7] The powder was then dried and phase purity of the milled particles was confirmed with a PANalytical X'Pert powder diffractometer using Cu Kα radiation (1.54183 Å).

Polycrystalline powder with the nominal composition $[(Sr_{0.625}Ba_{0.375})_{1.96}Eu_{0.01}Dy_{0.03}]MgSi_2O_7$ (SBMSO) was prepared *via* high-temperature solid-state synthesis using $SrCO_3$ (98%; Alfa Aesar), $BaCO_3$ (98%; Johnson Mathey), MgO (99.99%; Sigma-Aldrich), SiO_2 (99.5%; Sigma-Aldrich), Eu_2O_3 (99.9%; Materion Advanced Chemicals), and Dy_2O_3 (99.99%; Sigma-Aldrich). As a flux, 5 wt.% H_3BO_3 (99.98%; Sigma-Aldrich) was added. The reagents were hand-ground in an agate mortar and pestle for 30 min and then placed in a shaker mill (Spex 8000) for 45 min. The mixture was pressed into a pellet and heated at 1150 °C for 6 hrs in a reducing atmosphere of 5% H_2/95% N_2 with heating and cooling rates of 3 °C/min. The powder was then reground and sintered again at 1000 °C for 4 hrs with the same reducing atmosphere and ramp rates as the initial heating. The particle size of the product was reduced by ball milling in anhydrous ethanol for 10 days in a ceramic milling jar with zirconia grinding media. The powder was dried and phase purity of the final product was confirmed using a PANalytical X'Pert powder diffractometer using Cu Kα radiation (1.54183 Å).[20]

The particle size distribution of the dry, ball-milled SAO and SBMSO particles was then reduced by differential centrifugal sedimentation (Beckman Coulter Avanti J-E centrifuge) using anhydrous ethanol as the solvent to separate the smaller particles.[7]

2.2.2 Silica Encapsulation of Nanophosphors

A volume of 1 mL of fractionated PLNPs (2 mg/mL) was pipetted into a 2 mL microcentrifuge tube. In a different tube, a solution was prepared by adding 221.6 μL of anhydrous ethanol and 246.7 μL of DI water (Millipore Milli-Q), then adding 6.7 μL of tetraethyl orthosilicate (TEOS; 99%; Sigma-Aldrich). The mixture was added to the tube with the PLNPs, and it was placed in a bath sonicator (Fisher Scientific FS30) for 5 min. A volume of 25 μL of aqueous ammonium hydroxide (28 - 30%; Sigma-Aldrich) was added to the suspension, followed by sonication for another 30 min. The tube with nanophosphors was placed on a room temperature rotator for 7.5 hrs. Finally, the particles were washed three times by adding 1 mL of anhydrous ethanol and centrifuging (Eppendorf Centrifuge 5418) to settle the particles and remove the supernatant. The PLNPs were sonicated and vortexed thoroughly during the washings to minimize the formation of aggregates.[7]

The particle size of the bare and encapsulated nanophosphors was determined by observing the particles dispersed in ethanol under a transmission electron microscope (TEM; JEM-2010F) and the colloidal stability of the silica-encapsulated nanophosphors was confirmed by measuring the zeta potential of particles dispersed in ethanol using a Zetasizer (Malvern).

2.2.3 Functionalization of Nanophosphors with Antibodies

For silanization, 1 mL of silica-encapsulated PLNPs in ethanol (2 mg/mL) was transferred into a 2 mL microcentrifuge tube. The solution was centrifuged for 3 min at 3000 rcf and the top 216 μL of ethanol was removed and discarded. A second solution was prepared by adding 155 μL of TEOS, 5 μL of

triethoxysilylbutyraldehyde (TESBA; Gelest), and 1393 μL of anhydrous ethanol. 10 μL of this solution was added to the nanophosphors re-suspended in ethanol. Another solution was prepared by adding 189 μL of DI water and 16.7 μL of aqueous ammonium hydroxide and this solution was also added to the nanophosphor suspension. The mixture was sonicated for 10 min in a bath sonicator and then placed on a room temperature rotator at 20 rpm for 12 hrs. Finally, the PLNPs were washed with 1 mL of anhydrous ethanol at least three times. In each wash, particles were centrifuged at 3000 rcf for 3 min to remove as much supernatant as possible.

Following silanization, the PLNPs were washed once with DI water and once with phosphate-buffered saline, pH 8 (PBS; Takara Bio) to prepare them for bioconjugation. The nanoparticles were re-suspended in 700 μL of PBS (pH 8) and sonicated for 5 min. 50 μg (50 μL of 1 mg/mL stock solution) of monoclonal mouse anti-β hCG antibodies (ABBCG-0402; Arista Biologicals, Inc.) or monoclonal mouse anti-PSA antibodies ([8301] ab403; abcam) were then added to the PLNP suspension and mixed by vortexing. A solution of 1 M $NaBH_3CN$ (Thermo Scientific) in PBS (pH 8) was prepared, and 250 μL of that solution was added to the nanophosphor suspension. This combination was sonicated for 5 min and then placed on a room temperature rotator at 20 rpm for 2 hrs.

Finally, the PLNPs were washed once with PBS (pH 7.4) to prepare them for passivation. The particles were re-suspended in 200 μL of PBS. A solution of 40 mg/mL bovine serum albumin (BSA; 98%; Sigma-Aldrich) in PBS (pH 7.4) was prepared, and 750 μL was added to the nanophosphors. A volume of 50 μL of 1 M $NaBH_3CN$ was also added to the nanophosphor suspension. After 5 min of sonication, the nanophosphors were placed on a room temperature rotator at 20 rpm for 3 hrs followed by washing three times with PBS (pH 7.4). The particles were subsequently re-suspended in 100 μL of borate storage buffer (10 mM sodium borate (J.T. Baker), 150 mM NaCl (Macron), 0.1% BSA, 0.04% 40,000 avg. mol. wt.

polyvinylpyrrolidone (PVP-40; Sigma-Aldrich), 0.025% Tween 20 (Sigma-Aldrich), pH 8.5) and stored in a 4 °C refrigerator.

2.2.4 Constructing LFA Strips

LFA strips with Standard 14 sample pad, FF80HP nitrocellulose membrane, and CF5 absorbent pad (Cytiva) were assembled on an adhesive backing card (MIBA-020; DCN Diagnostics). The conjugate pad was not used since these LFAs were run only for the experimental purpose. To prepare the LFA strips for the hCG assay, polyclonal goat anti-α hCG antibodies (ABACG-0500; Arista Biologicals, Inc.) and polyclonal goat anti-mouse antibodies (ABGAM-0500; Arista Biologicals, Inc.) were diluted from the stock solution to 1 mg/mL in PBS for the test line and control line, respectively. These antibodies were striped on the nitrocellulose membrane using a BioDot dispenser (XYZ30600124) at a rate of 1 μL/cm. The striped membrane was dried at 37 °C for 30 min in an incubator (Robbins Scientific Micro Hybridization Incubator 2000) and then cut into 3 mm wide strips using a ZQ2000 Guillotine Cutter (Kinbio). For the assays including PSA, on the same 3 mm wide LFA test strips, polyclonal goat anti-PSA antibodies (AF1344; R&D systems; 1 μL of 0.3 mg/mL) and polyclonal goat anti-mouse antibodies (1 μL of 0.3 mg/mL) were spotted manually since we did not have enough amount of concentrated antibodies to make strips using the BioDot, as PSA antibodies are expensive. The antibody-spotted strips were then dried at 37 °C for 30 min in an incubator.

2.2.5 Smartphone-Based Imaging of Nanophosphors

An iPhone 5S and a 3-D printed attachment were used for the smartphone-based imaging. The 3-D printed attachment was designed to hold a lateral flow assay cartridge (part number MICA-125; DCN Diagnostics), such that the result window of the cartridge is aligned with the rear camera of the iPhone and occupying most of the field of view when the cartridge is fully inserted into the attachment. A proprietary software application called “Luminostics” was used to control the flash and the rear camera of the iPhone. The flash

excites the nanophosphors for ~3 s, and after switching off the flash, the camera captures the images after ~100 ms time delay. The camera captures four images and gives the average result.[17] Each test was run in triplicate to confirm the reliability of the test and imaging software.

2.3 Results and Discussion

2.3.1 Nanophosphor Reporters

LFAs require nanoparticles to effectively flow through membranes with pore sizes ranging from less than one micrometer to a few micrometers. The commercially purchased powder and bulk synthesized powder both initially consist of large particles of about 10 - 15 μm.[7] Therefore, milling and fractionation by differential centrifugal sedimentation of inorganic phosphors are necessary for reducing the particle size to the nano-scale. Small particle size also minimizes gravitational sedimentation and increases the surface-area-to-volume ratio to maximize the capacity for the conjugation of antibodies.[7, 31] After the fractionation of the particles from the bulk powder, the TEM images of the bare particles are shown in Figure 2.2a and Figure 2.2b. The particle size of SAO and SBMSO are ~200 nm and ~250 nm, respectively.

One limitation of PLNPs is that SAO nanoparticles, in particular, are sensitive to aqueous environments and will decompose with any prolonged exposure to water. However, the water stability of the nanophosphors is greatly improved by encapsulating the particles in a silica shell. A modified Stöber process was used here for the silica encapsulation of the particles, and the TEM images of encapsulated particles confirm the formation of a silica shell around the particle. (Figures 2.2c and 2.2d). This also enables the later reaction with trialkoxysilanes, which is a popular method to introduce reactive groups on silica/glass surfaces.[7] After the silica encapsulation, the zeta potential was measured to confirm the colloidal stability. Zeta potential is caused by the surface charge and the magnitude of zeta potential indicates the degree of electrostatic repulsions between the particles in a dispersion. Therefore, a greater zeta potential usually prevents aggregation and hence correlates to the colloidal stability of the nanoparticles. Generally,

colloids of a zeta potential greater than ±30 mV are considered stable.[32] The zeta potential of silica-encapsulated SAO and SBMSO were -37 mV and -48 mV, respectively, indicating good colloidal stability after silica encapsulation.

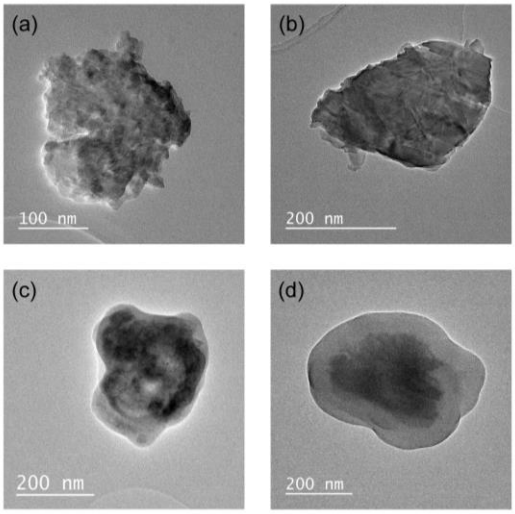

Figure 2.2. Transmission electron microscope (TEM) images of (a) bare SAO, (b) bare SBMSO, (c) silica-encapsulated SAO, (d) silica-encapsulated SBMSO.

Functionalizing the PLNPs with antibodies then required reacting the silica-encapsulated nanophosphors with triethoxysilylbutyraldehyde (TESBA) to introduce surface aldehydes that react with primary amines on the antibodies to form stable secondary amine bonds under reductive amination conditions in the presence of sodium cyanoborohydride. Finally, BSA was added to block any unreacted aldehyde sites to reduce non-specific binding.[7, 17]

X-ray photoelectron spectroscopy (XPS) was employed to confirm functionalization at each stage of the process. As shown in Figure 2.3a (top), the spectrum of the ball-milled (unencapsulated) SAO shows the Sr 3s, Sr 3p, Sr 3d peaks reside at 357.7 eV, 269.7 eV, and 134.5 eV whereas the Al 2s and Al 2p peaks are at 119.3 eV and 74.5 eV, respectively. No other signals were detected except for C, which likely stems from impurities and/or surface contamination. The spectrum of SAO encapsulated with silica in Figure 2.3a

(middle) shows prominent Si 2s and Si 2p peaks at 156.8 eV and 105.6 eV, respectively, while the Sr and Al peaks are significantly reduced, indicating the particles are fully encapsulated with silica. Finally, the spectrum of SAO after functionalization with the antibodies in Figure 2.3a (bottom) shows the presence of the N 1s peak at 404 eV, indicating the presence of a protein on the surface of the nanophosphors.[7] In the same manner, the spectrum of milled bare SBMSO in Figure 2.3b (top) shows Sr 3p, Sr 3d, Ba 4d peaks at 270.1, 134.9 eV, and 90.1 eV, respectively, two Mg KLL peaks at 306.9 eV and 353.3 eV, and peaks at 153.3 eV (Si 2s) and 102.9 eV (Si 2p). The spectrum of SBMSO encapsulated with silica in Figure 2.3b (middle) again shows prominent Si 2s and Si 2p peaks at 155.0 and 103.8 eV, respectively, with the Sr, Ba, and Mg peaks all significantly reduced, indicating that these particles also are encapsulated with silica. Finally, the spectrum of antibody-conjugated SBMSO in Figure 2.3b (bottom) shows N 1s peak at 398.7 eV, signifying the conjugation of a protein to the surface of the nanophosphors.[33] These results confirm that the PLNPs are encapsulated with silica, and the antibodies are successfully conjugated to the nanophosphors.[7, 33]

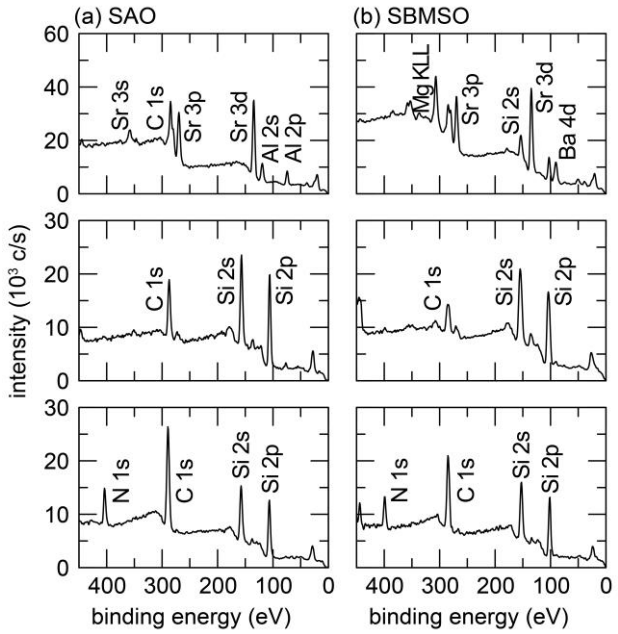

Figure 2.3. XPS spectra of (a) SAO and (b) SBMSO at different stages of functionalization: (top) milled bare, (middle) after silica encapsulation, (bottom) after functionalization with antibodies.

2.3.2 Applying Functionalized Multicolor Nanophosphors in an LFA Format

The assay buffer and the particle concentration were optimized to minimize non-specific binding and improve limits of detection. The contents of all four buffers created are provided in the Supporting Information. The optimal assay buffer (buffer D) selected based on the least non-specific binding and brightest test result line contains 50 mM NaCl, 0.1% Tween 20, 10 mM Tris HCl, 0.25% PVP-40, and 0.1% BSA (pH 8). The SAO and SBMSO particle concentrations were also optimized and found to be 0.13 mg/mL and 1 mg/mL, respectively. Two model analytes (hCG and PSA) were thereafter used to test the possibility of using SAO and SBMSO particles as different reporters in a multiplex LFA for the detection of two different analytes simultaneously. The analyte and antibody-conjugated SAO and SBMSO complexes were first independently tested for binding with anti-hCG antibodies and anti-PSA antibodies on LFA strips under optimum conditions. The samples were prepared by spiking the analyte into the buffer solution. The positive samples contain the analyte, and the negative samples contain distilled water instead of the analyte. To run the assays, 40 μL of buffer solution consisting of nanophosphors (diluted to the optimized concentration) and 10 ng/mL of the desired analyte was added to the sample pad of each strip. The strips were then allowed to run for 20 min and then imaged using the FluorChem imaging system (Alpha Innotech). Each test was run in triplicate to confirm the reliability of the test. As shown in Figure 2.4, the complexes of analyte and antibody-conjugated SAO or SBMSO nanophosphors bind well with both anti-hCG antibodies and anti-PSA antibodies on the test line with minimum non-specific binding in the individual assays proving both PLNPs can be used as optical reporters.

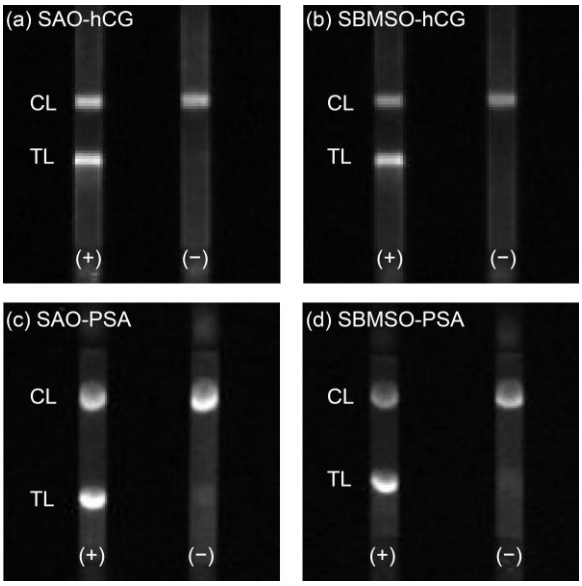

Figure 2.4. Binding of (a) 0.13 mg/mL SAO in hCG assay, (b) 1 mg/mL SBMSO in hCG assay, (c) 0.13 mg/mL SAO in PSA assay, and (d) 1 mg/mL SBMSO in PSA assay using buffer D. These grayscale images were collected using the FluorChem imaging system.

2.3.3 Point-of-Care Smartphone-Based Imaging of Nanophosphors

The FluorChem images display bright signals from the LFA strips with nanophosphors; however, the images are monochromatic. Taking advantage of the different emission colors allows significant differentiation of the two reporters beyond only spatial resolution. The tests were therefore imaged using the camera on an iPhone 5S smartphone that is coupled to the LFA through a custom-designed attachment and "Luminostics" application that operates the phone's LED flash as an excitation source for the nanophosphors and the camera for image capturing.[17] This testing format is a significant advantage as a POC test considering the ubiquitous availability and compact nature of the smartphone and LFA and also the low-cost (≈USD 5) and the simplicity of the design of the 3D-printable smartphone attachment.[17] The PLNPs can both be excited by the phone's flash with SAO emitting a green photon ($\lambda_{max} \approx 520$ nm)[31] and SBMSO emitting a blue photon ($\lambda_{max} \approx 460$ nm).[20] The app to operate the flash and camera employs time-gated imaging to decrease the background signal by introducing a 100 ms time delay that allows the LED light to decay before image capture. SAO and SBMSO were successfully imaged in this smartphone-based

time-gated imaging system owing to their long emission lifetimes[17, 20], as shown in Figure 2.5. Therefore, this system could lead to a rapid, low-cost, and reliable multiplex diagnostic test that will enable individuals to monitor their health anytime, anywhere.

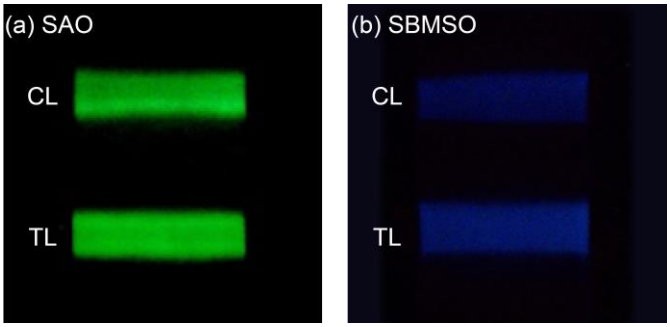

Figure 2.5. (a) SAO and (b) SBMSO detected on iPhone 5S. The color images were collected using an iPhone 5s rear camera.

The limit of detection (LOD) of PSA using SAO particles and hCG using SBMSO particles were determined by varying the concentration of each antigen from 0.02 -10 ng/mL and calculating the ratio of the test line (TL) intensity to the control line (CL) intensity. The intensities of TL and CL were measured using NIH ImageJ, and the background was subtracted to correct any non-specific adsorption. The tests were run in triplicate and the average intensity ratio of TL/CL and the associated standard deviation were determined, as shown in Figure 2.6. The results indicate the LODs of 0.1 ng/mL of PSA with SAO and 1 ng/mL of hCG with SBMSO. The LOD of previously reported serum PSA lateral flow assays is around 0.3 - 0.8 ng/mL.[34-36] The analytical sensitivities of the commercially available hCG lateral flow tests vary with most of the urine-based tests having LODs around 2.25 ng/mL,[37, 38] according to the WHO 4th International Standard, and the most sensitive tests having LODs between 0.5 - 0.9 ng/mL.[17, 38, 39] Therefore, the LODs of this minimally-optimized smartphone-based LFA for PSA and hCG are already competitive with commercially available tests.

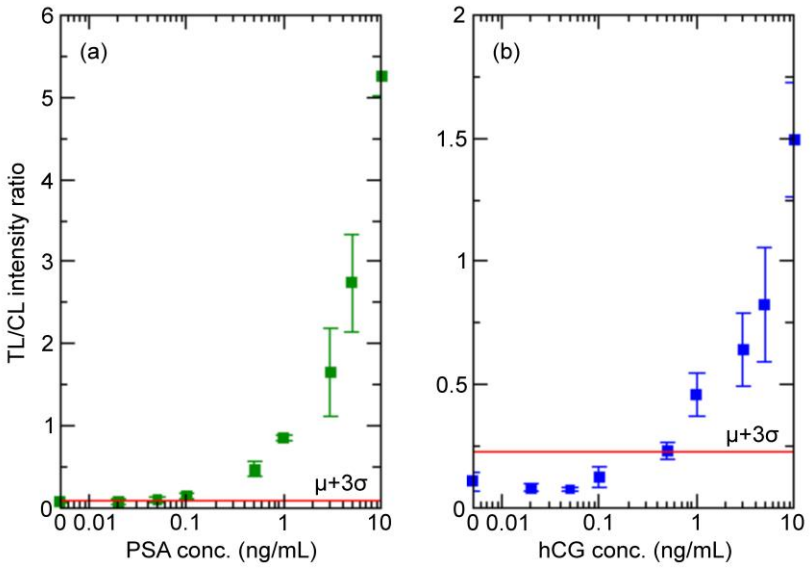

Figure 2.6. Serial dilution of (a) PSA with SAO and (b) hCG with SBMSO detected on the iPhone 5S. The red line signifies the detection limit cutoff taken as the mean plus three times the standard deviation (μ+3σ) of the no-analyte control tests.

2.3.4 Developing Multi-line Spatially-Resolved and Single-line Spectrally-Resolved Multicolor Duplex Assays

To develop a multiplex assay, hCG and PSA proteins were used as model analytes. Even though these model proteins do not occur together in biological samples, there are commercially available high-affinity antibodies that allowed us to show the ability of the high sensitivity detection of nanophosphor reporters. In addition, since hCG and PSA have been commonly used in previous LFA studies, we would be able to compare our LOD with previously reported values for different types of reporters to prove the high sensitivity detection of nanophosphor reporters.

Specific binding of the complexes of analyte and antibody-conjugated nanophosphors to the desired antibodies on the LFA strips in the presence of other analytes and antibodies is a critical factor in developing a multiplex assay format. To examine the capability of specific binding, LFAs were first constructed that contain two test regions and one control region on the same membrane, as illustrated in Figure 2.7a. The

strips have anti-PSA and anti-hCG antibodies spotted at the first and second test region, respectively (Figures 2.7b and 2.7c), and anti-mouse antibodies spotted at the control region. A solution of PLNPs functionalized with anti-hCG antibodies was then added to the sample pad along with hCG, and the results show that it is possible for SAO and SBMSO functionalized with anti-hCG antibodies to flow past the first spot with anti-PSA antibodies and form a bright positive band at the second spot where anti-hCG antibodies are located. In Figures 2.7d and 2.7e, anti-hCG antibodies are placed in the first spot and anti-PSA antibodies are placed in the second spot. A solution containing PLNPs functionalized with anti-PSA antibodies and PSA antigen was added to the sample pad. In this case, anti-PSA conjugated SAO and SBMSO flow through the first spot and form a positive band at the second spot. Each test was run in triplicate to confirm the reliability of the test. In all cases, binding is only observed at the desired test region, and most importantly, there is virtually zero-non-specific binding, indicating that the antibody-conjugated nanophosphors can bind specifically in the presence of multiple different analytes and antibodies.

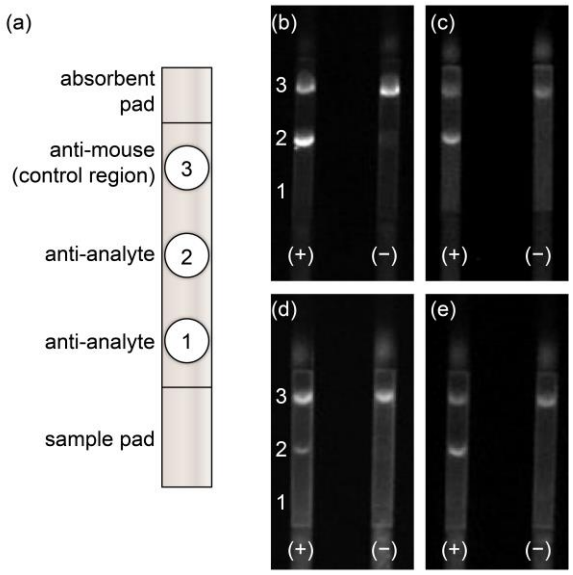

Figure 2.7. (a) Schematic representation. Specific binding of (b) SAO with anti-hCG antibodies, (c) SBMSO with anti-hCG antibodies, (d) SAO with anti-PSA antibodies, (e) SBMSO with anti-PSA antibodies. These grayscale images were collected using the FluorChem imaging system.

The specific binding ability of antibody-conjugated SAO and SBMSO allows developing a multiplex assay to detect multiple analytes simultaneously. Therefore, a spatial duplex assay was developed using SAO conjugated to anti-PSA antibodies and SBMSO conjugated to anti-hCG antibodies to detect a solution containing a dilute mixture of PSA and hCG antigens. Spatially-resolved multiplex assays differentiate analytes by physically separating the detections sites.[40, 41] As illustrated in Figure 2.8, two test regions were placed on the nitrocellulose membrane by spotting polyclonal anti-PSA antibodies (spot 1) and polyclonal anti-hCG antibodies (spot 2). Anti-mouse antibodies were spotted in the control region. A solution containing 0.13 mg/mL SAO nanophosphors functionalized with monoclonal anti-PSA antibodies and 10 ng/mL PSA in the optimized assay buffer was prepared. A second solution containing 1 mg/mL SBMSO nanophosphors functionalized with monoclonal anti-hCG antibodies and 10 ng/mL hCG in an optimized assay buffer was also prepared. 40 μL of each solution was mixed in another microcentrifuge tube and then loaded onto the sample pad. The strip was allowed to run for 20 min, followed by washing with 80 μL of assay buffer to remove unbound reporter particles. Finally, the LFA strip was imaged using the iPhone 5S (Figure 2.8). It is clear that the SAO particles are localized at the first test region containing anti-PSA antibodies, as indicated by the green band, and SBMSO particles are only bound at the second test region containing anti-hCG antibodies, as shown by the blue band. The control region is blue-green because both SAO and SBMSO particles bind with the anti-mouse antibodies in the control region. These results prove that these two compounds can be successfully used for the simultaneous detection of two different analytes in the same sample with minimal non-specific binding and that the two emission signals can be detected at the same time.

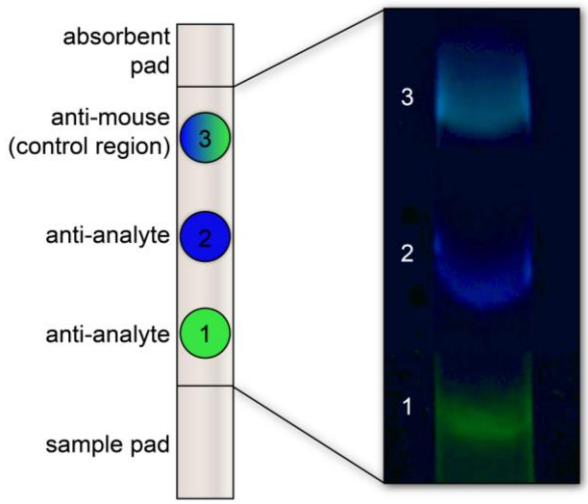

Figure 2.8. Spatial duplex LFA using SAO for anti-PSA antibodies (green) on spot 1 and SBMSO for anti-hCG antibodies (blue) on spot 2 imaged in color using iPhone 5S. The control region is a mixture of SAO and SBSMO and therefore appears bluish-green.

With the ability to discriminate the analytes based on spatial separation as well as the color of the reporter, the multiplex assay was performed varying the concentration of one analyte while maintaining the concentration of the other analyte constant at its LOD to confirm the limits of detection of the assay in a multiplex format. First, the LOD of PSA in the multiplex assay was tested by varying the PSA concentration from 0.02 - 10 ng/mL in the presence of a constant concentration of 1 ng/mL of hCG. The calculated intensity ratios of test spot1/control spot are shown in Figure 2.9a. The detection limit cutoff, which is the mean plus three times the standard deviation ($\mu+3\sigma$) of the no-analyte controls, is marked by the red horizontal line. Based on this analysis, shown in Figure 2.9a, the LOD is found to be 0.1 ng/mL, which is in agreement with the previous result of SAO in the single-plex format. The blue line shows the intensity ratio of test spot2/control spot at the constant concentration of 1 ng/mL hCG, and it remains nearly constant at different concentrations of PSA. Next, to find the LOD of hCG in the multiplex format, a concentration series from 0.02 - 10 ng/mL of hCG was used in the presence of a constant concentration of 0.1 ng/mL of PSA. The calculated intensity ratios of test spot2/control spot are shown in Figure 2.9b. In this case, the LOD is 1 ng/mL of hCG. The green line shows the intensity ratio of test spot1/control spot at the constant

concentration of 0.1 ng/mL PSA, and it also remains nearly constant at different hCG concentrations. These results indicate that the multiplex format does not change the LODs found in the individual assays. Moreover, the intensity ratio of the test region/control region for the target analyte is independent of the concentration of the other analyte. Therefore, SAO and SBMSO, in conjugation with the POC smartphone testing platform can be used for the highly sensitive, concurrent detection of two different analytes.

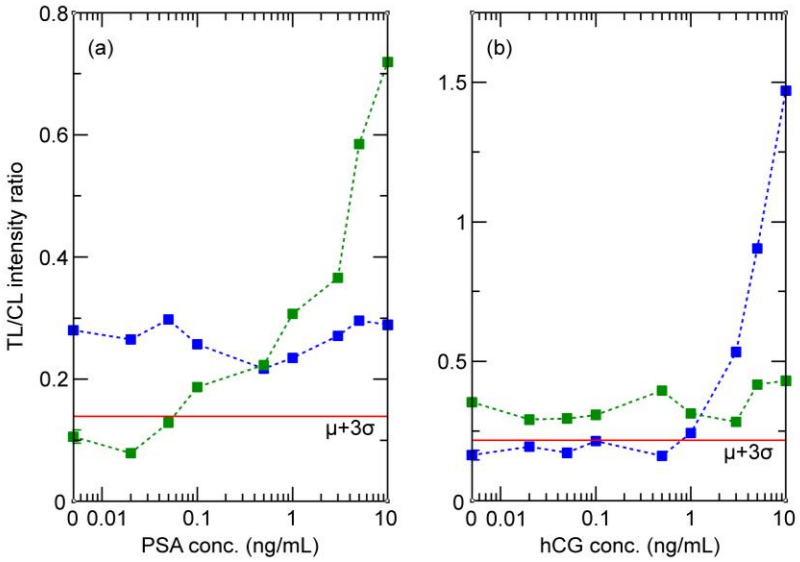

Figure 2.9. Serial dilution of (a) PSA with SAO in the presence of 1 ng/mL hCG and (b) hCG with SBMSO in the presence of 0.1 ng/mL PSA detected on the iPhone 5S.

Although these LFA strips show excellent LODs, any traditional reporter can be used in the multiplex formation using spatial separation of the test lines. One of the major advantages of using reporters that produce different optical signatures is the ability to also spectrally resolve their signal. Thus, in a spectral multiplex assay, different analytes are detected on a single detection site using different color labels for each analyte.[25, 40] Therefore, the above system was also developed as a spectral duplex assay where both types of capture antibodies are spotted at the same test region. As illustrated in Figure 2.10a, both polyclonal anti-PSA and polyclonal anti-hCG antibodies were spotted in the test region. Anti-mouse antibodies were spotted in the control region. A solution containing 0.13 mg/mL SAO nanophosphors functionalized with monoclonal anti-PSA antibodies and 10 ng/mL PSA in the optimized assay buffer was prepared. A second

solution containing 1 mg/mL SBMSO nanophosphors functionalized with monoclonal anti-hCG antibodies and 10 ng/mL hCG in an optimized assay buffer was also prepared. 40 µL of each solution was mixed, loaded onto the sample pad, and the strip was allowed to run for 20 min. It was then washed with 80 µL of assay buffer. Finally, the LFA strip was imaged using the iPhone 5S platform. As shown in Figure 2.10a, SAO and SBMSO particles are both captured at the test region, and the control region is signified by the blue-green emission.

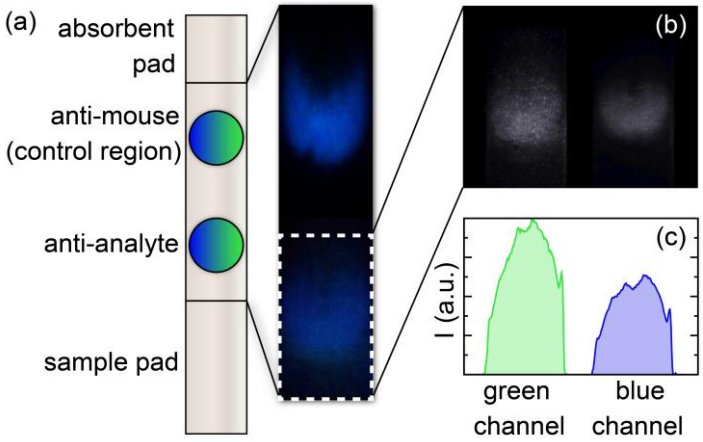

Figure 2.10. Spectral duplex LFA detected on iPhone 5S. (a) SAO conjugated to anti-PSA antibodies (green) and SBMSO conjugated to anti-hCG antibodies (blue), both bind at the test region in the presence of PSA and hCG analytes indicating a positive result. Decomposing the signal at the test region (b) reveals two distinct signals (c) that correspond to the green and blue color channels of the smartphone camera. These color images were collected and processed using the iPhone 5S and the associated application.

Decomposing the signal at the test region by post-processing the image into the green color channel and blue color channel (Figure 2.10b) reveals the presence of both green and blue signatures that can be plotted to reveal a relative intensity of the two channels (Figure 2.10c). This spectral assay is especially useful to analyze samples containing antibodies that are not specific to a particular pathogen (e.g., acute febrile illnesses).[25] In that case, two different colors can be associated with two different pathogens and by analyzing the color composition of the test region, the causative pathogen can be identified. Finally, the same spectral duplex assay was performed with different concentrations of PSA and hCG antigens as shown in Figure 2.11a. The LFA strips were imaged on the iPhone 5S and the green and blue colors of the test

region of each strip were separated and plotted in Figure 2.11b as a function of antigen concentration. In this spectral multiplex format, minimal non-specific binding is observed in the no-analyte control. Nevertheless, for the remainder of the strips, when the signal is decomposed into the green and blue channels, the signal intensity of the no-analyte control is very low compared to the positive samples. As shown in Figure 2.11b, the green and blue intensities increase with increasing concentrations of PSA and hCG, respectively. Therefore, this system is capable of quantitative detection of multiple analytes concurrently.

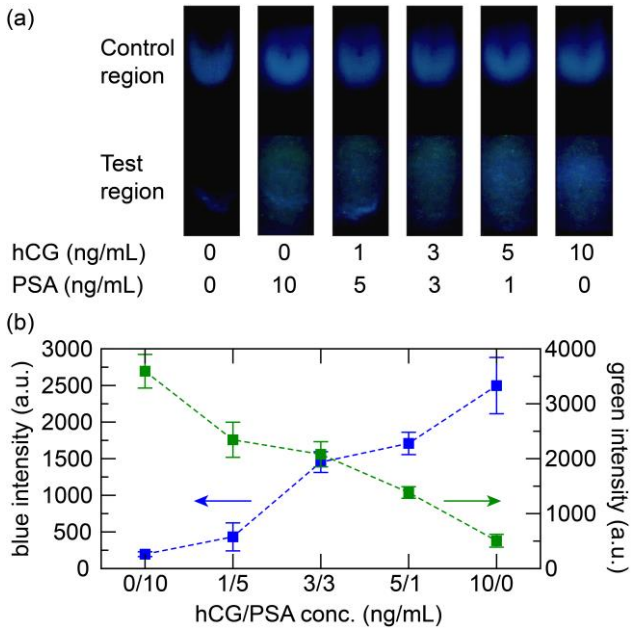

Figure 2.11. (a) iPhone images of LFA strips with varying concentrations of PSA and hCG. (b) Intensities of green and blue channels of the test region with varying concentrations of PSA and hCG. The color images were collected using an iPhone 5s rear camera.

2.4 Conclusions

This work demonstrated a new multiplex LFA capable of detecting two analytes simultaneously using PLNPs as reporters. Wet milling is necessary to reduce the particle size of both nanophosphor reporters, and differential centrifugal sedimentation can be used to fractionate smaller particles. The water stability

of particles was enhanced using a modified Stöber process to make a silica shell around the particles. Facile bioconjugation schemes such as reductive amination can subsequently link the antibodies onto the silica surface of the particle. The resulting antibody-conjugated SAO and SBMSO can simultaneously detect PSA and hCG proteins giving more sensitive and reliable results than the other conventional reporters. More importantly, the long emission lifetime of PLNPs eliminates the need for continuous excitation, which is required for standard fluorescence measurements; there is a substantially lower background signal and no need for advanced optical hardware. Therefore, PLNPs can be imaged using a smartphone-based time-gated imaging system, which enables the development of a simple, fast, and inexpensive POC diagnostic method to detect analytes in color quickly. SAO and SBMSO PLNPs can be successfully detected whether they are bound on two different lines (spatially resolved) or at the same test region (spectrally resolved) to detect PSA and hCG concurrently. It is also possible to integrate the emission intensity independently and determine the ratio of the analytes contained within a sample. Therefore, this system shows outstanding potential for the future development of a highly sensitive, quantitative detection tool for multiple analytes.

2.5 Acknowledgments

The authors thank the Department of Chemistry at the University of Houston for providing startup funds and NIH (Grant. No. 1R01AR072742-01) and CDC (Grant. No. 1U01CK000512-01) for funding this research. The authors also thank Drs. Andrew Paterson and Balakrishnan Raja, formerly in the RCW laboratory and now at Luminostics, Inc. for helping with the protocol for the functionalization of nanophosphors and providing the “Luminostics” application for smartphone-based imaging. The authors also thank Heather Goux for training on LFA and Angelica Cobb for help in the synthesis of SBMSO and fractionation of particles.

Bibliography

(1) Vashist, S. K. Point-of-Care Diagnostics: Recent Advances and Trends. *Biosensors (Basel)* **2017,** *7* (4), 62.

(2) Price, C. P. Point of Care Testing. *Br Med J* **2001,** *322*, 1285–1288.

(3) Hu, J.; Wang, S.; Wang, L.; Li, F.; Pingguan-Murphy, B.; Lu, T. J.; Xu, F. Advances in Paper-Based Point-of-Care Diagnostics. *Biosens Bioelectron* **2014,** *54*, 585–597.

(4) Kozel, T. R.; Burnham-Marusich, A. R. Point-of-Care Testing for Infectious Diseases: Past, Present, and Future. *J Clin Microbiol* **2017,** *55*, 2313–2320.

(5) Sajid, M.; Kawde, A.-N.; Daud, M. Designs, Formats and Applications of Lateral Flow Assay: A Literature Review. *Journal of Saudi Chemical Society* **2015,** *19* (6), 689–705.

(6) Koczula, K. M.; Gallotta, A. Lateral Flow Assays. *Essays Biochem* **2016,** *60* (1), 111–120.

(7) Paterson, A. S.; Raja, B.; Garvey, G.; Kolhatkar, A.; Hagstrom, A. E.; Kourentzi, K.; Lee, T. R.; Willson, R. C. Persistent Luminescence Strontium Aluminate Nanoparticles as Reporters in Lateral Flow Assays. *Anal Chem* **2014,** *86* (19), 9481–9488.

(8) Chun, P. Colloidal Gold and Other Labels for Lateral Flow Immunoassays. In *Lateral Flow Immunoassay*; Wong, R. C., Tse, H. Y., Eds.; Humana Press: New York, NY, 2009; pp 75–93.

(9) Zhang, C.; Zhang, Y.; Wang, S. Development of Multianalyte Flow-Through and Lateral-Flow Assays Using Gold Particles and Horseradish Peroxidase as Tracers for the Rapid Determination of Carbaryl and Endosulfan in Agricultural Products. *J Agric Food Chem.* **2006,** *54* (7), 2502–2507.

(10) Yang, W.; Li, X. B.; Liu, G. W.; Zhang, B. B.; Zhang, Y.; Kong, T.; Tang, J. J.; Li, D. N.; Wang, Z. A Colloidal Gold Probe-Based Silver Enhancement Immunochromatographic Assay for the Rapid Detection of Abrin-a. *Biosens Bioelectron* **2011,** *26* (8), 3710–3713.

(11) Lee, L. G.; Nordman, E. S.; Johnson, M. D.; Oldham, M. F. A Low-Cost, High-Performance System for Fluorescence Lateral Flow Assays. *Biosensors (Basel)* **2013,** *3* (4), 360–373.

(12) Foubert, A.; Beloglazova, N. V.; De Saeger, S. Comparative Study of Colloidal Gold and Quantum Dots as Labels for Multiplex Screening Tests for Multi-Mycotoxin Detection. *Anal Chim Acta* **2017,** *955*, 48–57.

(13) Zheng, Q.; Jockusch, S.; Zhou, Z.; Blanchard, S. C. The Contribution of Reactive Oxygen Species to the Photobleaching of Organic Fluorophores. *Photochemistry and Photobiology* **2014,** *90* (2), 448–454.

(14) Mahler, B.; Spinicelli, P.; Buil, S.; Quelin, X.; Hermier, J. P.; Dubertret, B. Towards Non-Blinking Colloidal Quantum Dots. *Nat Mater* **2008,** *7* (8), 659–664.

(15) Walling, M. A.; Novak, J. A.; Shepard, J. R. Quantum Dots for Live Cell and *In Vivo* Imaging. *Int J Mol Sci* **2009,** *10* (2), 441–491.

(16) Ye, Z.; Tan, M.; Wang, G.; Yuan, J. Novel Fluorescent Europium Chelate-Doped Silicananoparticles: Preparation, Characterization and Time-Resolved Fluorometric Application. *J. Mater. Chem.* **2004**, *14* (5), 851–856.

(17) Paterson, A. S.; Raja, B.; Mandadi, V.; Townsend, B.; Lee, M.; Buell, A.; Vu, B.; Brgoch, J.; Willson, R. C. A Low-Cost Smartphone-Based Platform for Highly Sensitive Point-of-Care Testing with Persistent Luminescent Phosphors. *Lab Chip* **2017,** *17* (6), 1051–1059.

(18) Liu, J.; Lécuyer, T.; Seguin, J.; Mignet, N.; Scherman, D.; Viana, B.; Richard, C. Imaging and Therapeutic Applications of Persistent Luminescence Nanomaterials. *Adv. Drug Deliv. Rev.* **2019,** *138*,193–210.

(19) Maldiney, T.; Richard, C.; Seguin, J.; Wattier, N.; Bessodes, M.; Scherman, D. Effect of Core Diameter, Surface Coating, and PEG Chain Length on the Biodistribution of Persistent Luminescence Nanoparticles in Mice. *ACS Nano* **2011,** *5* (2), 854–862.

(20) Finley, E.; Cobb, A.; Duke, A.; Paterson, A.; Brgoch, J. Optimizing Blue Persistent Luminescence in $(Sr_{1-\delta}Ba_{\delta})_2MgSi_2O_7:Eu^{2+},Dy^{3+}$ via Solid Solution for Use in Point-of-Care Diagnostics. *ACS Appl Mater Interfaces* **2016,** *8* (40), 26956–26963.

(21) Willson, R.; Paterson, A. Phosphorescent Reporters. EP3036530A1, June 29, 2016.

(22) Li, J.; Macdonald, J. Multiplexed Lateral Flow Biosensors: Technological Advances for Radically Improving Point-of-Care Diagnoses. *Biosens Bioelectron* **2016,** *83*, 177–192.

(23) Hanafiah, K. M.; Arifin, N.; Bustami, Y.; Noordin, R.; Garcia, M.; Anderson, D. Development of Multiplexed Infectious Disease Lateral Flow Assays: Challenges and Opportunities. *Diagnostics (Basel)* **2017,** *7* (3), 51.

(24) Chen, Y.; Chen, Q.; Han, M.; Zhou, J.; Gong, L.; Niu, Y.; Zhang, Y.; He, L.; Zhang, L. Development and Optimization of a Multiplex Lateral Flow Immunoassay for the Simultaneous Determination of Three Mycotoxins in Corn, Rice and Peanut. *Food Chem.* **2016,** *213*, 478–484.

(25) Lee, S.; Mehta, S.; Erickson, D. Two-Color Lateral Flow Assay for Multiplex Detection of Causative Agents Behind Acute Febrile Illnesses. *Anal. Chem.* **2016,** *88*, 8359–8363.

(26) Xu, Y.; Liu, Y.; Wu, Y.; Xia, X.; Liao, Y.; Li, Q. Fluorescent Probe-Based Lateral Flow Assay for Multiplex Nucleic Acid Detection. *Anal. Chem.* **2014,** *86*, 5611–5614.

(27) Wu, F.; Yuan, H.; Zhou, C.; Mao, M.; Liu, Q.; Shen, H.; Cen, Y.; Qin, Z.; Ma, L.; Li, L. S. Multiplexed Detection of Influenza A Virus Subtype H5 and H9 via Quantum Dot-Based Immunoassay. *Biosens. Bioelectron.* **2016,** *77*, 464–470.

(28) Taranova, N. A.; Berlina, A. N.; Zherdev, A. V.; Dzantiev, B. B. 'Traffic Light' Immunochromatographic Test Based on Multicolor Quantum Dots for the Simultaneous Detection of Several Antibiotics in Milk. *Biosens. Bioelectron.* **2015**, *63*, 255–261.

(29) Brgoch, J.; Finley, E. Blue Emitting Persistent Phosphor Compositions as Diagnostic Reporters. US20180080874A1, filed September 21, 2016, patent pending.

(30) Yen, C.-W.; de Puig, H.; Tam, J. O.; Gomez-Marquez, J.; Bosch, I.; Hamad-Schifferli, K.; Gehrke, L. Multicolored Silver Nanoparticles for Multiplexed Disease Diagnostics: Distinguishing Dengue, Yellow Fever, and Ebola Viruses. *Lab Chip* **2015,** *15*, 1638–1641.

(31) Finley, E.; Paterson, A. S.; Cobb, A.; Willson, R. C.; Brgoch, J. Reducing Particle Size of Persistent Luminescent $SrAl_2O_4:Eu^{2+},Dy^{3+}$ *via* Microwave-Assisted, Reverse Micelle Synthesis. *Opt. Mater. Express* **2017,** *7*, 2597–2616.

(32) Schierz, A.; Zanker, H. Aqueous Suspensions of Carbon Nanotubes: Surface Oxidation, Colloidal Stability and Uranium Sorption. *Environ. Pollut.* **2009**, *157* (4), 1088–1094.

(33) NIST X-ray Photoelectron Spectroscopy Database. https://srdata.nist.gov/xps/Default.aspx (accessed April 10, 2019).

(34) Andreevaa, I. P.; Grigorenkoa, V. G.; Egorova, A. M.; Osipov, A. P. Quantitative Lateral Flow Immunoassay for Total Prostate Specific Antigen in Serum. *Anal. Lett.* **2016,** *49*, 579–588.

(35) Li, X.; Li, W.; Yang, Q.; Gong, X.; Guo, W.; Dong, C.; Liu, J.; Xuan, L.; Chang, J. Rapid and Quantitative Detection of Prostate Specific Antigen with a Quantum Dot Nanobeads-Based Immunochromatography Test Strip. *Appl. Mater. Interfaces* **2014,** *6*, 6406−6414.

(36) Barnett, J. M.; Wraith, P.; Kiely, J.; Persad, R.; Hurley, K.; Hawkins, P.; Luxton, R. An Inexpensive, Fast and Sensitive Quantitative Lateral Flow Magneto-Immunoassay for Total Prostate Specific Antigen. *Biosensors* **2014,** *4*, 204–220.

(37) Gnoth, C.; Johnson, S. Strips of Hope: Accuracy of Home Pregnancy Tests and New Developments. *Geburtshilfe Frauenheilkd.* **2014,** *74* (7), 661–669.

(38) Silva de Moraes, G.; Cristovam, R.; Savaris, R. F. Comparative Analysis of the Accuracy of Urinary hCG Tests *In Vitro*. *Rev Assoc Med Bras* **2011,** *57* (5), 506–512.

(39) Cole, L. A.; The Utility of Six Over-the-Counter (Home) Pregnancy Tests. *Clin Chem Lab* Med. **2011,** *49* (8), 1317–1322.

(40) Anfossi, L.; Nardo, F. D.; Cavalera, S.; Giovannoli, C.; Baggiani, C. Multiplex Lateral Flow Immunoassay: An Overview of Strategies towards High-throughput Point-of-Need Testing. *Biosensors (Basel).* **2018**, *9* (1), 2.

(41) Boutal, H.; Vogel, A.; Bernabeu, S.; Devilliers, K.; Creton, E.; Cotellon, G.; Plaisance, M.; Oueslati, S.; Dortet, L.; Jousset, A.; Simon, S.; Naas, T.; Volland, H. A Multiplex Lateral Flow Immunoassay for the Rapid Identification of NDM-, KPC-, IMP- and VIM-type and OXA-48-like Carbapenemase-Producing Enterobacteriaceae. *J Antimicrob Chemother* **2018,** *73*, 909–915.

Supporting Information

Optimizing the Assay Buffer

Running the antibody-conjugated SAO and SBMSO in an LFA first requires a suitable assay buffer. Four different buffers generically labeled A, B, C, and D were each tested to detect hCG with anti-hCG conjugated SAO PLNPs. These buffers consist of different types of buffering agents (e.g., HEPES, Tris HCl), blockers such as BSA to reduce non-specific binding and surfactants such as Tween 20 to minimize particle aggregation. The compositions of the buffers are given in Table S2.1. In these assays, anti-hCG conjugated SAO was added directly to the sample pad along with antigen hCG. 40 μL of buffer solution containing 0.1 mg/mL SAO and 10 ng/mL hCG was added to the sample pad using a pipette. The strips were allowed to run for 20 min to ensure maximum binding. They were then imaged using an Alpha Innotech FluorChem imaging system (Figure S2.1). In the ideal case, there should be two bands present, one at the test line (TL) and one at the control line (CL) for the positive tests and only one band present at the control line for the negative tests. According to Figure S2.1a, buffer A does not produce bands at the test line for the positive tests even though it shows very faint bands at the control line. Also, the sample pad and the interface between the sample pad and the membrane are bright implying that most of the particles are stuck at the beginning of the strip. Buffer B (Figure S2.1b) gives clear bands for binding at the test line and control line for the positive tests, but there is non-specific binding at the test line for the negative tests. Buffer C (Figure S2.1c) also shows clear binding on test and control lines for the positive tests, and there is a clear difference at the test line between positive and negative tests. However, there are also faint bands at the test line of the negative tests. Furthermore, in Figures S2.1b and 2.1c, the sample pad is bright, indicating that buffers B and C do not carry the particles properly towards the membrane. Finally, buffer D was formulated by adding BSA to buffer C to reduce non-specific binding (Figure 2.1d). The need for BSA in the buffer suggests surface passivation may not be complete and could be further optimized. Nevertheless, it gives the brightest test line for the positive tests and zero non-specific binding for the negative tests. Also, there are fewer particles stuck at the sample pad compared to the other buffers. SBMSO

particles were also tested with buffer D, and they produced similar results (Figure 2.1e) showing excellent binding for the positive test lines and minimal non-specific binding in the negative control tests. Therefore, buffer D was selected as the optimum buffer to run all LFA tests in this study.

Table S2.1. The composition of buffers A, B, C, and D.

Buffer A	Buffer B	Buffer C	Buffer D
100 mM NaCl 0.1% Tween 20 0.5% Sucrose 1% PEG 3750 0.1% SDS 0.01% BSA 1M HEPES (pH=7.5)	50 mM NaCl 0.1% Tween 20 10 mM Tris HCl 0.25% PVP-40 1M HEPES (pH=8)	50 mM NaCl 0.1% Tween 20 10 mM Tris HCl 0.25% PVP-40 (pH=8)	50 mM NaCl 0.1% Tween 20 10 mM Tris HCl 0.25% PVP-40 0.1% BSA (pH = 8)

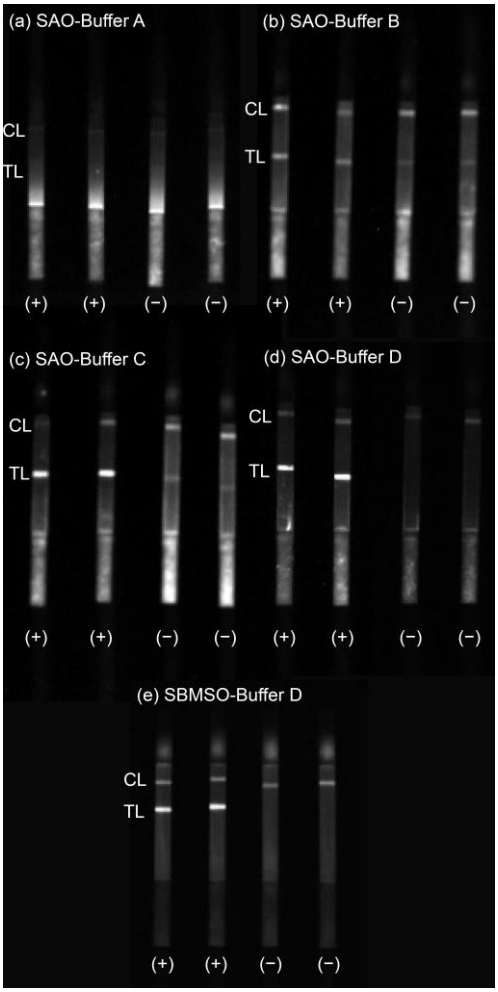

Figure S2.1. Optimizing the assay buffer for SAO and SBMSO using anti-hCG conjugated PLNPs shows buffer D yields the best test results with a clear test and control line for the positive test (+) and minimal non-specific binding in the negative test (-).

Optimizing the Particle Concentration

To optimize the particle concentration for SAO and SBMSO, hCG assays were run using the same conditions as above but with different PLNP concentrations, and the FluorChem images of the strips are shown in Figure S2.2. The optimum particle concentration was selected as the concentration that gives the brightest test line while still showing a clear control line. According to the plots in Figure S2.3, 0.13 mg/mL is suitable for SAO, whereas 1 mg/mL is optimal for SBMSO and as shown in Figures 2.4a and 2.4b, these

particle concentrations did not show any non-specific binding. Therefore, these optimized concentrations were used to run all the LFAs in the study.

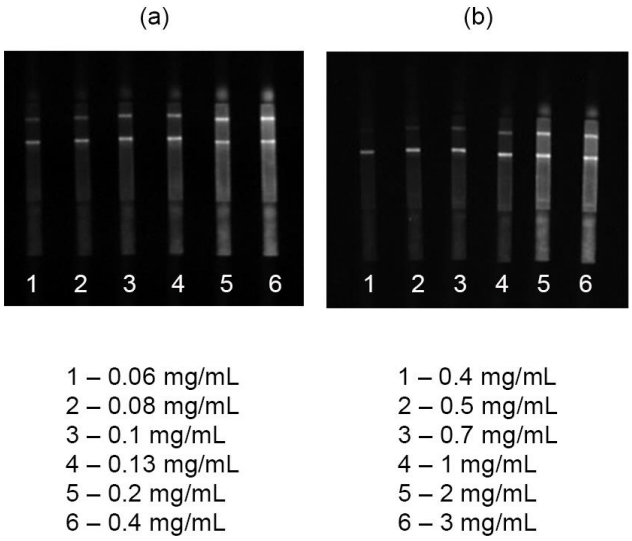

Figure S2.2. Optimizing particle concentration for (a) SAO and (b) SBMSO.

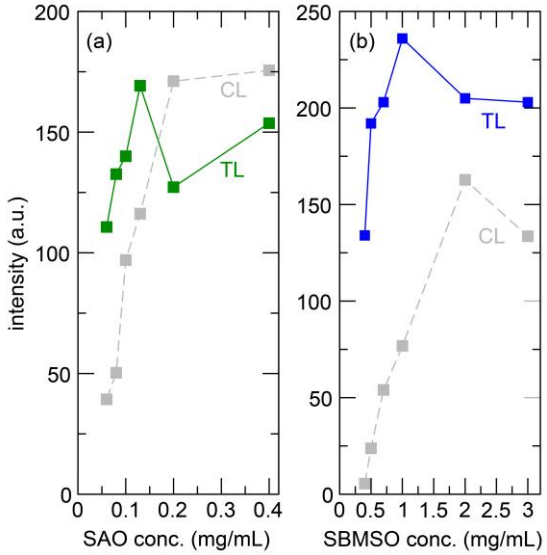

Figure S2.3. Optimum particle concentration for (a) SAO and (b) SBMSO was determined by the maximum intensity of the test line detected by the FluorChem imaging system as a function of concentration. The FluorChem images used to measure the intensities of the test lines are shown in Figure S2.2**.**

Limits of Detection of Individual Assays on iPhone 5S

The iPhone images of SBMSO in trials 1, 2, and 3 used to calculate the average intensity ratio of the test line/control line at different hCG concentrations are shown in Figure S2.4. A similar set of iPhone images of SAO were used to calculate the average intensity ratio of the test line/control line at different concentrations of PSA.

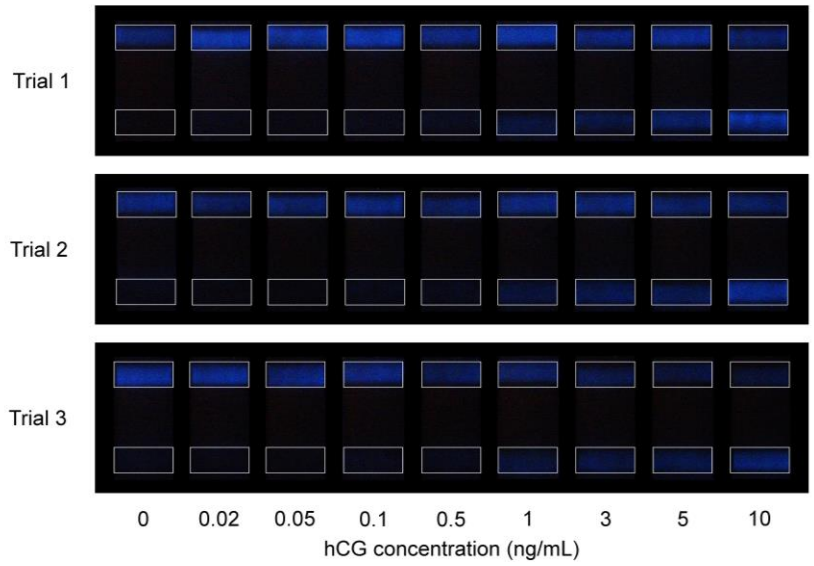

Figure S2.4. iPhone images of SBMSO at different concentrations of hCG.

Limits of Detection of Multiplex Assay on iPhone 5S

The iPhone images of SAO and SBMSO in the multiplex assay that used to calculate the intensity ratio of the test region/control region at different concentrations of hCG in the presence of a constant concentration of 0.1 ng/mL of PSA are shown in Figure S2.5. A similar set of iPhone images were used to calculate the intensity ratio of the test region/control region at different concentrations of PSA in the presence of a constant concentration of 1 ng/mL of hCG.

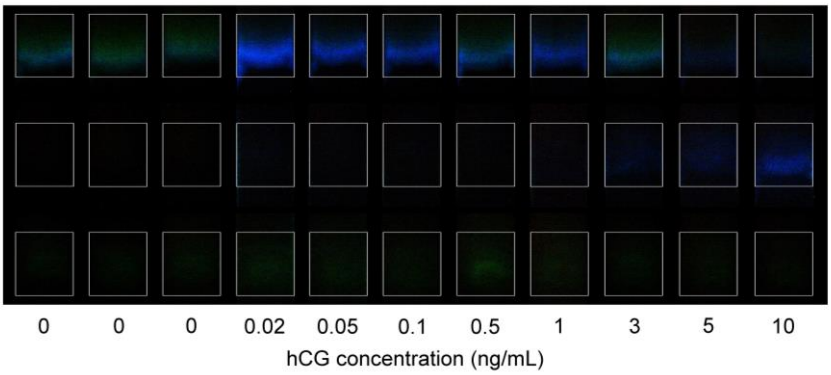

Figure S2.5. iPhone images of SBMSO and SAO at different concentrations of hCG and a constant concentration of 0.1 ng/mL of PSA.

Note: Figures S2.1, S2.4, and S2.5 are updated from the published forms which appeared in the Journal of Analytical Methods since the figures in the publication have some image duplication due to mislabeling of LFA images and mistakes in figure making. Figure S2.1 here is remade to correct the image duplication. The experiments to find the limits of detection of individual assays and limits of detection of spatial multiplex assay on iPhone 5S were repeated and new results are included in Figures S2.4 and S2.5. The corresponding graphs in the main text (Figures 2.6 and 2.9) are also updated according to the new results. These changes do not affect the limits of detection of the assays and do not have any impact on the final conclusions of the published research work.

CHAPTER 3

SMARTPHONE-BASED RPA-LFA FOR THE POINT-OF-CARE DETECTION OF CUTANEOUS LEISHMANIASIS USING NANOPHOSPHOR REPORTERS

3.1 Introduction

Cutaneous leishmaniasis is a vector-borne disease caused by the protozoan parasites of the genus *Leishmania* and transmitted by the bite of an infected female sandfly. Cutaneous leishmaniasis generally presents as ulcerated skin lesions, often leaving life-long scars, stigma and may result in severe disability. Sandflies transmitting cutaneous leishmaniasis are found throughout Central and South America and in some parts of Asia and Africa, impacting an estimated 700,000 to 1.2 million people worldwide annually.[1, 2] Cutaneous leishmaniasis is a treatable disease, and early diagnosis could decrease morbidity by preventing the development of large dermal lesions. Additionally, it could limit outbreaks caused by transmission *via* undiagnosed people.

Polymerase chain reaction (PCR) diagnosis of cutaneous leishmaniasis has high sensitivity and specificity, enabling identification to the species level and allowing species-specific treatment. Cutaneous leishmaniasis has been detected by kinetoplast DNA (kDNA)-targeted PCR with 98.7% sensitivity.[3] However, PCR tests require expensive equipment and trained personnel, limiting access for people in endemic regions with limited infrastructure. Cutaneous leishmaniasis can also be diagnosed using other conventional laboratory diagnostic methods like direct microscopy or culturing of skin specimens, although these methods are relatively insensitive and time-consuming, and require trained personnel.[1, 4, 5]

A promising alternative to PCR is recombinase polymerase amplification (RPA), an isothermal nucleic acid amplification method requiring minimal equipment and sample preparation. It works over a wide range of ambient temperatures making RPA valuable in low-resource settings, whereas PCR is restricted to a

laboratory equipped with thermal cyclers.[6, 7] The mechanism of RPA reaction is illustrated in Figure 3.1. RPA reaction mixtures are composed of several essential proteins: recombinase and single-strand DNA binding protein to substitute for the usual heat denaturation step in PCR and strand-displacing DNA polymerase to execute exponential DNA amplification. These proteins coordinate with accessory components such as a recombinase loading factor, crowding agent, energy/fuel components (e.g., adenosine triphosphate, ATP), and salt molecules to perform the RPA reaction.[8, 9] The RPA reaction starts with the binding of a recombinase (T4 UvsX) to the oligonucleotide primers and probes with the help of the loading factor (T4 UvsY). This forms a nucleoprotein filament that scans the double-stranded DNA template, searching for a homologous sequence. Once the homologous sequence is located, the filament invades the duplex DNA forming a D-loop structure to initiate a strand exchange reaction while a single-stranded DNA binding protein (T4 gp32) binds to the displaced DNA strand and stabilizes the resulting D loop. After this strand exchange reaction, the recombinase dissembles and becomes available to initiate another strand displacement reaction with a new pair of primers. The DNA polymerase then initiates the primer elongation from the free 3′-OH end of the primer. As the polymerization continues, strand synthesis occurs from both directions, and the two parental strands get separated, forming two duplexes of DNA. This results in the exponential accumulation of amplified duplex DNA, consisting of the sequence between the forward and reverse primers.[8-10]

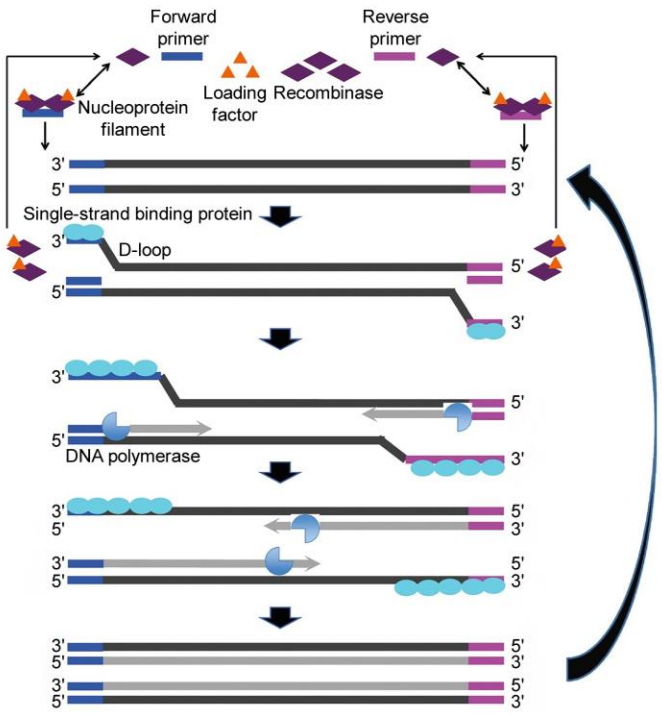

Figure 3.1. Mechanism of RPA reaction. The recombinase, assisted by the loading factor, binds with primers to form a nucleoprotein filament. The filament searches for a homologous sequence in the double-stranded DNA template. Once the homology is found, the filament invades the duplex DNA while the displaced DNA strand is stabilized by the binding of single-stranded DNA binding proteins. The recombinase then disassembles and DNA polymerase starts the DNA amplification from the 3′-OH end of the primers, subsequently resulting in two duplexes of DNA (Reproduced from reference 8 with permission from the Royal Society of Chemistry).

End-point RPA is most commonly read by lateral flow assay (LFA), which is a simple paper-based device used to detect analytes in POC settings.[7] End-point RPA combined with LFA detection was first demonstrated in 2006 in the detection of 10 copies of three methicillin-resistant *Staphylococcus aureus* isoforms (MRSA I-III) distinguishing them from methicillin-sensitive *Staphylococcus aureus*.[11, 12] Since then, RPA-LFA has been developed for the use in many fields including medical diagnostics,[11, 13, 14] food and agriculture industry,[11, 15, 16] and veterinary diagnostics[11, 17, 18]. Previously RPA-LFA was also applied to a field molecular test for detecting cutaneous *Leishmania Viannia spp*. infection using a gold nanoparticle-based LFA. These tests showed an analytical sensitivity equivalent to 0.1 parasites per reaction.[4] Furthermore, the diagnostic performance of an RPA-LFA for cutaneous leishmaniasis was demonstrated

using 118 patient samples in an endemic setting in Colombia and found 87% sensitivity and 86% specificity in the reference lab scenario and 75% sensitivity and 89% specificity in the field scenario.[19]

Here, we expanded on efforts to develop a highly sensitive and economical RPA-LFA by replacing gold nanoparticle LFA reporters with persistent luminescent nanophosphors. $[(Sr_{0.625}Ba_{0.375})_{1.96}Eu_{0.01}Dy_{0.03}]MgSi_2O_7$ (SBMSO) is a blue-emitting inorganic solid-state compound substituted with rare-earth ions Eu^{2+} and Dy^{3+}. When excited with UV/blue light, it emits long-lasting luminescence (>9 min) even after the termination of excitation. The long luminescence lifetime allows time-resolved measurements with a reduced excitation/autofluorescence background, thereby increasing sensitivity.[20] Compared to conventional LFA reporters like gold nanoparticles, organic fluorophores, and quantum dots, persistent luminescent nanophosphors have been shown to have enhanced sensitivity, resistance to photobleaching, and they also avoid the need for continuous excitation and expensive optical hardware.[21, 22] In this study, we have compared the sensitivity of SBMSO nanophosphors and commonly used gold nanoparticles in detecting cutaneous leishmaniasis by RPA-LFA. We have also combined smartphone-based imaging techniques with RPA-LFA to develop a user-friendly and straightforward POC test for cutaneous leishmaniasis.

3.2 Experimental Section

3.2.1 Recombinase Polymerase Amplification of *Leishmania Viannia*

All the evaluations were performed using purified DNA from *Leishmania (Viannia) panamensis* (HOM/COL/84/1099), which was isolated from a patient in Colombia and later delivered to the University of Texas Medical Branch at Galveston by Dr. Saravia (CIDEIM's *Leishmania* repository, Cali, Colombia). The design of RPA primers for amplifying the *Leishmania* kDNA minicircle conserved sequence has been described previously.[4] The biotinylated forward primer (5′-biotin-GATGAAAATGTACTCCCCGACATGCCTCTG-3′) and 5′-fluorescein (FAM) containing reverse primer

(5′-FAM-CTAATTGTGCACGGGGAGGCCAAAAATAGCGA-3′) were purchased from Integrated DNA Technologies, USA. Primer sequence specificity was confirmed by BLAST searches in the database of the *Leishmania Viannia* subgenus. End-point RPA reactions were carried out in a CFX OPUS Real-Time qPCR System (Bio-Rad) using TwistAmp Basic reagents (TwistDx) and labeled forward and reverse primers. It is important to note that the TwistAmp Basic kit was used instead of the TwistAmp nfo kit, which contains the nfo probe to reduce non-specific amplification[23] because it was not available in the market for purchase when these experiments were carried out. Betaine was added to the RPA reaction mixture to reduce non-specific amplification.[24, 25]

Briefly, each lyophilized RPA enzyme pellet was rehydrated with 29.5 µL of primer-free rehydration buffer and mixed with 2.5 µL of each primer (10 µM). 10 ng of purified *Leishmania* (kDNA) (~600 parasites/reaction) was used as the test sample, and 10 ng of Vero cell DNA (derived from green monkey kidney cells) was used as the negative control. The test samples and controls were prepared and diluted in nuclease-free water containing 3 M betaine (Sigma-Aldrich). Lastly, 2.5 µL of 280 mM magnesium acetate solution was added to each tube and mixed well to start the reaction, and the tubes were incubated at 40º C for 40 min. Then each 50 µL RPA reaction was divided into two 25 µL fractions and one fraction was purified with a silica membrane-based QIAquick PCR Purification Kit (Qiagen) according to the manufacturer's recommendation. The other fraction was left unpurified for further use. The amplified products were stored at -20 °C until use.

3.2.2 Gel Electrophoresis of Parasite DNA Amplicons

Amplicons were analyzed by a 1.5% agarose gel electrophoresis in 1X TAE (Tris/acetic acid/EDTA) buffer and visualized by 1000-fold dilution of SYBR Green I (Thermo Fisher Scientific) staining. 10 µL of the amplified product combined with 2 µL of 6X Gel Loading Dye, Purple (New England BioLabs Inc.) and 2 µL of pre-diluted SYBR Green I was incubated briefly and added to each well. The gel was run for ~1 hr

at 100 V. A Quick-Load 100 bp DNA ladder (New England BioLabs Inc.) was used to characterize the size of the amplicons.

3.2.3 Quantification of Parasite DNA Amplicons

Double-stranded DNA (dsDNA) in amplicons were quantified using the QuantiFluor dsDNA system (Promega). A Lambda dsDNA standard curve (0.05 - 200 ng/well) was prepared in 1X TE buffer according to the manufacturer's recommended protocol. The QuantiFluor dsDNA dye was diluted 1:400 in 1X TE buffer. A volume of 200 µL of QuantiFluor dsDNA dye was pipetted to each well of a multiwell plate (Corning 96-well flat black) intended for unknown, blank, or standard samples. 10 µL of the prepared dsDNA standards were added to each respective standard sample well, 10 µL of 1X TE buffer was added to the blank well, and 4 µL of 5X diluted unknown samples were added to each respective unknown sample well. The multiwell plate was covered with foil paper and was put on a plate shaker to mix the components in each well thoroughly. After 5 min, the fluorescence was measured at $504nm_{Ex}/531nm_{Em}$ using a plate reader (Tecan). Finally, the dsDNA concentration of unknown samples was estimated based on the lambda DNA standard curve.

3.2.4 Preparation of LFA Strips

LFA strips consisting of Standard 14 sample pad, FF80HP nitrocellulose membrane, and CF5 absorbent pad (Cytiva) were assembled on an adhesive backing card (MIBA-020; DCN Diagnostics). Test line (TL) and control line (CL) stripes were deposited on the nitrocellulose membrane with 1 mg/mL polyclonal goat anti-biotin antibodies (ab6643; abcam) and 1 mg/mL polyclonal goat anti-mouse antibodies (ABGAM-0500; Arista Biologicals, Inc.), respectively using a BioDot dispenser (XYZ30600124) at a rate of 1 µL/cm. The striped membrane was dried at 37 °C for 30 min in an incubator (Robbins Scientific Micro Hybridization Incubator 2000) and then cut into 3 mm wide strips using a ZQ2000 Guillotine Cutter (Kinbio).

3.2.5 Synthesis and Functionalization of SBMSO Reporters

Polycrystalline powder of $[(Sr_{0.625}Ba_{0.375})_{1.96}Eu_{0.01}Dy_{0.03}]MgSi_2O_7$ (SBMSO) was synthesized *via* high-temperature solid-state synthesis as described in our previous work.[22] Briefly, a stoichiometric hand-ground mixture of $SrCO_3$, $BaCO_3$, MgO, SiO_2, Eu_2O_3, and Dy_2O_3 with 5 wt.% H_3BO_3 was pressed into a pellet and heated at 1150 °C for 6 hrs in a reducing atmosphere of 5% H_2/95% N_2 with heating and cooling rates of 3 °C/min. The powder was then reground and sintered again at 1000 °C for 4 hrs with the same reducing atmosphere and ramp rates as the initial heating. The product's particle size was reduced by ball milling, and the particles of ~250 nm were isolated by differential centrifugal sedimentation in anhydrous ethanol. The particles were then silica-encapsulated using a modified Stöber process as described previously.[22] Briefly, a solution of 221.6 μL of anhydrous ethanol, 246.7 μL of DI water, and 6.7 μL of tetraethyl orthosilicate (TEOS) was added to 1 mL of SBMSO (2 mg/mL). The mixture was sonicated in a bath sonicator (Fisher Scientific FS30) for 5 min, and 25 μL of 30% aqueous ammonium hydroxide was added to the suspension, followed by sonication for another 30 min. Then, the tube with nanophosphors was placed on a room temperature rotator at 20 rpm for 7.5 hrs. Finally, the particles were washed three times with 1 mL of anhydrous ethanol.

The particles were then conjugated with antibodies by reductive amination chemistry.[22] 1 mL of silica-encapsulated nanophosphors dispersed in ethanol (2 mg/mL) in a 2 mL microcentrifuge tube was centrifuged for 3 min at 3000 rcf. The top 216 μL of the ethanol was removed, and 10 μL of a mixture of 155 μL of TEOS, 5 μL of triethoxysilylbutyraldehyde (TESBA), and 1393 μL of anhydrous ethanol was added to the nanophosphor solution, followed by 189 μL of DI water and 16.7 μL of aqueous ammonium hydroxide. The mixture was sonicated for 10 min in a bath sonicator and then placed on a room temperature rotator at 20 rpm for 12 hrs. The particles were then washed with 1 mL of anhydrous ethanol at least three times.

The nanophosphors were washed with DI water and then with PBS, pH 8. They were then re-suspended in 700 µL of PBS (pH 8) and sonicated for 5 min, and 50 µL of 1 mg/mL monoclonal mouse anti-FITC antibodies (ab112511; abcam) was added, and the solution was vortexed. A volume of 250 µL of 1 M $NaBH_3CN$ in PBS (pH 8) was added, and the solution was sonicated for 5 min and then placed on a room temperature rotator at 20 rpm for 2 hrs.

The nanophosphors were then washed once with PBS (pH 7.4) and re-suspended in 200 µL of PBS. For passivation, 750 µL of 80 mg/mL BSA in PBS (pH 7.4) and 50 µL of 1 M $NaBH_3CN$ was added to the nanophosphor suspension. After 5 min of sonication, nanophosphors were placed on a room temperature rotator at 20 rpm for 3 hrs followed by washing three times with PBS (pH 7.4). The nanophosphors were subsequently re-suspended in 100 µL of borate storage buffer (10 mM sodium borate, 150 mM NaCl, 0.1% BSA, 0.04% PVP-40 (40,000 avg. mol. wt.), 0.025% Tween 20, pH 8.5) and stored at 4 °C.

3.2.6 Detection of Parasite DNA Amplicons on Lateral Flow Assay

Serial dilutions of both purified and unpurified DNA amplicons were prepared and run on commercial gold nanoparticle-based LFA strips designed to detect biotin- and FITC-labeled amplicons (Milenia HybriDetect 1; TwistDx). 2 µL of DNA sample and 48 µL of manufacturer-supplied running buffer were added to the sample pad, and the colored bands were observed by eye after 5 min. The same dilution series of purified and unpurified DNA amplicons were run on lab-made LFA strips with SBMSO reporters. 2 µL of DNA sample, 5 µL of anti-FITC antibody-conjugated SBMSO nanophosphors (1 mg/mL) mixed with 43 µL of running buffer (50 mM NaCl, 0.1% Tween 20, 10 mM Tris HCl, 0.25% PVP-40, and 1% BSA, pH = 8) were added to the sample pad, and the strip was run for 20 min. The LFA strips were inserted in a 3-D printed attachment that can be attached to the smartphone and were illuminated and imaged using the "Luminostics" application on an iPhone 5S.[26] The images were analyzed using NIH ImageJ[27] by measuring the area under the peaks to calculate the TL/CL intensity ratio.[22]

Next, to demonstrate the feasibility of the smartphone-based RPA-LFA for point-of-care detection of cutaneous leishmaniasis, a dilution series of *Leishmania (V.) panamensis* DNA in nuclease-free water was run with RPA, varying the initial DNA amount from 10^{-4} - 10^{3} parasites/reaction using the protocol described in section 3.2.1. The unpurified DNA amplicons were run both on commercial LFA strips with gold nanoparticles and LFA strips with SBMSO reporters as described above. Finally, the limit of detection (LOD) for gold nanoparticle-based LFA was compared to the LOD for the SBMSO nanophosphor-based LFA.

3.3 Results and Discussion

3.3.1 Characterization of the *Leishmania Viannia panamensis* DNA Amplicons from RPA Reaction

The mitochondrial DNA of protist parasites of the class *Kinetoplastida* exists as a large nucleoid consisting of two circular, concatenated genomes; maxicircles (approximately 20 - 50 copies per parasite) and minicircles (10 - 20,000 copies per parasite).[28] *Leishmania* is a member of the *Kinetoplastida* class that contains ~10,000 kDNA minicircles per parasite, each comprising a conserved region of ~120 bp.[29, 30] This study used RPA primers targeting polyploid kDNA minicircles and amplifying the conserved region of *Leishmania (V.) panamensis*. Here, 10 ng of *Leishmania (V.) panamensis* DNA (~600 parasites/reaction) were used as the template, and 10 ng Vero cell DNA was used as the negative control. Gel electrophoresis of the purified and unpurified RPA reaction mixtures showed the amplicons at the expected size (~120 bp) and the absence of non-specific products or primer dimers (Figure 3.2). As expected, the unpurified amplicons in the RPA reaction mixture appeared as smears around the expected band on the gel (Figure 3.2, lane 3 and lane 4) since protein-DNA crowding agents in the RPA reaction mixture are known to affect amplicon migration.[7, 31] Lane 5 which contains Vero cell DNA did not show non-specific amplification. Therefore, we successfully performed RPA reactions using readily available basic RPA reagents, and adding 3 M betaine to the RPA reaction mixture helps to reduce non-specific amplification.

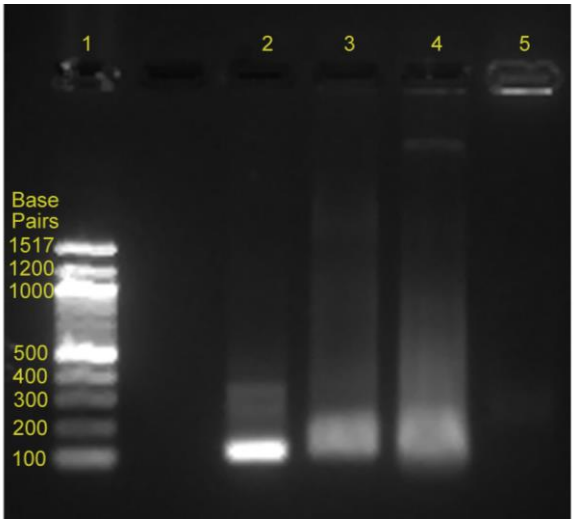

Figure 3.2. Agarose gel electrophoresis of RPA products. 10 ng of *Leishmania (V.) panamensis* DNA (~600 parasites/reaction) was used as the template, and 10 ng Vero cell DNA was used as the negative control. 10 µL of each RPA reaction was loaded on the gel. Lane: (1) DNA ladder (100 - 1517 bp), (2) Purified DNA amplicons, (3) Unpurified DNA amplicons sample 1, (4) Unpurified DNA amplicons sample 2, (5) Vero cell DNA amplicons.

3.3.2 Quantification of RPA Products

The purified and unpurified RPA products were quantified using the fluorescent dsDNA binding dye-based QuantiFluor dsDNA system. The dsDNA concentration of purified *Leishmania* DNA amplicons was estimated at 20.3 ng/µL and that of unpurified *Leishmania* DNA amplicons at 11.7 ng/µL based on a lambda dsDNA standard curve (Figure 3.3).

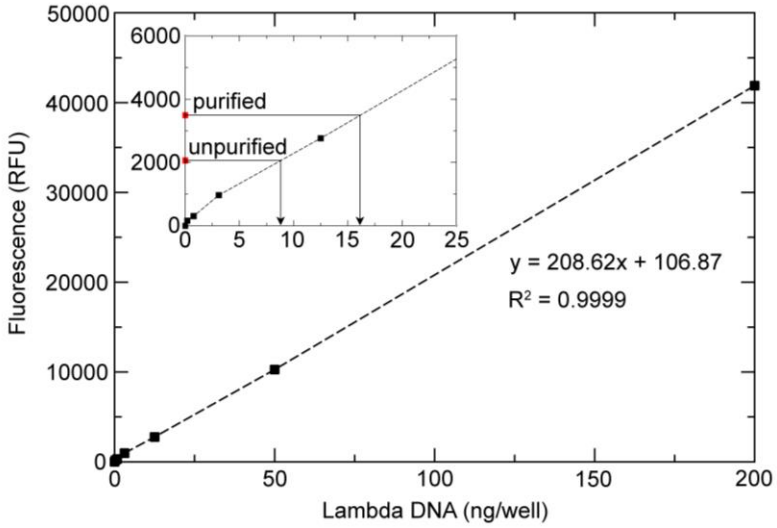

Figure 3.3. The dsDNA standard curve obtained from the QuantiFluor dsDNA system. The inset shows the fluorescence obtained for 4 µL of 5X diluted purified and unpurified RPA products (in red) and their respective dsDNA concentrations. According to the standard curve, the dsDNA amount of purified and unpurified samples is 16.23 and 9.37 ng/well, respectively. Therefore, the dsDNA concentration of the undiluted purified and unpurified amplicons is 20.3 and 11.7 ng/µL, respectively.

3.3.3 Detection of RPA Products by Lateral Flow Assay

RPA products were run on commercial gold nanoparticle-based LFA strips and lab-made LFA strips with SBMSO reporters and the LFA architecture is shown in Figure 3.4. The primers used were designed to label the DNA amplicons with fluorescein (FITC/FAM) and biotin for detection with monoclonal mouse anti-FITC antibody-conjugated reporter particles in the conjugate pad and capture on anti-biotin antibodies on the test line. The excess reporter particles are captured by the anti-mouse antibodies on the control line. Therefore, if the test is positive, LFA shows two lines on the membrane, whereas a negative test shows only a control line.

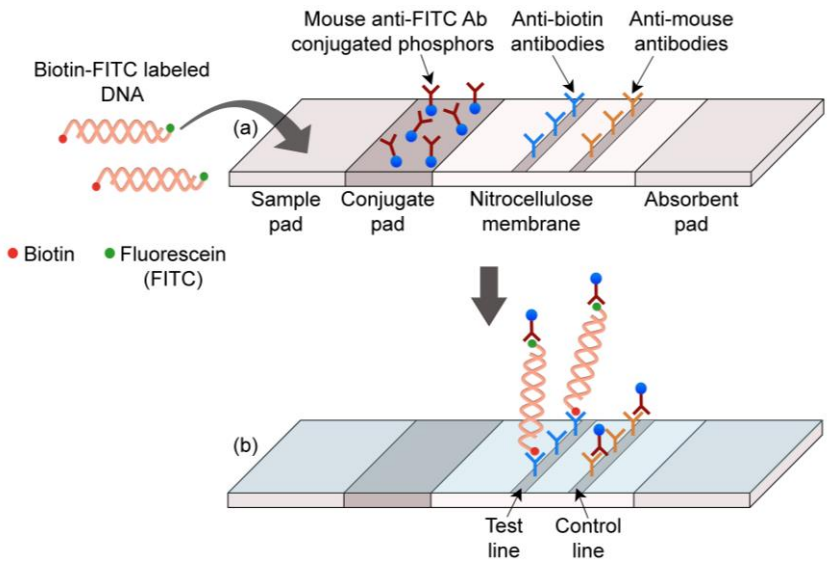

Figure 3.4. LFA architecture used to detect RPA products. (a) DNA amplicon labeled with biotin and FITC first binds with reporter particles conjugated with monoclonal mouse anti-FITC antibodies immobilized at the conjugate pad. (b) This complex then travels along the nitrocellulose membrane and binds with anti-biotin antibodies at the test line. Anti-mouse antibodies capture the excess reporters at the control line. Positive samples show two bands at the test and the control lines, and the negative samples show only a control line.

First, a dilution series of the purified RPA products were run with both gold nanoparticle-based LFA and SBMSO nanophosphor-based LFA. The LOD of gold nanoparticles for the purified RPA products was visually estimated to be 5 ng/mL (Figure 3.5a). The strips with SBMSO nanophosphors were imaged using an iPhone 5S (Figure 3.5b) and the LOD was estimated as the lowest concentration detected above the cutoff, which is the mean plus three times the standard deviation ($\mu+3\sigma$) of the blanks, no-analyte samples, as shown in Figure 3.5c. The LOD of purified RPA products with SBMSO nanophosphors was 0.05 ng/mL, 100-fold lower than that for gold nanoparticles. These results also show that anti-FITC antibody-conjugated SBMSO reporters can successfully bind with amplified *Leishmania* DNA in the RPA product.

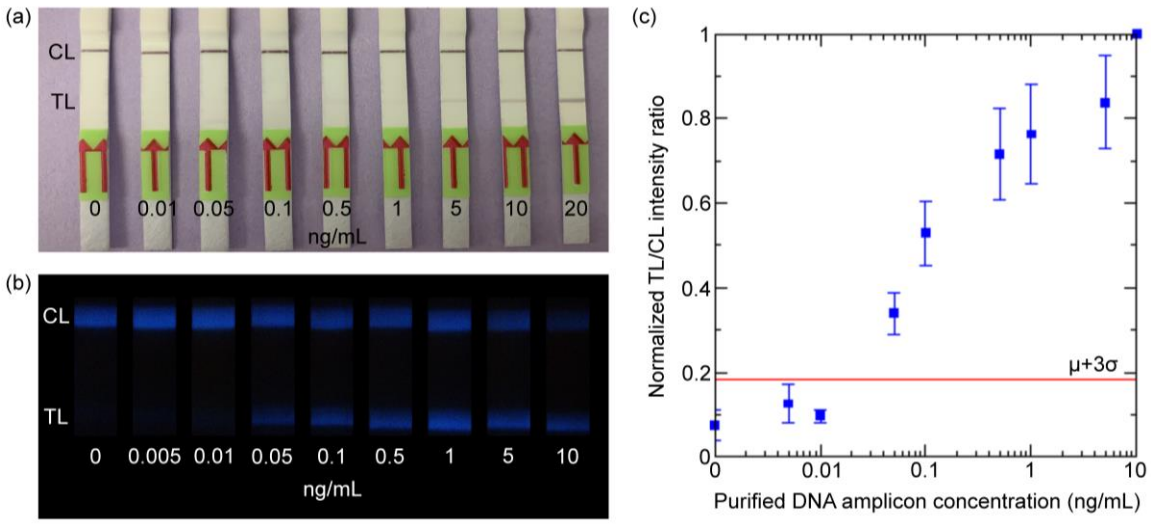

Figure 3.5. Detection of purified RPA products run on LFA strips. (a) Visual detection of purified RPA products run on commercial gold nanoparticle-based LFA strips. (b) Smartphone images of purified RPA products run on lab-made LFA strips with SBMSO nanophosphor reporters. (c) Normalized TL/CL intensity ratio of SBMSO reporters against the concentration of purified DNA amplicons. Three trials were run for each concentration, and the average was calculated. The red line signifies the detection limit cutoff taken as the mean plus three times the standard deviation (μ+3σ) of the no-analyte control tests.

Next, a dilution series of the unpurified RPA products was run with gold nanoparticles (Figure 3.6a) and SBMSO nanophosphors (Figure 3.6b). For the unpurified product, gold nanoparticles show the same LOD (5 ng/mL) as the purified product, although the test line bands are dimmer than the purified product. As plotted in Figure 3.6c, the SBMSO nanophosphors show a LOD of 0.1 ng/mL, 50-fold lower than with gold nanoparticles. SBMSO nanophosphors show less sensitivity in the detection of unpurified products compared to purified RPA products, potentially due to excess primers, proteins, and RPA reagents in the sample. However, these results show that the remaining RPA reaction mixture does not give substantial non-specific binding on LFA. This result is potentially very significant because it suggests the ability to use unpurified products from minimal volume RPA reactions, reducing complexity and cost.

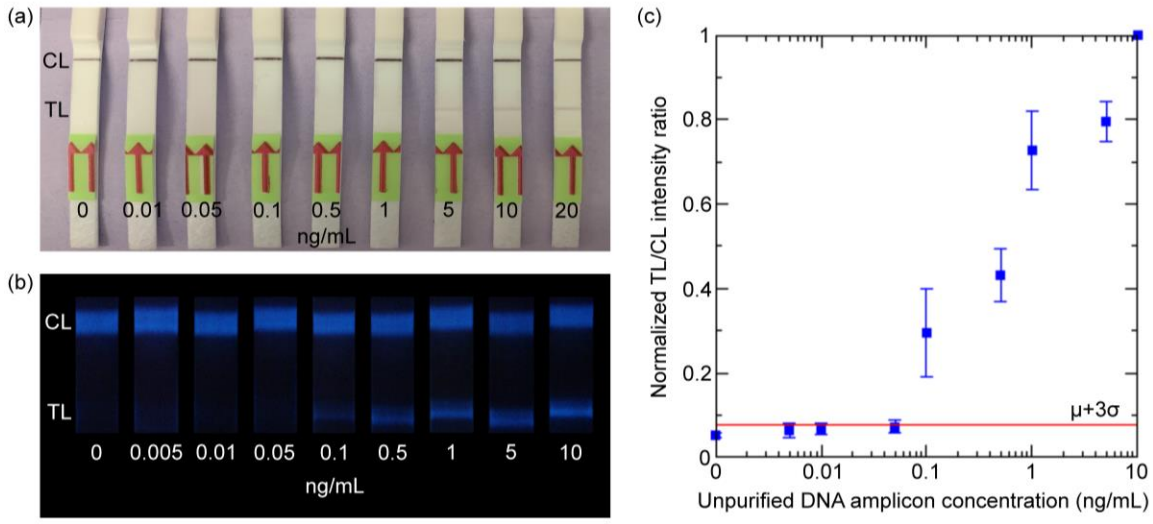

Figure 3.6. Detection of unpurified RPA products run on LFA strips. (a) Visual detection of unpurified RPA products run on commercial gold nanoparticle-based LFA strips. (b) Smartphone images of unpurified RPA products run on lab-made LFA strips with SBMSO nanophosphor reporters. (c) Normalized TL/CL intensity ratio of SBMSO reporters against the concentration of unpurified DNA amplicons. Three trials were run for each concentration, and the average was calculated. The red line signifies the detection limit cutoff taken as the mean plus three times the standard deviation (μ+3σ) of the no-analyte control tests.

As the next step, the feasibility of this assay for POC diagnosis of cutaneous leishmaniasis was tested by running RPA reactions with varying *Leishmania* parasite DNA concentrations ranging from 10^{-4} to 10^{3} parasites/reaction. The unpurified amplified products were run on gold nanoparticle-based LFA (Figure 3.7a) and SBMSO nanophosphor-based LFA (Figure 3.7b). The gold nanoparticles show a LOD of 1 parasite per reaction, while the SBMSO nanophosphors demonstrate the ability to detect 0.01 parasites per reaction (Figure 3.7c), making SBMSO nanophosphors 100-fold more sensitive in detecting *Leishmania* in unpurified RPA products. Therefore, these results indicate that the nanophosphor reporters are potential compounds to develop more sensitive, reliable, and cost-effective POC tests to diagnose infectious diseases.

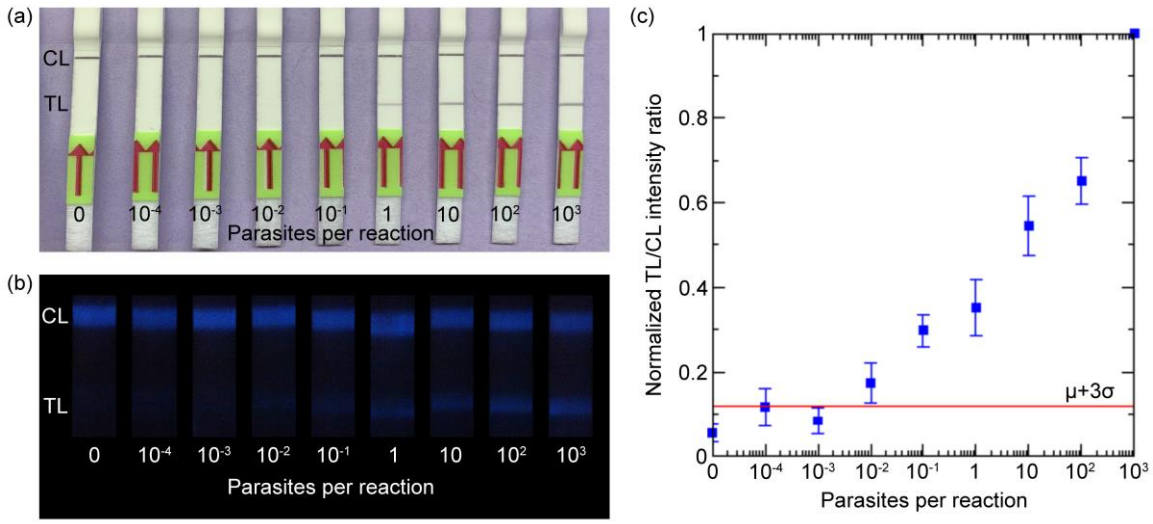

Figure 3.7. Detection of the amplicons of *Leishmania* parasite DNA dilution series run on LFA strips. (a) Visual detection of the amplicons of *Leishmania* parasite DNA dilution series run on commercial gold nanoparticle-based LFA strips. (b) Smartphone images of the amplicons of the *Leishmania* parasite DNA dilution series run on lab-made LFA strips with SBMSO nanophosphor reporters. (c) Normalized TL/CL intensity ratio of SBMSO reporters against parasites per RPA reaction. Three trials were run for each concentration, and the average was calculated. The red line signifies the detection limit cutoff taken as the mean plus three times the standard deviation (μ+3σ) of the no-analyte control tests.

3.4 Conclusions

The early detection of cutaneous leishmaniasis is essential to improve treatment effectiveness to decrease disease morbidity and avoid long-term complications. We have developed a smartphone-based LFA combined with recombinase polymerase amplification for rapid and sensitive detection of cutaneous leishmaniasis using $[(Sr_{0.625}Ba_{0.375})_{1.96}Eu_{0.01}Dy_{0.03}]MgSi_2O_7$ nanophosphors as reporters. The nanophosphor-based LFA shows 50 - 100 times greater sensitivity than gold-nanoparticle-based LFAs in detecting *Leishmania* DNA from RPA products. The high sensitivity of this method can be achieved using a minimal volume (2 μL) of the RPA reaction, allowing significant reduction of reagent usage, thereby reducing cost. Therefore, this approach is promising for the rapid, sensitive, and cost-effective POC detection of cutaneous leishmaniasis, especially in resource-limited settings. In the future, this approach can also be applied for more sensitive, reliable, and accurate diagnosis of other infectious diseases by using nanophosphor reporters as an alternative to conventional colorimetric reporters such as gold nanoparticles.

3.5 Acknowledgments

This work was funded in part by NIAID/NIH (Grants No. 1R43AI118180-01A1 and 1R01AR072742-01) and CDC (Grant No. 1U01CK000512-01 and Contract No. 200-2017-M-94591). The authors also acknowledge the NIH Rapid Acceleration of Diagnostics (RADx) Project. The authors thank Drs. Bruno L. Travi and Thomas Shelite at the University of Texas Medical Branch at Galveston for generously providing *Leishmania Viannia* parasite DNA. The authors also thank Drs. Andrew Paterson and Balakrishnan Raja, formerly in the RCW laboratory and now at Clip Health, for providing the "Luminostics" application for smartphone-based imaging.

Bibliography

(1) Mitropoulos, P.; Konidas, P.; Durkin-Konidas, M. New World Cutaneous Leishmaniasis: Updated Review of Current and Future Diagnosis and Treatment. *J. Am. Acad. Dermatol.* **2010**, *63* (2), 309–322.

(2) https://www.cdc.gov/parasites/leishmaniasis/epi.html (accessed November 5, 2021).

(3) Bensoussan, E.; Nasereddin, A.; Jonas, F.; Schnur, L. F.; Jaffe, C. L. Comparison of PCR Assays for Diagnosis of Cutaneous Leishmaniasis. *J. Clin. Microbiol.* **2006**, *44* (4), 1435–1439.

(4) Saldarriaga, O. A.; Castellanos-Gonzalez, A.; Porrozzi, R.; Baldeviano, G. C.; Lescano, A. G.; de Los Santos, M. B.; Fernandez, O. L.; Saravia, N. G.; Costa, E.; Melby, P. C.; Travi, B. L. An Innovative Field-Applicable Molecular Test to Diagnose Cutaneous *Leishmania Viannia Spp.* Infections. *PLoS Negl. Trop. Dis.* **2016**, *10* (4), e0004638.

(5) Vega-López, F. Diagnosis of Cutaneous Leishmaniasis. *Curr. Opin. Infect. Dis.* **2003**, *16* (2), 97–101.

(6) https://www.twistdx.co.uk/rpa/ (accessed November 15, 2021).

(7) Lobato, I. M.; O′Sullivan, C. K. Recombinase Polymerase Amplification: Basics, Applications and Recent Advances. *TrAC - Trends Anal. Chem.* **2018**, *98*, 19–35.

(8) Li, J.; Macdonald, J.; von Stetten, F. Review: A Comprehensive Summary of a Decade Development of the Recombinase Polymerase Amplification. *Analyst* **2019**, *144* (1), 31–67.

(9) Daher, R. K.; Stewart, G.; Boissinot, M.; Bergeron, M. G. Recombinase Polymerase Amplification for Diagnostic Applications. *Clin. Chem.* **2016**, *62* (7), 947–958.

(10) Li, J.; Macdonald, J. Advances in Isothermal Amplification: Novel Strategies Inspired by Biological Processes. *Biosens. Bioelectron.* **2015**, *64*, 196–211.

(11) Zhang, Y.; Hu, J.; Li, Q.; Guo, J.; Zhang, G. Detection of Microorganisms Using Recombinase Polymerase Amplification with Lateral Flow Dipsticks. In *Immunological Methods in Microbiology*; Pavia, C. S., Gurtler, V., Eds.; Academic Press, 2020; pp 319–349.

(12) Piepenburg, O.; Williams, C. H.; Stemple, D. L.; Armes, N. A. DNA Detection Using Recombination Proteins. *PLoS Biol.* **2006**, *4* (7), e204.

(13) Shelite, T. R.; Uscanga-Palomeque, A. C.; Castellanos-Gonzalez, A.; Melby, P. C.; Travi, B. L. Isothermal Recombinase Polymerase Amplification-Lateral Flow Detection of SARS-CoV-2, the Etiological Agent of COVID-19. *J. Virol. Methods* **2021**, *296*, 114227.

(14) Xia, S.; Chen, X. Single-Copy Sensitive, Field-Deployable, and Simultaneous Dual-Gene Detection of SARS-CoV-2 RNA via Modified RT–RPA. *Cell Discov.* **2020**, *6*, 37.

(15) Ivanov, A. V.; Safenkova, I. V.; Zherdev, A. V.; Dzantiev, B. B. Nucleic Acid Lateral Flow Assay with Recombinase Polymerase Amplification: Solutions for Highly Sensitive Detection of RNA Virus. *Talanta* **2020**, *210*, 120616.

(16) Ghosh, D. K.; Kokane, S. B.; Gowda, S. Development of a Reverse Transcription Recombinase Polymerase Based Isothermal Amplification Coupled with Lateral Flow Immunochromatographic Assay (CTV-RT-RPA-LFICA) for Rapid Detection of *Citrus tristeza* Virus. *Sci. Rep.* **2020**, *10*, 20593.

(17) Fan, J.; Chen, W.; Zhang, Y.; Liu, Z.; Li, X.; Ding, H.; Yi, L.; Chen, J.; Zhao, M. Development of a Reverse-Transcription Recombinase Polymerase Amplification Assay with a Lateral Flow Assay for Rapid Detection of Avian Orthoavulavirus 1. *J. Vet. Diagn. Invest.* **2021**, *33* (2), 308–312.

(18) Salazar, A.; Ochoa-Corona, F. M.; Talley, J. L.; Noden, B. H. Recombinase Polymerase Amplification (RPA) with Lateral Flow Detection for Three *Anaplasma* Species of Importance to Livestock Health. *Sci. Rep.* **2021**, *11*, 15962.

(19) Cossio, A.; Jojoa, J.; Castro, M. D. M.; Castillo, R. M.; Osorio, L.; Shelite, T. R.; Saravia, N. G.; Melby, P. C.; Travi, B. L. Diagnostic Performance of a Recombinant Polymerase Amplification Test—Lateral Flow (RPA-LF) for Cutaneous Leishmaniasis in an Endemic Setting of Colombia. *PLoS Negl. Trop. Dis.* **2021**, *15* (4), e0009291.

(20) Finley, E.; Cobb, A.; Duke, A.; Paterson, A.; Brgoch, J. Optimizing Blue Persistent Luminescence in $(Sr_{1-\delta}Ba_{\delta})_2MgSi_2O_7:Eu^{2+},Dy^{3+}$ via Solid Solution for Use in Point-of-Care Diagnostics. *ACS Appl. Mater. Interfaces* **2016**, *8* (40), 26956–26963.

(21) Paterson, A. S.; Raja, B.; Garvey, G.; Kolhatkar, A.; Hagström, A. E. V.; Kourentzi, K.; Lee, T. R.; Willson, R. C. Persistent Luminescence Strontium Aluminate Nanoparticles as Reporters in Lateral Flow Assays. *Anal. Chem.* **2014**, *86* (19), 9481–9488.

(22) Danthanarayana, A. N.; Finley, E.; Vu, B.; Kourentzi, K.; Willson, R. C.; Brgoch, J. A Multicolor Multiplex Lateral Flow Assay for High-Sensitivity Analyte Detection Using Persistent Luminescent Nanophosphors. *Anal. Methods* **2020**, *12* (3), 272–280.

(23) TwistDx; TwistAmp DNA Amplification Kits Assay Design Manual; TwistDx: United Kingdom, 2018; pp 22–26.

(24) Zou, Y.; Mason, M. G.; Botella, J. R. Evaluation and Improvement of Isothermal Amplification Methods for Point-of-Need Plant Disease Diagnostics. *PLoS One* **2020**, *15* (6), e0235216.

(25) Luo, G. C.; Yi, T. T.; Jiang, B.; Guo, X. L.; Zhang, G. Y. Betaine-Assisted Recombinase Polymerase Assay with Enhanced Specificity. *Anal. Biochem.* **2019**, *575*, 36–39.

(26) Paterson, A. S.; Raja, B.; Mandadi, V.; Townsend, B.; Lee, M.; Buell, A.; Vu, B.; Brgoch, J.; Willson, R. C. A Low-Cost Smartphone-Based Platform for Highly Sensitive Point-of-Care Testing with Persistent Luminescent Phosphors. *Lab Chip* **2017**, *17* (6), 1051–1059.

(27) Schneider, C. A.; Rasband, W. S.; Eliceiri, K. W. NIH Image to ImageJ: 25 Years of Image Analysis. *Nat. Methods* **2012**, *9* (7), 671–675.

(28) Simpson, L. The Genomic Organization of Guide RNA Genes in Kinetoplastid Protozoa: Several Conundrums and Their Solutions. *Mol. Biochem. Parasitol.* **1997**, *86* (2), 133–141.

(29) Degrave, W.; Fernandes, O.; Campbell, D.; Bozza, M.; Lopes, U. Use of Molecular Probes and PCR for Detection and Typing of *Leishmania* - a Mini-Review. *Mem Inst Oswaldo Cruz*. **1994**, *89* (3), 463–469.

(30) Kocher, A.; Valière, S.; Bañuls, A. L.; Murienne, J. High-Throughput Sequencing of kDNA Amplicons for the Analysis of *Leishmania* Minicircles and Identification of Neotropical Species. *Parasitology* **2018**, *145* (5), 585–594.

(31) Glais, L.; Jacquot, E. Detection and Characterization of Viral Species/Subspecies Using Isothermal Recombinase Polymerase Amplification (RPA) Assays. In *Plant Pathology Techniques and Protocols*, 2nd ed.; Lacomme, C., Ed.; Humana Press, 2015; pp 207–225.

CHAPTER 4

POINT-OF-CARE ANTIGEN AND SEROLOGICAL DETECTION OF HUMAN MONOCYTIC EHRLICHIOSIS INFECTION WITH CHEMILUMINESCENT LATERAL FLOW ASSAYS

4.1 Introduction

Human Monocytic Ehrlichiosis (HME) is an emerging life-threatening zoonosis in humans caused by *Ehrlichia chaffeensis*, an obligately intracellular bacterium. It is transmitted by the bite of the Lone Star tick (*Amblyomma americanum*) and has a clinical presentation ranging from a mild febrile illness to severe multi-organ system failure, making differential diagnosis challenging. HME was first reported in the United States in 1987, and since then, the number of cases reported to the Center for Disease Control (CDC) has increased steadily. It is now the most prevalent life-threatening tick-borne disease in the United States, with a predominant prevalence extending from the east coast, the south, and westward to Texas.[1-3]

HME prognosis is very favorable when the non-standard antibiotic doxycycline is administered early. Therefore, prompt diagnosis is vital and is often made using one of the several standard laboratory diagnostic methods, including detecting Ehrlichial DNA by polymerase chain reaction (PCR) and serological detection of specific antibodies using indirect immunofluorescence assay. However, the instrumentation required for these laboratory tests is not often readily available in small rural clinics that generally serve high-prevalence areas, leading to misdiagnosis or underdiagnosis.[1, 3] Access to a rapid point-of-care (POC) test would undoubtedly improve the diagnosis of HME. Fortunately, advances in the immunomolecular characterization of *Ehrlichia chaffeensis* revealed that *Ehrlichia* tandem repeat proteins (TRPs), which are major immunoreactive secreted effector proteins that are highly expressed and abundantly secreted extracellularly could provide an ideal target for POC diagnostics.[4, 5] More recently, McBride *et al*. discovered that proteins expressed by *Ehrlichia chaffeensis* in the tick host and injected into humans by tick bites produce a detectable serological response sufficiently early to be clinically actionable

upon detection. These proteins could also serve as the basis for developing accompanying POC diagnostics. Therefore, we developed two different types of lateral flow assays (LFAs): an antigen detection LFA for TRPs and an antibody detection LFA for the serological response to the tick-expressed protein (A9), using chemiluminescence-based reporters, as a proof-of-concept for the POC detection of HME.

Chemiluminescence-based immunoassays determine the concentration of analytes in a sample based on the intensity of the luminescence produced due to a chemical reaction. In recent years, chemiluminescence-based assays have gained increasing attention because, compared to other optical methods, chemiluminescence has a high signal-to-noise ratio, resulting in increased sensitivity. It also shows a wide linear range, enabling quantitative analysis. Moreover, readout instruments for chemiluminescent signals are simpler than most other optical readout systems.[6, 7] Several types of chemiluminescence methods have been incorporated into LFAs to develop simple, rapid, and sensitive tests for POC diagnostics.[8] This work used an indirect chemiluminescent method to establish two separate antigen detection LFAs for two different proteins: TRP 32 and 120, where the energy from a chemical reaction excites another luminescent material that acts as the reporter. For the antibody detection assay for A9 protein, we used enzyme-based reporting (HRP) as the label, which produces a chromogenic or a chemiluminescent signal depending on the substrate. The resulting pair of tests showed excellent capability in detecting HME based on an antigen or serological test.

4.2 Experimental Section

4.2.1 Development of Antigen Detection LFA

4.2.1.1 Preparation of LFA Strips

LFA strips with Standard 14 sample pad, FF80HP nitrocellulose membrane, and CF5 absorbent pad (Cytiva) were assembled on an adhesive backing card (MIBA-020; DCN Diagnostics). On the membrane, 2 mg/mL polyclonal rabbit anti-TRP 32 or anti-TRP 120 antibodies (provided by Dr. Jere McBride at the

University of Texas Medical Branch at Galveston) were striped on the test line (TL) and 1 mg/mL polyclonal goat anti-rabbit antibodies (ab6702; abcam) were striped on the control line (CL) using a BioDot dispenser (XYZ30600124) at a rate of 1 µL/cm. The striped membrane was dried at 37 ºC for 30 min in an incubator (Robbins Scientific Micro Hybridization Incubator 2000) and then cut into 4 mm wide strips using a ZQ2000 Guillotine Cutter (Kinbio).

4.2.1.2 Antibody Conjugation of Reporter Particles

The optical reporters used for TRP antigen detection were prepared by pipetting 25 µL of 0.2 µm 2% carboxylate-modified FluoSpheres (365/415) (Invitrogen) into a 2 mL microcentrifuge tube, followed by washing twice with 300 µL of 50 mM MES buffer, pH 5.8 (99%; Sigma-Aldrich), and centrifuging (Eppendorf Centrifuge 5418) at 15,000 rcf for 10 min and removing the supernatant. The particles were then re-suspended in 95 µL of 50 mM MES buffer (pH 5.8) and sonicated (Fisher Scientific FS30) for 5 - 10 min.

Solutions of 10 mg/mL N-(3-Dimethylaminopropyl)-N′-ethylcarbodiimide hydrochloride (EDC; commercial grade; Sigma-Aldrich) and 5 mg/mL N-Hydroxysuccinimide (NHS; 98%; Sigma-Aldrich) were freshly prepared in 50 mM MES buffer (pH 5.8). A volume of 2.34 µL of EDC and 18.4 µL of NHS were added to the particles, and the solution was put on a room temperature rotator at ~20 rpm for 30 min. After 30 min, the activation solution was removed by centrifuging at 15,000 rcf for 10 min and removing the supernatant. The particles were washed once with phosphate-buffered saline, pH 7.4 (PBS; Takara Bio) by centrifuging at 16,000 rcf for 10 min and removing the supernatant. The particles were re-suspended in 100 µL of PBS and the solution was sonicated for 5 - 10 min. Following sonication, 35 µg of polyclonal rabbit anti-TRP 32 or anti-TRP 120 antibodies were added to the particle solution and the solution was incubated on a rotator at room temperature for 3 hrs. The solution was removed by centrifuging at 16,000 rcf for 10 min and removing the supernatant once again. A volume of 300 µL of 4% bovine serum albumin

(BSA; 98%; Sigma-Aldrich) in PBS was subsequently added to the antibody-conjugated particles and the solution was put on a rotator at room temperature overnight. The solution was then removed by centrifuging at 16,000 rcf for 10 min and decanting the supernatant. The particles were washed three times by re-suspending the particles in 300 µL of PBS. Each time, the re-suspended particles were sonicated for 5 - 10 min and centrifuged at 16,000 rcf for 10 min, followed by removing the supernatant. Finally, antibody-conjugated particles were re-suspended in 100 µL of 1% BSA in PBS solution and stored at 4 °C.

4.2.1.3 Detection of TRPs using an LFA with Human Serum

Two different dilution series of TRP 32 and TRP 120 were prepared in PBS. 5 µL of each diluted TRP sample was mixed with 5 µL of 1 mg/mL anti-TRP antibody-conjugated reporter particles in 90 µL of 40% human serum. The particles and the serum were diluted in dilution buffer containing PBS (pH 7.4), 0.5% Tween 20 (molecular biology grade; Sigma-Aldrich) and 0.5% BSA. A volume of 80 µL of the mixed solution was then added to the sample pad. 12 mM bis(2,4,6-trichlorophenyl) oxalate (TCPO; 98%; Tokyo Chemical Industry Co., Ltd.) was prepared in 1:2 of tributyl O-acetylcitrate (98%; Sigma-Aldrich) and butyl benzoate (99%; Sigma-Aldrich). A 3% H_2O_2 solution was made in tert-butanol (99.5%; Sigma-Aldrich). Once the strips were dry, 50 µL of the glow reagent containing 1:1 of 12 mM TCPO and 3% H_2O_2 was added to each strip using a multichannel pipette. The strips were placed inside a lab-made 3-D printed dark box and imaged using the Pro mode of a Samsung Galaxy Note 8. The blue channel was separated and the TL/CL intensity ratio at each concentration was measured by integrating the area under the peaks using NIH ImageJ[9] software.

4.2.1.4 Detection of TRPs using an LFA with Whole Human Blood

To detect TRPs in whole human blood samples, the sample pads of the LFA strips were replaced with FR2 0.7 mm blood filters (mdi Membrane Technologies) to filter out red blood cells. A glass fiber conjugate pad (grade 8950; Ahlstrom-Munksjö) was used to immobilize antibody-conjugated reporter particles. A

solution of 5 µL of 1 mg/mL anti-TRP (32/120) antibody-conjugated reporter particles diluted in conjugate dilution buffer (PBS, 0.5% Tween 20, 1% BSA and 1% sucrose (99.5%; Sigma-Aldrich), pH 7.4) were spotted on the conjugate pad and let it dry overnight. A dilution series of TRPs (32/120) was prepared in PBS. 5 µL of each diluted TRP (32/120) sample was spiked into 45 µL of 40% whole human blood diluted in sample dilution buffer containing PBS (pH 7.4), 0.5% Tween 20 and 1% BSA. A volume of 40 µL of the mixed solution was added to the blood filter. After ~2 min, three washing steps were carried out with 80 µL of washing buffer containing PBS (pH 7.4), 0.5% Tween 20, and 0.1 mM hydroxylamine hydrochloride ($H_2NOH{\cdot}HCl$) (99%; Sigma-Aldrich). Once the strips were dry, 50 µL of the glow reagent (1:1 of 12 mM TCPO and 3% H_2O_2) was added to each strip using a multichannel pipette. The strips were placed inside a 3-D printed dark box and imaged using the Pro mode of the Samsung Galaxy Note 8. The blue channel was separated, and the TL/CL intensity ratio of each concentration was measured by integrating the area under the peaks using NIH ImageJ software.

4.2.2 Development of Antibody Detection LFA

4.2.2.1 Preparation of LFA Strips

LFA strips with Standard 14 sample pad and conjugate pad, Fusion 5 glass fiber membrane, and CF7 absorbent pad (Cytiva) were assembled on an adhesive backing card (MIBA-020; DCN Diagnostics). A tick-expressed protein called A9 that produces a serological response in patients at the early stage of HME was initially provided by Dr. Jere McBride at the University of Texas Medical Branch at Galveston and later produced in-house by Suman Nandy using *in-vitro* transcription and translation. The A9 protein and polyclonal goat anti-rabbit antibodies (ab6702; abcam) were mixed with 50 mM sodium acetate buffer, pH 3.8 (99%; Sigma-Aldrich) in 1:1 ratio and striped on the test line (1.5 mg/mL) and control line (1 mg/mL), respectively using the BioDot dispenser (XYZ30600124) at a rate of 1 µL/cm. The striped membrane was dried at 37 ºC for 30 min in an incubator (Robbins Scientific Micro Hybridization Incubator 2000) and then cut into 4 mm wide strips using a ZQ2000 Guillotine Cutter (Kinbio). 10 µL of goat anti-rabbit antibody-

conjugated HRP reporters (7074; Cell Signaling Technology) diluted 1:50 in 1% BSA in PBS was immobilized on the conjugate pad, and the strips were dried overnight.

4.2.2.2 Detection of Anti-A9 Antibodies using LFA with Human Serum

The initial antibody detection assay was developed using polyclonal anti-A9 antibodies provided by Dr. Jere McBride at the University of Texas Medical Branch at Galveston that were generated in rabbits and purified using the Melon gel IgG spin purification kit (Catalog no. 45206; Thermo Fisher Scientific). A dilution series of anti-A9 antibodies was prepared in PBS. 10 µL of diluted anti-A9 antibodies was spiked into 90 µL of 30% human serum diluted in dilution buffer containing PBS (pH 7.4), 1% Tween 20, 1% Triton X-100 (Sigma-Aldrich), 0.5% Polyethylene Glycol (PEG; 3350 avg. mol. wt.; Sigma-Aldrich) and 1% BSA. The mixed solution was added to the sample pad. The strips were then washed twice by adding 100 µL of washing buffer containing PBS (pH 7.4) and 0.5% Tween 20 in 3 min intervals. Next, 50 µL of the Pierce 1-step ultra TMB blotting solution (Thermo Scientific) was added to the membrane and the development of color at the test line and control line was observed. The experiment described above was repeated to compare the chromogenic signal with the chemiluminescent signal, but instead of adding TMB, a luminol mixture was added as the substrate for HRP. The luminol mixture was prepared by mixing Lumigen ECL Ultra (TMA-6) solution A and B in 1:1 ratio. The chemiluminescent signal was imaged on the FluorChem imaging system (Alpha Innotech).

4.2.2.3 Detection of Anti-A9 Antibodies in Clinical Samples

The feasibility of the antibody detection assay for human anti-A9 antibodies was investigated by analyzing 24 clinical human serum samples provided by Dr. Jere McBride at the University of Texas Medical Branch at Galveston. The A9 protein and protein A (AGPTA-0101; Arista Biologicals, Inc) were mixed with 50 mM sodium acetate buffer (pH 3.8) in 1:1 ratio and spotted on the test line (1.5 mg/mL) and control line (1 mg/mL), respectively. First, 20 µL of serum sample was mixed with 80 µL of dilution buffer containing

PBS (pH 7.4), 1% Tween 20, 1% Triton X-100, 0.5% PEG 3350, and 2% BSA, and the mixed solution was added to the sample pad. The strips were washed twice with 100 µL of washing buffer containing PBS (pH 7.4) and 0.5% Tween 20. 100 µL of goat anti-human antibody-conjugated HRP reporters (ab6858; abcam) diluted 1:20,000 in 2% BSA in PBS were added to the conjugate pad. The anti-human antibody conjugated HRP reporters were not pre-immobilized on the conjugate pad since further optimization of the reporter concentration might be required. Another washing was carried out by adding 100 µL of the washing buffer. 50 µL of the TMB blotting solution was added to the membrane, and the development of color at the test line and control line was observed. The images of the strips were taken by iPhone XS, and the intensity of the TL and CL was measured by integrating the area under the peaks using NIH ImageJ software. The TL/CL intensity ratio was calculated, and statistical analysis was done by generating a receiver operating characteristic (ROC) curve using IBM SPSS Statistics software.

4.3 Results and Discussion

4.3.1 Antigen Detection LFA

The architecture of a sandwich antigen detection assay is illustrated in Figure 4.1. When the sample containing TRP is added to the sample pad, it migrates to the conjugated pad and binds with anti-TRP antibodies conjugated to reporter particles. This complex then travels along the nitrocellulose membrane and at the test line, makes a sandwich complex between anti-TRP antibodies conjugated to reporters and the capture anti-TRP antibodies immobilized at the test line. Any excess labeled rabbit anti-TRP antibodies bind with anti-rabbit antibodies at the control line. The positive test shows two colored lines at the test line and the control line, whereas a negative test shows only one colored line at the control line.

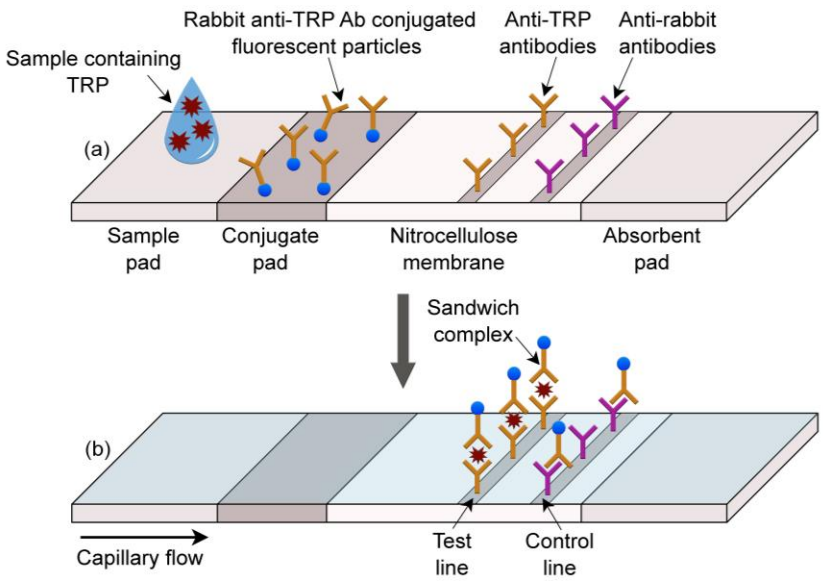

Figure 4.1. The architecture of sandwich antigen detection LFA for HME protein TRP 32 or TRP 120. (a) The TRP in the sample travels to the conjugate pad and binds with rabbit anti-TRP antibody-conjugated reporter particles. (b) This analyte-antibody-reporter complex then travels to the nitrocellulose membrane and binds with anti-TRP antibodies at the test line. Anti-rabbit antibodies capture any excess reporters at the control line. Positive samples show two bands at the test line and the control line, and the negative samples show only one band at the control line.

4.3.1.1 Detection of TRPs in Human Serum

Two separate sandwich antigen detection LFAs were developed to detect TRP 32 and 120 in human serum. When running serum samples, instead of using a conjugate pad, the antibody-conjugated reporter particles were added to the sample pad along with the sample. After running the strips, the glow reagent (TCPO + H_2O_2) was added to the strips, followed by smartphone imaging to detect the presence of the chemiluminescent reporter. TCPO and H_2O_2 react to produce peroxy acid ester (or 1,2-dioxetanedione), which breaks down spontaneously due to its instability, releasing CO_2. The fluorescent dye reporters absorb the energy produced upon decomposition, exciting the molecule. As the dye relaxes to the electronic ground state, photons are emitted, resulting in a colorful, long-lasting emission[10, 11] that can be imaged using a smartphone camera.

A smartphone image of LFAs of a TRP 32 dilution series in 40% human serum is shown in Figure 4.2a, and its blue channel image separated by ImageJ is shown in Figure 4.2b. The plot of TL/CL intensity ratio against TRP 32 concentration is shown in Figure 4.2c. Triplicates were run for each TRP 32 concentration, and the limit of detection (LOD) was calculated using the cutoff, mean plus three times the standard deviation of no-analyte samples (μ+3σ). The LOD of TRP 32 in 40% serum was between 0.5 ng/mL - 1 ng/mL.

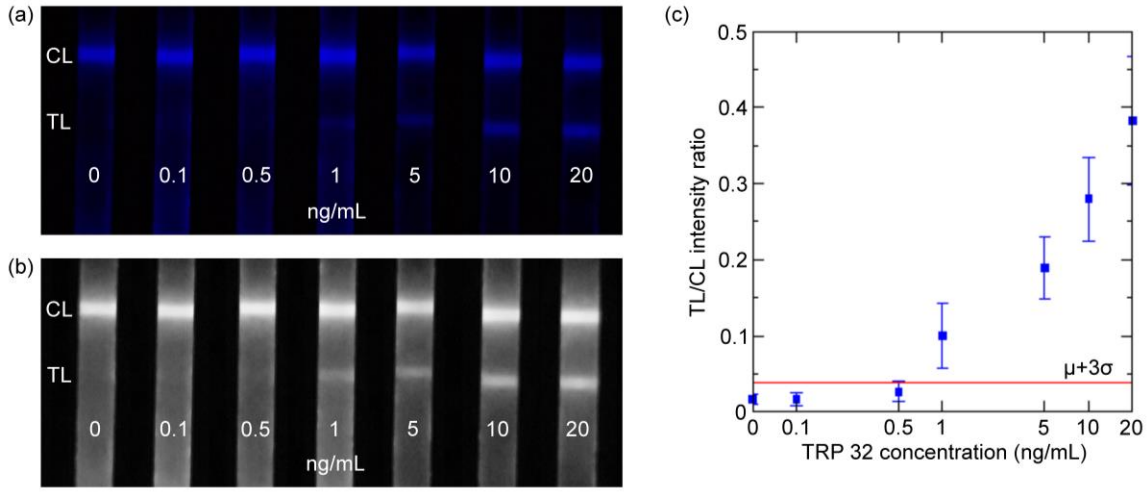

Figure 4.2. Detection of TRP 32 in 40% human serum. (a) Smartphone image of the LFAs of TRP 32 dilution series. (b) The blue channel image of the TRP 32 dilution series in (a) separated by ImageJ. (c) The plot of TL/CL intensity ratio vs. TRP 32 concentration (The limit of detection taken as the μ+3σ of the no-analyte samples is shown by the red line).

Similarly, a smartphone image of LFAs of a TRP 120 dilution series in 40% human serum is shown in Figure 4.3a and its blue channel image separated by ImageJ is shown in Figure 4.3b. The LOD of TRP 120 was between 1 ng/mL - 5 ng/mL as shown in Figure 4.3c. These results indicate that this smartphone-based chemiluminescent LFA can be used successfully to detect TRPs in serum. It is also important to note that this sandwich LFA is designed using polyclonal antibodies for both detection and capture antibodies, which helps reduce the assay's cost. Therefore, this system can be further developed for simple, fast, and cost-effective POC detection of HME.

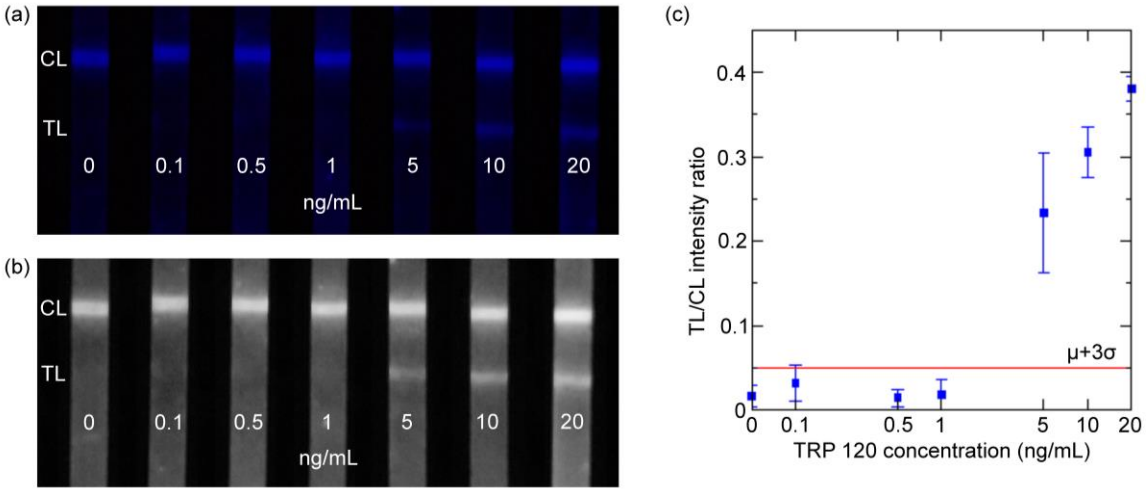

Figure 4.3. Detection of TRP 120 in 40% human serum. (a) Smartphone image of the LFAs of TRP 120 dilution series. (b) The blue channel image of the TRP 120 dilution series in (a) separated by ImageJ. (c) The plot of TL/CL intensity ratio vs. TRP 120 concentration (The limit of detection taken as the μ+3σ of the no-analyte samples is shown by the red line).

4.3.1.2 Detection of TRPs in Whole Human Blood

LFA strips were then constructed to detect the TRPs in blood samples. This involved adding a blood filter to remove the red blood cells before the membrane, as shown in Figure 4.4a.[12] The samples were run in 40% blood and once the glow reagent was added to the strips, the bands were not initially visible, or they were blurry (Figure 4.4b). This is likely due to the degradation of H_2O_2 in the glow reagent by the catalase enzyme in the blood. Therefore, the strips were washed three times with 80 μL of washing buffer containing 0.1 mM $HONH_2 \cdot HCl$, which acts as a catalase inhibitor,[13] and then the bands were easily visible, as shown in Figure 4.4c.

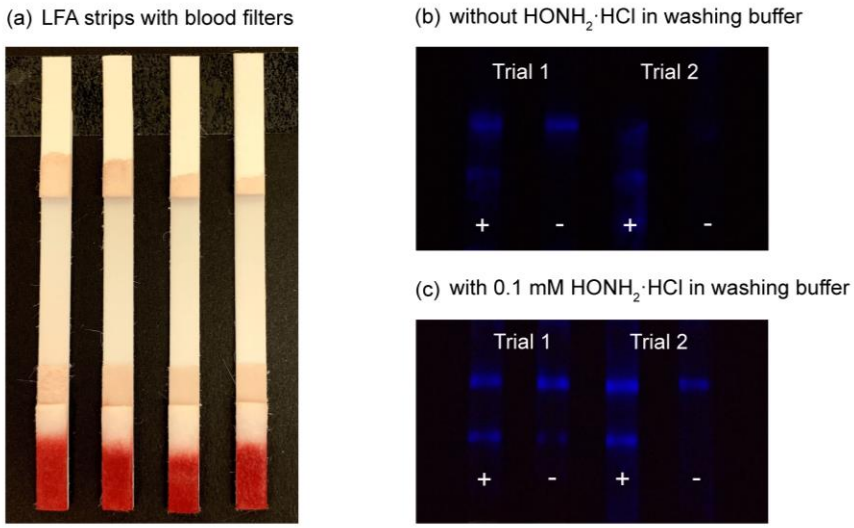

Figure 4.4. Modifications of the LFA to detect TRPs in whole human blood. (a) A blood filter at the beginning of each strip traps the red blood cells, and only the serum runs along the nitrocellulose membrane. (b) When the glow reagent is added to the LFA strips with blood, the bands are not clearly visible or blurred. (c) Adding catalase inhibitor (0.1 mM $HONH_2 \cdot HCl$) in the washing buffer helps to obtain clearer bands.

After running a dilution series of TRP 32 and TRP 120 in 40% whole human blood, the strips were imaged using the smartphone and the blue channel was separated to measure the TL/CL intensity ratio at each concentration using ImageJ. The plot of TL/CL intensity ratio vs. TRP 32 concentration is shown in Figure 4.5a and it shows the LOD between 0.5 ng/mL - 1 ng/mL. Figure 4.5b shows the TL/CL intensity ratio vs. TRP 120 concentration, and the LOD is between 1 ng/mL - 5 ng/mL. The initial results indicate that this LFA format using chemiluminescent optical reporters works in serum and blood with similar limits of detection. Further experiments need to be done to better understand the matrix effect of the whole blood. The antigen detection directly from blood samples helps to reduce the sample preparation time and cost. Therefore, this LFA is well-suited to be developed as a fast, reliable, and cheap POC test for HME antigen detection.

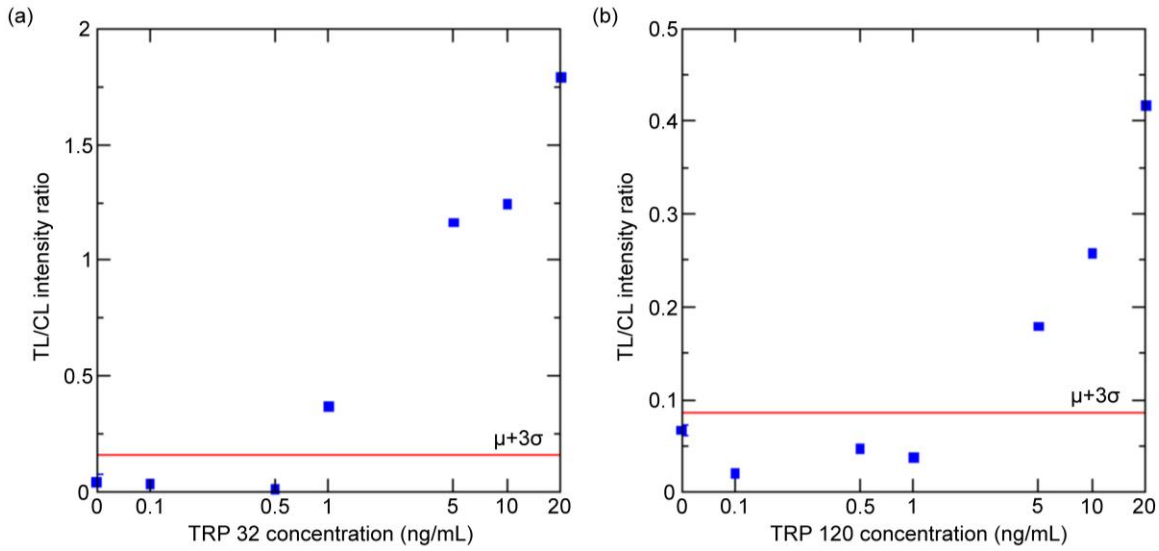

Figure 4.5. Detection of TRP 32 and TRP 120 spiked in 40% whole human blood. TL/CL intensity ratios (n=1) at different (a) TRP 32 and (b) TRP 120 concentrations. Triplicates were run for the blank sample to determine the detection limit cutoff (the red line), which is the mean plus three times the standard deviation (μ+3σ) of the no-analyte samples.

4.3.2 Antibody Detection LFA

4.3.2.1 Detection of Anti-A9 Antibodies in Human Serum

The antibody detection assay was initially developed to test purified polyclonal anti-A9 antibodies generated in rabbits to test the specific binding between the A9 protein immobilized on the membrane and anti-A9 antibodies in the sample. A9 protein of 3 mg/mL and anti-rabbit antibodies of 2 mg/mL were mixed with 50 mM sodium acetate buffer (pH 3.8) in 1:1 ratio to immobilize on test line and control line of the Fusion 5 glass fiber membrane, respectively (final concentration on the test line = 1.5 mg/mL and the control line = 1 mg/mL). Fusion 5 membrane is hydrophilic and non-protein binding, and it has a permanent negative charge. Therefore, proteins are mixed with a low pH buffer to make them positively charged, which results in the adhesion of the protein to the membrane.[14] The architecture of the antibody detection assay is shown in Figure 4.6. Anti-A9 antibodies were spiked into the human serum to study any matrix effect.

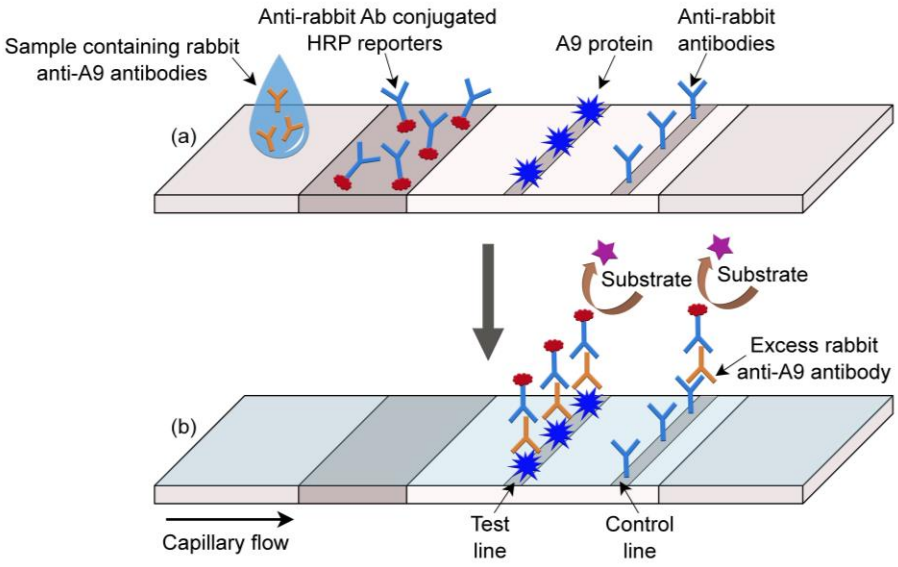

Figure 4.6. LFA architecture of the antibody detection assay developed in the rabbit system. (a) When the sample containing rabbit anti-A9 antibodies is applied to the sample pad, they bind with anti-rabbit antibody-conjugated HRP reporters at the conjugate pad. (b) This complex binds with the A9 protein on the test line *via* anti-A9 antibodies. Any excess rabbit anti-A9 antibodies bind with anti-rabbit antibodies at the control line. Upon the addition of the substrate, a signal appears at the test line and the control line if the sample is positive, whereas a signal appears only at the control line if the sample is negative.

A dilution series of rabbit anti-A9 antibodies in 30% human serum was run, and TMB blotting solution was added as the substrate for HRP for chromogenic detection. According to visual observation, the results provided in Figure 4.7a suggest the LOD is ~1 µg/mL. The experiment was repeated using the same dilution series, and then the luminol mixture was added as the substrate for HRP to generate a chemiluminescent signal. FluorChem images of the strips are shown in Figure 4.7b, revealing a visual LOD of ~500 ng/mL. The chemiluminescent signal has a better sensitivity than the chromogenic signal. In these tests, the control line is faint or invisible at low concentrations since the sample doesn't have enough excess rabbit anti-A9 antibodies to bind with anti-rabbit antibodies at the control line.

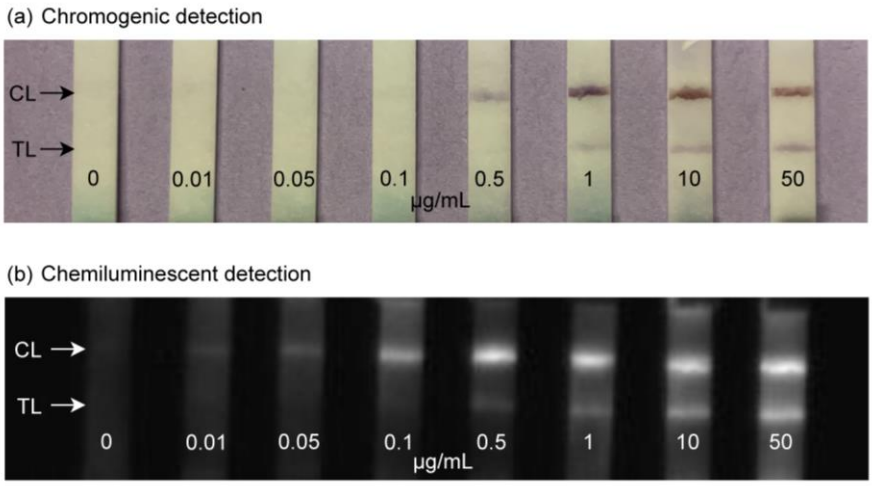

Figure 4.7. Comparison of chromogenic detection vs. chemiluminescent detection. (a) TMB was added as the substrate for HRP, and the visual LOD is ~1 µg/mL. (b) The luminol mixture was added as the substrate for HRP. The FluorChem image shows a visual LOD of ~500 ng/mL.

4.3.2.2 Detection of Anti-A9 Antibodies in Clinical Samples

After confirming the specific binding of anti-A9 antibodies with A9 protein, the assay was modified and used to test human anti-A9 antibodies in clinical human serum samples. The architecture of the antibody detection LFA used is shown in Figure 4.8. When the serum-containing anti-A9 antibodies are added to the sample pad, they migrate to the conjugate pad and bind with anti-human antibody-conjugated HRP reporters. This complex then binds with the A9 protein immobilized at the test line. The human antibodies in serum then bind with protein A at the control line. Protein A was used as the control line as it strongly binds with human IgG[15] and generates a strong signal at the control line, and also it's inexpensive. If the sample is positive, upon adding the substrate of HRP, it produces color at both the test and control lines, whereas if the sample is negative, it generates only one line at the control line.

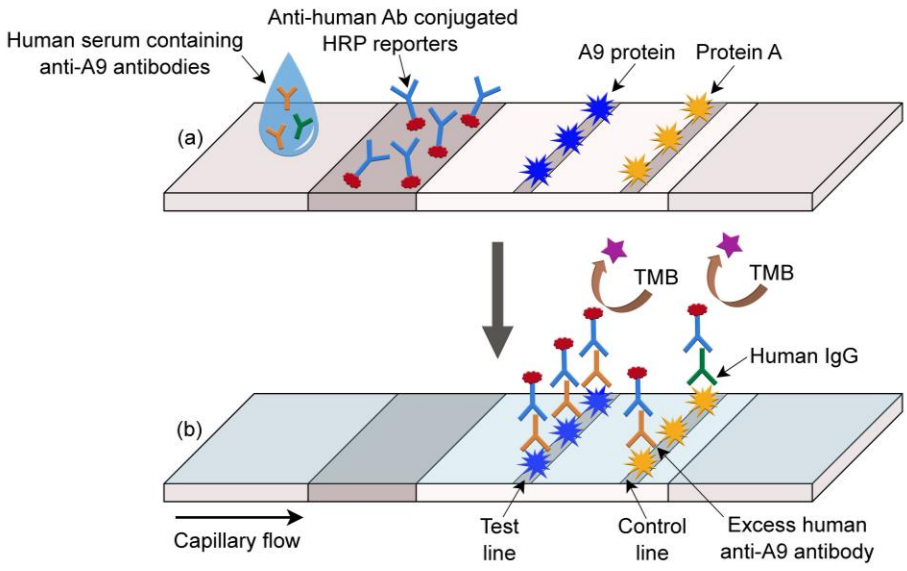

Figure 4.8. LFA architecture of the antibody detection assay adapted to test human samples. (a) When the human serum containing anti-A9 antibodies is applied to the sample pad, they bind with anti-human antibody-conjugated HRP reporters at the conjugate pad. (b) This complex binds with the A9 protein at the test line *via* anti-A9 antibodies. Human antibodies in the serum bind with protein A at the control line. Upon adding the substrate (TMB), positive samples give two bands at the test line and the control line and negative samples give one band only at the control line.

A small number of clinical serum samples (N = 24) were tested using the developed antibody detection LFA and 20/24 samples are in good agreement with ELISA results, resulting in 89.5% sensitivity and 60% specificity, as demonstrated in Table 4.1. A statistical analysis of the clinical data was done by generating a receiver operating characteristic (ROC) curve, which is a plot of sensitivity vs. 1-specificity or true positive rate vs. false positive rate of the test (Figure 4.9). The area under the curve (AUC) of the ROC curve indicates the diagnostic accuracy of the test, and it can have values from 0 to 1. A value of 0 indicates a perfectly inaccurate test, whereas a value of 1 indicates a perfectly accurate test. A value of 0.5 represents a random chance assay, which has no discriminatory ability. A functional test shows a value between 0.5 and 1. As the diagnostic test accuracy improves, the AUC approaches 1.[16, 17] The AUC of the ROC curve obtained from IBM SPSS software was 0.947, which indicates that this test is indeed valid. In these preliminary tests, TMB substrate was added for the signal generation to ease signal detection. This assay can be modified to generate a chemiluminescent signal to achieve better sensitivities and combined with a

smartphone-based chemiluminescent detection system to make it a more reliable and user-friendly POC test.

Table 4.1. The 2X2 table obtained from the initial clinical sample testing (TP = True Positive, FP = False Positive, FN = False Negative, TN = True Negative).

	Gold Standard (ELISA)		
Test	Positive	Negative	Total
Positive	TP = 17	FP = 2	TP + FP = 19
Negative	FN = 2	TN = 3	FN + TN = 5
Total	TP + FN = 19	FP + TN = 5	N = 24

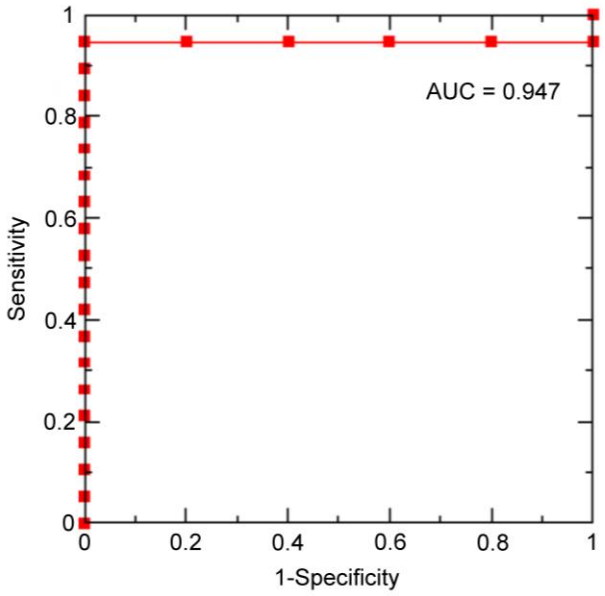

Figure 4.9. The ROC curve generated from the initial clinical data to determine the diagnostic accuracy of the test. The area under the curve (AUC) is 0.947, indicating that this test can potentially be used for the serological detection of HME. (AUC = 1 represents a perfect test).

4.4 Conclusions

In this work, we developed two different types of LFAs: antigen detection and antibody detection, as a proof-of-concept for the POC testing of HME. The antigen detection LFA was created using two types of tandem repeat proteins, and a chemiluminescence-based reaction of TCPO and H_2O_2 was used to generate the signal. The signal detection was done using smartphone-based techniques revealing limits of detection of <1 ng/mL and <5 ng/mL for TRP 32 and TRP 120, respectively, in human serum and whole human blood. It shows that TRPs are valuable targets for developing POC rapid diagnostic tests for the detection of HME. These tests can also be made simple and user-friendly by combining the LFA with smartphones. The antibody detection LFA was developed using a tick-expressed protein, A9, which gives a human serological response at the earlier stage of the disease. HRP was used as the reporter with the chromogenic and chemiluminescent signals compared by adding TMB and luminol mixture as the substrate, respectively. Although the chemiluminescent signal showed enhanced sensitivity, chromogenic detection was used for the initial analysis of clinical samples because of the ease of signal detection. The 20/24 samples show agreement with ELISA results, and the ROC curve indicates an AUC of 0.947, implying this is a likely useful test for serological detection of HME. Therefore, the A9 protein can be used for the early diagnosis of HME in POC settings. In the future, this antibody detection LFA can be further developed by using chemiluminescent signal detection methods to obtain more reliable results with high sensitivity.

4.5 Acknowledgements

This work was funded in part by NIAID/NIH (Grant No. 1R43AI118180-01A1 and 1R01AR072742-01) and CDC (Grant No. 1U01CK000512-01 and Contract No. 200-2017-M-94591). The authors also acknowledge the NIH Rapid Acceleration of Diagnostics (RADx) Project. The authors thank Dr. Jere McBride and Jignesh Patel at the University of Texas Medical Branch at Galveston for excellent collaboration and providing the protein targets and clinical samples. The authors also thank Suman Nandy for producing A9 protein by *in-vitro* transcription and translation, Dr. Binh Vu and Kristen Brosamer for

supporting with glow reagents and imaging, and Dr. Katerina Kourentzi for the help in clinical sample testing.

Bibliography

(1) Ismail, N.; Bloch, K. C.; McBride, J. W. Human Ehrlichiosis and Anaplasmosis. *Clin. Lab. Med.* **2010**, *30* (1), 261–292.

(2) https://www.cdc.gov/ehrlichiosis/stats/index.html (accessed December 3, 2021).

(3) Abusaada, K.; Ajmal, S.; Hughes, L. Successful Treatment of Human Monocytic Ehrlichiosis with Rifampin. *Cureus* **2016**, *8* (1), e444.

(4) Luo, T.; Zhang, X.; McBride, J. W. Major Species-Specific Antibody Epitopes of the *Ehrlichia chaffeensis* p120 and *E. canis* p140 Orthologs in Surface-Exposed Tandem Repeat Regions. *Clin. Vaccine Immunol.* **2009**, *16* (7), 982–990.

(5) Luo, T.; Patel, J. G.; Zhang, X.; Walker, D. H.; McBride, J. W. *Ehrlichia chaffeensis* and *E. canis* Hypothetical Protein Immunoanalysis Reveals Small Secreted Immunodominant Proteins and Conformation-Dependent Antibody Epitopes. *npj Vaccines* **2020**, *5* (1), 85.

(6) Wu, J.; Ju, H. X. Clinical Immunoassays and Immunosensing. In *Comprehensive Sampling and Sample Preparation*; Pawliszyn, J., Ed.; Academic Press, 2012; pp 143–167.

(7) Zhu, X.; Gao, T. Spectrometry. In *Nano-Inspired Biosensors for Protein Assay with Clinical Applications*; Li, G., Ed.; Elsevier, 2019; pp 237–264.

(8) Nguyen, V. T.; Song, S.; Park, S.; Joo, C. Recent Advances in High-Sensitivity Detection Methods for Paper-Based Lateral-Flow Assay. *Biosens. Bioelectron.* **2020**, *152*, 112015.

(9) Schneider, C. A.; Rasband, W. S.; Eliceiri, K. W. NIH Image to ImageJ: 25 Years of Image Analysis. *Nat. Methods* **2012**, *9* (7), 671–675.

(10) Delafresnaye, L.; Bloesser, F. R.; Kockler, K. B.; Schmitt, C. W.; Irshadeen, I. M.; Barner-Kowollik, C. All Eyes on Visible-Light Peroxyoxalate Chemiluminescence Read-Out Systems. *Chem. Eur. J.* **2020**, *26* (1), 114–127.

(11) Yuan, D. Q.; Kishikawa, N.; Yang, C.; Koga, K.; Kuroda, N.; Fujita, K. Fluorophore-Capped Cyclodextrins as Efficient Chemical-to-Light Energy Converters. *Chem. Commun.* **2003**, *3* (3), 416–417.

(12) Nazem, A. Viral Nanoparticles as Lateral Flow Assay Reporters: Analysis of Capture Kinetics, Stabilization, and Detection in Blood. Ph.D. Dissertation, University of Houston, Houston, TX, 2019.

(13) Sevag, M. G.; Shelburne, M.; Ibsen, M. Inhibition of Catalase by Hydroxylamine and *p*-Hydroxylaminobenzenesulfonamide and the Reversal of Inhibition by Serum, Crystalline Serum Albumin, and Hemin. *J. Biol. Chem.* **1942**, *144* (3), 711–717.

(14) Jones, K. FUSION 5: A New Platform for Lateral Flow Immunoassay Tests. In *Lateral Flow Immunoassay*; Wong, R. C., Tse, H. Y., Eds.; Humana Press: New York, NY, 2009; pp 115–129.

(15) https://www.neb.com/tools-and-resources/selection-charts/affinity-of-protein-ag-for-igg-types-from-different-species (accessed December 22, 2021).

(16) Zou, K. H.; O'Malley, A. J.; Mauri, L. Receiver-Operating Characteristic Analysis for Evaluating Diagnostic Tests and Predictive Models. *Circulation* **2007**, *115* (5), 654–657.

(17) Mandrekar, J. N. Receiver Operating Characteristic Curve in Diagnostic Test Assessment. *J. Thorac. Oncol.* **2010**, *5* (9), 1315–1316.

CHAPTER 5

CONCLUSIONS AND OUTLOOK

Reproduced with permission from *the Journal of Applied Bio Materials*

(*Appl. Bio Mater.* 2022, 5, 1, 82–96)

DOI: 10.1021/acsabm.1c01051

Adheesha N. Danthanarayana,[1] Jakoah Brgoch,[1,*] and Richard C. Willson[2,3,*]

[1]Department of Chemistry, University of Houston, Houston, Texas 77204, USA

[2]Department of Chemical and Biomolecular Engineering, University of Houston, Houston, Texas 77204, USA

[3]Department of Biology and Biochemistry, University of Houston, Houston, Texas 77204, USA

Luminescent reporters greatly enhance the sensitivity of lateral flow assays (LFAs) compared to conventional reporter molecules or nanomaterials such as gold nanoparticles. They enable quantitative detection by measuring the amount of luminescence and are available in multiple colors, allowing multiplex analyte detection. Luminescent reporters also have a myriad of other advantages. For example, organic fluorophores are among the most widely used reporters in biomedical applications such as bioimaging and diagnostics due to the vast range of compounds with desirable chemical and photophysical properties, but they are susceptible to photobleaching.[1] Quantum dots are resistant to photobleaching, and they display unique size-tunable optical properties. However, they are costly, have intermittent on/off behavior, and are often cytotoxic.[2, 3] Additionally, both reporters need continuous excitation, which leads to high background signals. Lanthanide chelates provide an excellent solution for background interference as they have a long luminescence lifetime, allowing time-resolved measurements which minimize the background signal and

avoid the need for advanced optical readers.[4] Yet, they tend to have photostability issues that cause reduced sensitivity when involved in time-resolved measurements unless a time delay is accurately calculated.[5] Persistent luminescent phosphors display a long luminescence lifetime and superior resistance for photobleaching, making them ideal for time-resolved measurements,[6] although there are a limited number of materials that can be applied in LFAs. Upconversion phosphors have the unique ability to absorb infrared radiation and re-emit in the visible region. The resulting large anti-Stokes shift eliminates the need for time-resolved measurements and allows background-free detection with high sensitivity.[7, 8] Finally, chemiluminescent reporter systems have gained attention since they show better sensitivities because of the lower background signal than photoluminescent reporters. However, chemiluminescence systems generally have low quantum efficiency resulting in weak luminescence, and are susceptible to various chemical interferences, limiting the application of chemiluminescent reporters in analytical assays.[9]

In this dissertation, the limit of detection (LOD) for different analytes is provided (in Chapter 1) with each type of luminescent reporter discussed, alongside the sensitivity range of each reporter class. However, the LOD depends on many factors such as sample matrix, antibodies, and detection method/reader device. Therefore, it is not ideal to compare LODs between different types of luminescent reporters. Compared to laboratory diagnostic methods such as PCR and ELISA, the sensitivity of point-of-care (POC) luminescence-based LFAs is poor. Therefore, many different approaches have been explored to improve sensitivity, such as doping luminescent reporters into nanomaterials such as silica and polystyrene to enhance the chemical stability and the luminescence properties and developing FRET-based assays to enhance the signal intensity.[10] The sensitivity can be further improved by developing more sensitive and user-friendly luminescence reader devices. Some luminescence-based LFAs are coupled with ubiquitous devices such as smartphones to allow people to monitor their health more quickly and easily. Furthermore, researchers have paid more attention on developing multiplex LFAs to improve the efficiency of POC diagnostics by reducing the time and cost of analyzing multiple analytes.

The research work presented herein shows that the persistent luminescent nanophosphors are potential compounds to be used to develop smartphone-based multiplex assays with LODs comparable to commercially available tests. Nucleic acid-based LFA coupled with isothermal amplification is another emerging type since it significantly improves the sensitivity and specificity by detecting organism-specific DNA or RNA. The research work presented in this dissertation shows that the persistent luminescent nanophosphors can be used as reporters to develop nucleic acid-based LFAs combined with smartphone-based detection to achieve better sensitivities compared to gold nanoparticle-based tests. The research also shows the use of chemiluminescent reporters to develop antigen and antibody detection LFAs as chemiluminescence can reach greater sensitivities of detection compared to absorbance and fluorescence assays due to its low background.

Moreover, the sensitivity of LFAs can be further enhanced by optimizing assay kinetics to maximize specific binding and minimize non-specific binding and by amplifying the signal by chemical enhancement or physical stimulus *via* a reader device. In addition, other assay parameters such as sample pretreatment, surface modification or blocking of the reporters, reporter size and concentration, running buffer, and membrane blocking can be optimized to enhance the sensitivity and specificity of the assay. Although a rapid development of LFAs has occurred in the last decade, some issues still need to be improved in the future. This includes reducing performance variations within the same technique, developing more sensitive and cost-effective reader devices, and developing more simple, convenient flow control strategies.[11-13]

These developments will indeed help escalate the use of luminescence-based LFAs in medical diagnostics and other fields such as the food and agriculture industry and environmental testing. LFAs have been developed using quantum dots to detect food contaminants, including pesticide residues[14], mycotoxins[15], and antibiotics such as chloramphenicol.[16] Eu(III) chelates have also been used to develop time-resolved

multiplex LFAs for simultaneous and quantitative detection of pesticides (chlorothalonil), mycotoxins (aflatoxin B_1 and zearalenone)[17], and β-lactam antibiotics[18] in food samples. Furthermore, quantum dot-based LFAs have been developed to detect cyanobacteria-produced microcystins in water[19] and for pathogen detection in bottled water.[20] With the increase in foodborne disease outbreaks and various diseases due to environmental pollution, in the future, LFAs will gain more attention to be used in the food and agriculture industries and in environmental testing to obtain accurate and reliable results in a few minutes rather than waiting hours or days for results from laboratory testing methods.

Bibliography

(1) Sajid, M.; Kawde, A. N.; Daud, M. Designs, Formats and Applications of Lateral Flow Assay: A Literature Review. *J. Saudi Chem. Soc.* **2015**, *19* (6), 689–705.

(2) Hötzer, B.; Medintz, I. L.; Hildebrandt, N. Fluorescence in Nanobiotechnology: Sophisticated Fluorophores for Novel Applications. *Small* **2012**, *8* (15), 2297–2326.

(3) Chandan, H. R.; Schiffman, J. D.; Balakrishna, R. G. Quantum Dots as Fluorescent Probes: Synthesis, Surface Chemistry, Energy Transfer Mechanisms, and Applications. *Sen. Actuators B Chem.* **2018**, *258*, 1191–1214.

(4) Gudgin Dickson, E. F.; Pollak, A.; Diamandis, E. P. Time-Resolved Detection of Lanthanide Luminescence for Ultrasensitive Bioanalytical Assays. *J. Photochem. Photobiol. B Biol.* **1995**, *27* (1), 3–19.

(5) Ye, Z.; Tan, M.; Wang, G.; Yuan, J. Novel Fluorescent Europium Chelate-Doped Silica Nanoparticles: Preparation, Characterization and Time-Resolved Fluorometric Application. *J. Mater. Chem.* **2004**, *14*, 851–856.

(6) Paterson, A. S.; Raja, B.; Garvey, G.; Kolhatkar, A.; Hagström, A. E. V.; Kourentzi, K.; Lee, T. R.; Willson, R. C. Persistent Luminescence Strontium Aluminate Nanoparticles as Reporters in Lateral Flow Assays. *Anal. Chem.* **2014**, *86* (19), 9481–9488.

(7) Chen, J.; Zhao, J. X. Upconversion Nanomaterials: Synthesis, Mechanism, and Applications in Sensing. *Sensors* **2012**, *12* (3), 2414–2435.

(8) Zhou, J.; Liu, Q.; Feng, W.; Sun, Y.; Li, F. Upconversion Luminescent Materials: Advances and Applications. *Chem. Rev.* **2015**, *115* (1), 395–465.

(9) Zhu, X.; Gao, T. Spectrometry. In *Nano-Inspired Biosensors for Protein Assay with Clinical Applications*; Li, G., Ed.; Elsevier, 2019; pp 237–264.

(10) Gong, X.; Cai, J.; Zhang, B.; Zhao, Q.; Piao, J.; Peng, W.; Gao, W.; Zhou, D.; Zhao, M.; Chang, J. A Review of Fluorescent Signal-Based Lateral Flow Immunochromatographic Strips. *J. Mater. Chem. B* **2017**, *5* (26), 5079–5091.

(11) Huang, Y.; Xu, T.; Wang, W.; Wen, Y.; Li, K.; Qian, L.; Zhang, X.; Liu, G. Lateral Flow Biosensors Based on the Use of Micro- and Nanomaterials: A Review on Recent Developments. *Microchim. Acta* **2020**, *187* (1), 70.

(12) Liu, Y.; Zhan, L.; Qin, Z.; Sackrison, J.; Bischof, J. C. Ultrasensitive and Highly Specific Lateral Flow Assays for Point-of-Care Diagnosis. *ACS Nano* **2021**, *15* (3), 3593–3611.

(13) Deng, Y.; Jiang, H.; Li, X.; Lv, X. Recent Advances in Sensitivity Enhancement for Lateral Flow Assay. *Microchim. Acta* **2021**, *188* (11), 379.

(14) Wang, S.; Liu, Y.; Jiao, S.; Zhao, Y.; Guo, Y.; Wang, M.; Zhu, G. Quantum-Dot-Based Lateral Flow Immunoassay for Detection of Neonicotinoid Residues in Tea Leaves. *J. Agric. Food Chem.* **2017**, *65* (46), 10107–10114.

(15) Beloglazova, N. V.; Sobolev, A. M.; Tessier, M. D.; Hens, Z.; Goryacheva, I. Y.; De Saeger, S. Fluorescently Labelled Multiplex Lateral Flow Immunoassay Based on Cadmium-Free Quantum Dots. *Methods* **2017**, *116*, 141–148.

(16) Berlina, A. N.; Taranova, N. A.; Zherdev, A. V.; Vengerov, Y. Y.; Dzantiev, B. B. Quantum Dot-Based Lateral Flow Immunoassay for Detection of Chloramphenicol in Milk. *Anal. Bioanal. Chem.* **2013**, *405* (14), 4997–5000.

(17) Wang, D.; Zhu, J.; Zhang, Z.; Zhang, Q.; Zhang, W.; Yu, L.; Jiang, J.; Chen, X.; Wang, X.; Li, P. Simultaneous Lateral Flow Immunoassay for Multi-Class Chemical Contaminants in Maize and Peanut with One-Stop Sample Preparation. *Toxins (Basel).* **2019**, *11* (1), 56.

(18) Li, X.; Pan, Z.; Li, M.; Jia, X.; Zhang, S.; Lin, H.; Liu, J.; Ma, L. Europium Chelate-Labeled Lateral Flow Assay for Rapid and Multiple Detection of β-Lactam Antibiotics by the Penicillin-Binding Protein. *Anal. Methods* **2020**, *12* (28), 3645–3653.

(19) Sun, J.; Li, Y.; Pi, F.; Ji, J.; Zhang, Y.; Sun, X. Using Fluorescence Immunochromatographic Test Strips Based on Quantum Dots for the Rapid and Sensitive Determination of Microcystin-LR. *Anal. Bioanal. Chem.* **2017**, *409* (8), 2213–2220.

(20) Morales-Narváez, E.; Naghdi, T.; Zor, E.; Merkoçi, A. Photoluminescent Lateral-Flow Immunoassay Revealed by Graphene Oxide: Highly Sensitive Paper-Based Pathogen Detection. *Anal. Chem.* **2015**, *87* (16), 8573–8577.